

Extended Jaynes-Cummings models in cavity QED

Jonas Larson



Dissertation for the degree of Doctor of Philosophy
Department of Physics
The Royal Institute of Technology, Albanova

Stockholm 2005

Cover: Pårte, Sarek Sweden, a cold evening in September.

*There's more to the picture
than meets the eye*

Neil Young

ISBN 91-7178-124-2

TRITA-FYS 2005:44

ISSN 0280-316X

ISRN KTH/FYS/-05:44- -SE

Printed by Universitetsservice US AB
Stockholm 2005

Avhandling

Jonas Larson

Laser Physics and Quantum Optics, Royal Institute of Technology, 2005

Abstract

Due to the improvement within cavity quantum electrodynamics experiments during the last decades, what was former seen as 'toy models' are today realized in laboratories. A controlled isolated coherent evolution of one or a few atoms coupled to a single mode inside a cavity is achievable. Such systems are well suited for studying purely quantum mechanical effects, and also for performing quantum gates, necessary for quantum computing. The Jaynes-Cummings model has served as a theoretical description of the interaction. However, as the experimental techniques are improved, for example, atom cooling, the use of multi-level atoms or multi-modes and driving of atoms or fields by external lasers, extensions of the original Jaynes-Cummings model are needed. In this thesis we study some of these extended models, and in particular multi-level models, time-dependent models and quantized motion models. Both analytical and numerical analysis are considered. The two-level structure of the Jaynes-Cummings model leads to applications of known solvable time-dependent two-level Schrödinger equations. In other cases, different forms of adiabatic approximate solutions are used, and with the analytically solvable models, the amplitudes of non-adiabatic contributions may be estimated. For higher dimensional systems, STIRAP and multi-STIRAP methods are applied. It is shown how the time-dependent models may be used for preparation of various kinds of non-classical states, and also to generate universal sets of quantum gates, both on atomic and field qubits. When the atoms are cooled to very low temperatures, their velocities must be treated quantum mechanically, and we have studied the dynamics of such cases for different coupling shapes. Again numerical and analytical approaches have been used and compared, wave-packet propagations of the atom, approaching and traversing the cavity, have been performed. For periodic couplings, standing wave cavity modes, the dynamics has been described by effective parameters; group velocity or atomic index of refraction and effective mass. Tunneling resonances for ultra cold atoms have been exhibited in the STIRAP models for certain initial conditions.

© Jonas Larson 2005

TRITA-FYS 2005:44 • ISSN 0280-316X • ISRN KTH/FYS/-05:44- -SE

Acknowledgment

Of course, the first and most important person for the research during my PhD. years is my supervisor Prof. Stig Stenholm. We have had a close collaboration always running smoothly. Even though he has been busy as any professor, I have never felt as standing still on the same old spot, the help has always been there. Not only when we have worked directly together has Stig been a resource and helpful hand, giving comments and suggestions. But maybe most important is the 'spring' of inspiration he has been for me, broadening my horizons in physics.

I have had the joy to work with some other people during these years, and they are warmly thanked here: Janne Salo, Barry Garraway and Erika Andersson. You have all been very helpful. I am also thankful to Prof. Fredrik Laurell for financial support during my last phd. period.

My huge family deserves all possible gratitude, cheering me along climbs and descents. My mother and father, my sisters and brother: Åsa, Odd, Hanna and Malin and all the rest: Smilla, Tilde, Carola, Martin, Sandra and Louise. I love you all so much, in you I have a safe spot. Finally a 'lily of the valley' goes to some friends: The sailors, Fredrik and the shoulder Jon.

The thesis is based on the following papers

- I** *Adiabatic state preparation in a cavity*
 J. Larson and S. Stenholm, *J. Mod. Opt.* **50**, 1663 (2003).
- II** *Photon filters in a microwave cavity*
 J. Larson and S. Stenholm, *J. Mod. Opt.* **50**, 2705 (2003).
- III** *Cavity field ensembles from non-selective measurements*
 J. Larson and S. Stenholm, *J. Mod. Opt.* **51**, 129 (2004).
- IV** *Dynamics of a Raman coupled model: entanglement and quantum computing*
 J. Larson and B. M. Garraway, *J. Mod. Opt.* **51**, 1691 (2003).
- V** *Cavity-state preparation using adiabatic transfer*
 J. Larson and E. Andersson, *Phys. Rev. A* **71**, 053814 (2005). Selected for publication in *Virtual Jour. Quant. Inf.* June issue (2005)
- VI** *Effective mass in cavity QED*
 J. Larson, J. Salo and S. Stenholm, *Phys. Rev. A* **72**, 013814 (2005).
- VII** *Level crossings in a cavity QED model*
 J. Larson, *Phys. Rev. A*, submitted (2005).
- VIII** *Scheme for generating entangled states of two field modes in a cavity*
 J. Larson, *Opt. Comm.*, to be submitted (2005).

Paper I

The first of three papers dealing with the original Jaynes-Cummings model with time-dependent parameters. The general idea of using parameters explicitly depending on time is introduced. It is shown how the system Hamiltonian is reduced to two coupled differential equations, and how known solvable time-dependent two-level models may be applied to the Jaynes-Cummings model. The Landau-Zener and the Demkov-Kunike models are studied. The use of repeated atomic conditional measurements are used to reshape the photon distribution, and the concept of *filter functions* is defined. Some analytical approximations are derived.

Paper II

In this paper the results from Paper I are applied to more physical models including numerical work on the standing wave mode coupling. The solvable time-dependent Rosen-Zener model is used to simulate a pulse shaped coupling. The adiabaticity constrains are studied for various forms of the coupling pulses.

Paper III

The final paper on the time-dependent Jaynes-Cummings model. Instead of using repeated conditional atomic measurements we analyze the situation of unconditional measurements, and some analytical results are derived. The Demkov-Kunike model is used to show how to prepare Fock states of the field.

Paper IV

Here a Λ atom interacting with two quantized modes is considered. An effective model, where one of the three atomic levels has been eliminated, is used. A large part of the paper considers the interaction of the atom with the fields either in coherent or squeezed states with large amplitudes. The disentanglement of the atom from the fields at specific times is studied and especially the state of the fields at those times. It is shown how entangled Schrödinger cat states are achieved. One part of the paper also investigate the model used for state preparation and quantum gate realization.

Paper V

In this paper we again use explicit time-dependence on the atom-field couplings, but for an extended Jaynes-Cummings model. The atom has two levels and it interacts with more than just one cavity field. The mode shape gives the specific time-dependence and by using overlapping cavities a situation much like STIRAP is obtained. The method is extended to contain more atoms and cavities and we mainly consider state preparation of the cavity fields. Again it is shown how to generate various entangled states. Numerical integration is used to test the adiabaticity constrains.

Paper VI

A complete quantum mechanical treatment, including the atomic center-of-mass motion, is considered in this and in the next paper. We only treat the situation with cosine shape of the coupling, either with infinite extent or with finite extent characterizing the cavity boundaries. The problem is treated both using Floquet theory and numerical wave-packet simulations. From the former we introduce the effective parameters as group velocity and effective mass, we also give some analytical approximations of the effective mass. The two methods are compared by calculating the effective parameters for the two approaches. Scattering and

reflection of the atom upon the cavity field, and the atomic dynamics in general, is analyzed.

Paper VII

This paper uses the full quantum treatment again, but with a linear force affecting the atom while traversing the cavity. The energy spectrum together with the acceleration theorem is used in order to understand the dynamics in terms of Bloch oscillations. Effective time-dependent models are derived to measure the non-adiabatic damping of the oscillations. The effect of the detuning is especially considered and from that we find a new kind of level crossing including three energy curves. One section explains how similar oscillations may be obtained from an oscillating detuning instead of a linear external force.

Paper VIII

The final paper gives a simple scheme for preparing entangled states of two cavity modes. A two-level atom is coupled to two modes with equal frequencies. Using an unitary transformation of the original Hamiltonian the standard Jaynes-Cummings one is obtained. The problem is analytically treated in the transformed basis and going back to the initial basis the evolution is found. It is shown how to generate entangled Schrödinger cat states of the two modes, either by using a large or vanishing atom-field detuning.

Contribution by the author

The general idea of using time-dependent parameters in the original Jaynes-Cummings model was due to Stig Stenholm. He also wrote part of Paper I. I have done the numerical work in all papers . The use of a standing wave mode coupling in Paper II is also due to Stig, while the adiabaticity analysis was my idea and I wrote the paper. Paper III was written by me and all ideas were also mine. In Paper IV Barry Garraway had the suggestion of studying the A model and he also gave the important reference on 'large amplitude' fields for the preparation of Schrödinger cat states. The analyses are done by me and I also wrote the paper. Paper V is written by both Erika Andersson and myself, she came up with the idea of including several cavities and atoms. I showed how to use the third atomic state $|q\rangle$ for state preparation, and I also introduced the 'star configuration'. The main question, asked by Stig, for Paper VI was how the concept of an effective mass is introduced in cavity QED. The original ideas did not lead to satisfactory results, which was sorted out by myself and Janne Salo. Janne also helped me with getting my codes correct. I wrote the main parts of the paper and most of the 'applications' suggested are mine. Paper VII and VIII are solely by me, but I had helpful discussions with Janne for the first of the two.

Papers not included in the thesis

- I *Spectral asymptotics for Schrödinger operators with periodic point interactions*
P. Kurasov and J. Larson, *J. Math. Anal. Appl.*, **266**, 127 (2002).

- II *Transient effects on electron spin observation*
J. Larson, B. M. Garraway and S. Stenholm, *Phys. Rev. A* **69**, 032103 (2004).

Contents

| | | |
|----------|---|-----------|
| 1 | Introduction | 3 |
| 2 | Cavity QED and the Jaynes-Cummings model | 7 |
| 2.1 | Cavity QED | 7 |
| 2.2 | Introducing the Jaynes-Cummings model | 9 |
| 2.2.1 | Derivation of the Jaynes-Cummings model | 9 |
| 2.2.2 | Conditional atomic measurement | 13 |
| 2.2.3 | Unconditional atomic measurement | 16 |
| 3 | Extended Jaynes-Cummings models | 17 |
| 3.1 | Multi-level Jaynes-Cummings models | 17 |
| 3.2 | Time dependent Jaynes-Cummings models | 20 |
| 3.2.1 | Adiabatic evolution with level crossings | 22 |
| 3.2.2 | STIRAP evolution in cavities | 22 |
| 3.3 | The Jaynes-Cummings model with quantized motion | 25 |
| 3.3.1 | Pulse-shaped atom-field coupling | 26 |
| 3.3.2 | Periodic atom-field coupling | 28 |
| 3.3.3 | Washboard potential | 32 |
| 3.3.4 | External atomic trap-potential | 34 |
| 4 | Dynamics of extended Jaynes-Cummings models | 35 |
| 4.1 | State preparation | 35 |
| 4.1.1 | Adiabatic preparation of Fock states | 35 |
| 4.1.2 | Adiabatic preparation of entangled states, chirped case | 37 |
| 4.1.3 | Adiabatic preparation of entangled states, STIRAP case | 38 |
| 4.1.4 | Non-adiabatic preparation of entangled states, Λ -atom case | 44 |
| 4.1.5 | Dispersive preparation of entangled states, V -atom case | 49 |
| 4.2 | Quantum computing | 51 |
| 4.2.1 | Adiabatic quantum computing, with field qubits | 51 |
| 4.2.2 | Adiabatic quantum computing, with atom qubits | 53 |

| | | |
|----------|--|-----------|
| 4.2.3 | Non-adiabatic quantum computing, with field qubits | 54 |
| 4.3 | Effects due to a quantized atomic motion | 55 |
| 4.3.1 | Effective parameters | 55 |
| 4.3.2 | Atom optics | 57 |
| 4.3.3 | Generalized Bloch oscillations and tunneling | 61 |
| 4.3.4 | STIRAP with quantized motion | 63 |
| 5 | Conclusion | 67 |
| A | Adiabaticity | 69 |
| B | Split operator method | 77 |
| | References | 79 |

Chapter 1

Introduction

The understanding of the most simple non trivial systems in quantum mechanics is, of course, a condition for possible interpretation of more complex, and possibly, more realistic models. It is also more likely that, with a small number of degrees of freedom, an analytical solutions may be found. Even if it has become possible to numerical solve for the system dynamics on todays computers, analytical solution directly gives an insight into the parameter dependence. If a large set of parameters is involved, also systems with a few degrees of freedom may be time consuming to solve numerically for the interesting parameter rangers. Maybe more important than understanding simple systems in order to achieve a deeper knowledge of 'larger' systems, is the fact that during the last decades it has become possible to experimentally realize the most simple fully quantum mechanical systems. The experimental works on simple dynamical systems include a broad collection in various fields in physics, such as, solid state physics, nuclear magnetic resonance, trapped ions, Bose-Einstein condensates, quantum optics, atom optics. Some of these are covered in the book [1]. One of the successful area is cavity quantum electrodynamics, or shortly *cavity QED* [2]. As with any physical model, the degrees of freedom that are not important for the evolution are left out, scaling down the system to contain a much smaller set of states. In cavity QED, the standard picture is that an atom interacts with a single mode of the cavity field, and due to energy conservation and selection rules only two atomic levels are included. The effective model thus describes interaction between a two-level particle and an harmonic oscillator. When the motion of the atom is not included in the description and the rotating wave approximation has been applied, the evolution is given by the analytically solvable Jaynes-Cummings (JC) model [3, 4]. This is the simplest non trivial model describing interaction between two different sub-systems. In spite of its simplicity, since it was first presented a huge amount of

theoretical and experimental work has been focused on it. Theoretical predictions are, collapse-revivals [5], atomic disentanglement [6, 7], field squeezing [8], non-demolition measurements [9], state reconstruction [10], single photon states *Fock states* [11], superposition of large amplitude coherent states (*Schrödinger cats*) [12], decoherence [13]. Many of these and other predictions have been verified in experiments [14, 15, 16, 17, 18, 19, 20, 21]. At about the same time as realization of cavity QED experiments began, a new sub-field of quantum mechanics; quantum information, developed explosively [1, 22]. The qubit, which carries the information, could either be decoded in the two-level atom or in the field state, usually the zero $|0\rangle$ or the one photon $|1\rangle$ Fock states. The applications towards quantum information and computing have been studied and also experimentally tested, see for example [17, 23].

Concurrently with the progress of cavity QED experiments, numerous extensions of the original JC model have been analyzed. Not only because of more sophisticated experimental set-ups and techniques, making it possible to increase the number of degrees of freedom in a controlled fashion, but also since in some situations the JC model is an approximation which might not be valid. For example, an atom traversing a cavity couples differently to the mode depending on its location along the cavity mode shape. Thus, the coupling should vary in strength during the interaction. With typical experimental parameters, the atomic kinetic energy largely exceeds the interaction energy and may thus be seen as a constant of motion. It is then legitimate to substitute the spatial dependence of the atom-field coupling g into a time-dependence; $x \rightarrow vt$, where v is the classical center-of-mass velocity of the atom. The model is then transformed into a time-dependent semi-classical one and one must solve the time-dependent Schrödinger equation. Note that the center-of-mass momentum should be large enough to be treated classically, but it cannot be too large, since then the atom will couple non-adiabatically to other cavity modes. In addition to the coupling g , there is another essential parameter in the JC model, namely the detuning Δ , which is the difference between the atomic transition and mode frequency. Naturally, a large detuning results in small energy exchange between the two sub-systems. Also the detuning may become time-dependent if either the mode or atomic transition frequencies are varied during the passage of the atom through the cavity. As the number of excitations is conserved in the JC model, the Schrödinger equation reduces to a system of two coupled first order differential equations. This situation has been studied for both analytically solvable models and using numerical integration of the coupled equations.

By using ultra cool atoms, the center-of-mass momentum may no longer be a constant of motion and the kinetic energy term cannot be rejected, neither can the spatial dependence of the coupling be replaced by its corresponding classical position. The dynamics is now described fully quantum mechanically and makes out

a great part of this thesis. We differentiate between two situations; the coupling has a pulse shape and disappears at $x = \pm\infty$, and when the coupling is periodic or quasi periodic. The first case is characterized by its transmission and reflection coefficients and by the non-classical tunneling resonances. While for the periodic coupling, the dynamics can be understood from the energy spectrum $E_\nu(k)$ consisting of continuous bands separated by gaps. Here ν is the band index and k the quasi momentum. In our analysis we have used both analytical results, exact or obtained from approximations, and numerical ones. The numerical results are obtained from wave-packet propagation. The effective parameters obtained from the coefficients of a series expansion of $E_\nu(k)$, have been verified in our wave-packet propagation results.

In addition to the above extensions of the original JC model, we have also considered, multi-mode and three level atom cases. These are direct generalizations of the JC model and here we have considered them both as time-dependent and position-dependent ones. For the time-dependent models, we have particularly studied the well known STIRAP model [24, 25], where the two couplings are pulse shaped and displaced in time. STIRAP is often used for population transfer between internal states, and here we show its applications in cavity QED and how it may be used for state preparation.

Central for the most part of the thesis is the concept of adiabaticity, and therefore one of the appendixes is devoted to this subject. The phenomenon is usually connected to having explicit time-dependence in the Hamiltonian, but we have seen above how one may, in certain parameter regimes, transform time-independent Hamiltonian into a time-dependent one. Another example is the *acceleration theorem* derived in an appendix. One aspect that is important for us is adiabatic elimination, which derives effective models by reducing the number of states, only including those that are significantly populated. This is often done for large detunings, where excitations are not likely to populate one or more of the internal levels.

The outline of the thesis is as follows.

In chapter 2 we present the idea of cavity QED and derive the standard JC model. Some of the most interesting phenomena of the model, such as entanglement, collapse-revivals and measurements are briefly discussed. Various extensions of the JC model, and some of their properties are introduced in the following chapter 3. The main three extensions are, as mentioned above, multi-level, time-dependent and quantized motion JC models. There is one subsection about a tilted periodic potential, where the atom, under certain conditions, shows an oscillatory motion. Most of the results are presented in chapter 4. One section deals with *state preparation*, where the models are used to initialize desirable quantum states, for example Fock or entangle states. It is also shown how to realize universal sets of quantum gates, both for field and atomic qubits. And finally the

dynamics of an atom with a quantized center-of-mass motion is studied, for a two-level atom and for a three-level atom, which represents the fully quantized version of the semiclassical STIRAP. The last chapter 5 concludes with a summery and future perspectives. Adiabaticity is considered in appendix A and the split operator method, used for numerical wave-packet propagation is discussed in appendix B.

Chapter 2

Cavity QED and the Jaynes-Cummings model

2.1 Cavity QED

QED describes the interaction between quantized light and matter, ranging from single photons and atoms to atomic gases or molecules and classical light fields. As the degrees of freedom for the system increase, the possible 'channels' for dissipation usually blow up, and the controllability of the system and its reversible evolution is lost. Thus, systems consisting of only few degrees of freedom are more likely to stay isolated from the surrounding environment. Even the most simple non-trivial systems have turned out to be difficult enough to keep isolated. By letting an atom be confined inside a cavity it is possible to consider only a few particular cavity modes and atomic transitions in the atom-field interaction, the rest of the internal states can be left out. Thus, the degrees of freedom can be considerably reduced due to the presence of the surrounding cavity.

The general set-up for cavity QED experiments is built on the following scheme: From an atom oven a beam of atoms leaks out through a hole, during the passage of a set of classical laser beams the atomic initial state is prepared. This includes to excite the atom to the desirable internal electronic state, and also to select the atomic velocities. This can be done simultaneously by controlling the doppler shifted laser frequencies such that only atoms with a certain velocity are excited. The atoms then enter the cavity, and the interaction time is set by the atomic velocity. The atoms that have too different initial velocities are never excited and will therefore pass through the cavity without affecting the field. The state preparation of the cavity field is done in different ways. It could be done by for example, previous atom-cavity interactions, atom-cavity-laser interactions, cavity-

laser interaction or simply just cooling of the cavity temperature. After the atoms exiting the cavity, ionization atomic detectors determine the atomic state. By using laser manipulations of the atom in the step between the cavity interaction and the detection, its state can be rotated by any angle and all possible atomic states can be detected.

In addition to the scheme above there exist several other possible setups, which will be partly discussed in this thesis.

The atoms used are usually Rubidium or Cesium, excited to high Rydberg states. These atomic states have several advantages, in particular a long decay time and a large dipole-element giving a strong atom-field coupling. The cavities have very high Q -values, because of the use of super-conducting closed or nearly closed walls. The low temperature also keeps the number of thermal photons down. Mostly used are cavities with Fabry-Perot geometries as in for example the groups of Prof. S. Haroche Course 3 in [1], Prof. H. J. Kimble [16] and Prof. G. Rempe [26]. In the experiments of Prof. H. Walther, a closed cylindrical cavity is used [27]. The forms of the cavities determine the shapes of the modes of the field. Thus, the construction of the cavity is strongly linked to the atoms used and to the experiment one has in mind. One general problem is stray fields around the entrance and exit holes of the atom. These tend to destroy the coherence of the atomic state. An advantage with the Fabry-Perot cavities is that the atom may be manipulated while it is inside the cavity, using external lasers or EM-fields. The experiments are performed within two different parameter regimes; the microwave or the optical. Usually the atom-field couplings g_0 are much larger in the optical regime due to a much smaller mode-volume. However, the relaxation times of the cavity κ^{-1} and of the atom Γ^{-1} are instead shorter than for microwave cavities. In order to have an evolution in which the coherent mechanism dominates over the incoherent ones coming from the losses we must have

$$\kappa, \Gamma \ll g_0. \quad (2.1)$$

In the table below we present some typical experimental parameter values for two groups working in the optical (Kimble and Rempe) and two in the microwave regime (Walther and Haroche), where $\Omega/2\pi$ is the transition frequency of the atom and τ is the transition time of the atom through the cavity.

| Group | $\Omega/2\pi$ | $g_0/2\pi$ | $\kappa/2\pi$ | $\Gamma/2\pi$ | τ |
|-----------------------|---------------|------------|---------------|---------------|--------------|
| Kimble <i>et al.</i> | 352 THz | 120 MHz | 40 MHz | 2.6 MHz | 0.05 μ s |
| Rempe <i>et al.</i> | 385 THz | 16 MHz | 1.4 MHz | 3 MHz | 3 μ s |
| Walther <i>et al.</i> | 21 GHz | 7 kHz | 0.4 Hz | 500 Hz | 80 μ s |
| Haroche <i>et al.</i> | 51 GHz | 48 kHz | 400 Hz | 5 Hz | 30 μ s |

Table 1. Experimental data.

2.2 Introducing the Jaynes-Cummings model

2.2.1 Derivation of the Jaynes-Cummings model

We now turn to the issue of finding the correct Hamiltonian describing the dynamics of a single atom interacting with the field inside the cavity. Here we assume the most simple situation; just one atomic transition and a single quantized mode of the cavity field is taken into account. The extensions of this model are discussed in the next chapter.

We leave out the procedure of quantization of the field, which can be find in any book on quantum optics [28, 29]. The full Hamiltonian describing an atom interacting with a EM-field is

$$H_{a-f} = \frac{1}{2m} [\mathbf{p} - q\mathbf{A}(\mathbf{x})]^2 + U(\mathbf{x}) + \hbar\omega \left(a^\dagger a + \frac{1}{2} \right) + H_{el}, \quad (2.2)$$

where \mathbf{p} , q , \mathbf{x} and m are the momentum, charge, position and mass of the atom, a^\dagger and a are creation and annihilation operators for the field mode and H_{el} is the Hamiltonian describing the electronic states of the atom. The vector potential operator is

$$\mathbf{A}(\mathbf{x}) = A_0 (\bar{\varepsilon} f(\mathbf{x}) a + \bar{\varepsilon}^* f^*(\mathbf{x}) a^\dagger), \quad (2.3)$$

where $\bar{\varepsilon}$ is the polarization vector and $f(\mathbf{x})$ is a function describing the field along the mode in the cavity. It gives the effective mode volume

$$V = \int d^3\mathbf{x} |f(\mathbf{x})|^2, \quad (2.4)$$

which relates to the constant A_0 as

$$A_0 = \sqrt{\frac{\hbar}{2\varepsilon_0\omega V}}. \quad (2.5)$$

Under the assumption that only one atomic transition couples to the mode, the electronic states may be labeled $|\pm\rangle$ and the electronic hamiltonian in (2.2) can be written

$$H_{el} = \frac{\hbar\Omega}{2}\sigma_z, \quad (2.6)$$

where Ω is the transition frequency and σ_z is the Pauli z -operator; $\sigma_z|\pm\rangle = \pm|\pm\rangle$. If we neglect multi-photon processes (leave out the \mathbf{A}^2 -term) and assume the

external atomic potential to be zero, $U = 0$, the Hamiltonian becomes

$$\begin{aligned} H_{a-f} &= H_{at} + H_{field} + H_{int}, \\ H_{at} &= \frac{\mathbf{p}^2}{2m} + \frac{\hbar\Omega}{2}\sigma_z, \\ H_{field} &= \hbar\omega \left(a^\dagger a + \frac{1}{2} \right), \\ H_{int} &= -\frac{q}{m} A_0 [(\mathbf{p} \cdot \hat{\varepsilon}) f(\mathbf{x}) a + (\mathbf{p} \cdot \hat{\varepsilon}^*) f^*(\mathbf{x}) a^\dagger]. \end{aligned} \tag{2.7}$$

In matrix representation within the atomic basis states, the interaction Hamiltonian is [29]

$$H_{int} = g(\mathbf{x}) (a^\dagger \sigma^- + a \sigma^+), \tag{2.8}$$

where σ^\pm are the raising and lowering operators for the atom and

$$g(\mathbf{x}) = -\frac{q}{m} \langle + | (\mathbf{p} \cdot \hat{\varepsilon}) | - \rangle f(\mathbf{x}) \sqrt{\frac{2}{\hbar\omega\varepsilon_0 V}}. \tag{2.9}$$

In deriving (2.8) we neglected the fast oscillating terms corresponding to virtual processes, called the *rotating wave approximation* (for corrections, see [30]), and we adjusted the phases of the states $|\pm\rangle$ such that $g(\mathbf{x})$ is real.

If we further assume that $g(\mathbf{x})$ is to a good approximation independent of \mathbf{x} , the atomic kinetic energy operator is a constant of motion and can be omitted, as may the constant vacuum term $\hbar\omega/2$. The resulting Hamiltonian is

$$\tilde{H} = \hbar\omega a^\dagger a + \frac{\hbar\Omega}{2}\sigma_z + g (a^\dagger \sigma^- + a \sigma^+), \tag{2.10}$$

which defines the Jaynes-Cummings (JC) model. The form of the coupling term is such that the number of excitations $N = a^\dagger a + \frac{1}{2}\sigma_z$ is preserved and it is customary to work within an interaction picture

$$H = \tilde{H} - \hbar\omega N = \frac{\Delta}{2}\sigma_z + g (a^\dagger \sigma^- + a \sigma^+). \tag{2.11}$$

Here $\Delta = \Omega - \omega$, is the atom-field detuning. A large detuning results in fast oscillating exponentials in the eigenfunctions of the Hamiltonian (2.11) and the population transfer between the states $|\pm\rangle$ decreases.

Since N is a constant of motion it is enough to solve the system for one particular value $n \pm \frac{1}{2}$ of N . Thus, in the interaction picture the Hamiltonian is of

block-diagonal form with 2×2 -blocks ($\hbar = 1$)

$$H_n = \begin{bmatrix} \frac{\Delta}{2} & g_0\sqrt{n} \\ g_0\sqrt{n} & -\frac{\Delta}{2} \end{bmatrix}. \quad (2.12)$$

Any Hermitian Hamiltonian for a two-level system can be transformed into the form (2.12), see [31]. The basis states are the so called *bare states* $|n-1, +\rangle$ and $|n, -\rangle$, where $|n\rangle$ is the n photon Fock state; $a|n\rangle = \sqrt{n}|n-1\rangle$. The eigenstates of H_n are

$$\begin{aligned} |\psi_+\rangle &= \cos\left(\frac{\theta}{2}\right)|+, n-1\rangle + \sin\left(\frac{\theta}{2}\right)|-, n\rangle, \\ |\psi_-\rangle &= \sin\left(\frac{\theta}{2}\right)|+, n-1\rangle - \cos\left(\frac{\theta}{2}\right)|-, n\rangle, \end{aligned} \quad (2.13)$$

where

$$\tan(\theta) = \frac{2g_0\sqrt{n}}{\Delta} \quad (2.14)$$

and with corresponding eigenvalues

$$E_{\pm} = \pm \sqrt{\left(\frac{\Delta}{2}\right)^2 + g_0^2 n}. \quad (2.15)$$

Note that for $\Delta = 0$, the angle $\theta = \pi/2$ and is thus independent of the parameters. This has important consequences, as will become clear in the following chapters, namely the two-level structure of the JC model can be separated into two disconnected sets regardless if the coupling is time-dependent or x -dependent.

A general state evolving under the Hamiltonian (2.11) can be written in the bare states as

$$|\Psi\rangle = c_0 a_-(0, t)|0, -\rangle + \sum_{n=1}^{\infty} c_n [a_+(n, t)|n-1, +\rangle + a_-(n, t)|n, -\rangle], \quad (2.16)$$

where c_n determines the initial photon distribution and the coefficients $a_{n\pm}(t)$ are the solution of the Schrödinger equation and read, according to equation (2.13),

$$\begin{aligned} a_-(n, t) &= \left[\cos\left(\frac{\Omega t}{2}\right) - \frac{i\Delta}{2\Omega} \sin\left(\frac{\Omega t}{2}\right) \right] e^{-i\Delta t/4} \\ a_+(n, t) &= \frac{ig_0\sqrt{n}}{\Omega} \sin\left(\frac{\Omega t}{2}\right) e^{i\Delta t/4}, \end{aligned} \quad (2.17)$$

for the initial condition $|a_{n-}(t=0)| = 1$ and $\Omega = \sqrt{\left(\frac{\Delta}{2}\right)^2 + g_0^2 n}$. The solutions become especially simple in the zero detuning case $\Delta = 0$,

$$\begin{aligned} a_-(n, t) &= \cos(g_0\sqrt{n}t) \\ a_+(n, t) &= \sin(g_0\sqrt{n}t). \end{aligned} \quad (2.18)$$

The oscillatory behaviour of the solutions is called *Rabi oscillations* and $g_0\sqrt{n}$ the *Rabi frequency*. Note that the Rabi frequency is depending on the number of photons in the mode. For an initial photon state with several coefficients c_n non-zero, the terms of the state (2.17) will oscillate with different frequencies resulting in general in a collapse of various atom and field quantities.

In experiments where the atom leaves the cavity, and only interacts with it for a certain time, we are interested in the asymptotic solutions $|a_\pm^\infty(n)|$ as $t \rightarrow \infty$. This assumes that the atom and the field do not couple for large values t .

A state of two composite systems A and B is said to be *entangled* if it can not be written as a direct product of separate states

$$|\Psi\rangle_{AB} \neq |\Psi\rangle_A \otimes |\Psi\rangle_B. \quad (2.19)$$

For *mixed states*, $\rho = \sum_i p_i |\psi_i\rangle\langle\psi_i|$, where the p_i s are classical probabilities satisfying $\sum_i p_i = 1$, entanglement is defined as

$$\rho_{AB} \neq \sum_i p_i \rho_A^i \otimes \rho_B^i, \quad (2.20)$$

for any sets of density operators $\{\rho_A^i\}$ and $\{\rho_B^i\}$ of system A and B respectively. It is clear from the form of the solution (2.17) of the JC model that the atom and the field are most likely to be entangled. There are several quantities that measures some kind of degree of entanglement, for example *purity*

$$p_A = \text{Tr}_A [\rho_A^2] \quad (2.21)$$

or *von Neumann entropy*

$$S_A = -\text{Tr}[\rho_A \log(\rho_A)], \quad (2.22)$$

where ρ_A is the *reduced density operator*, $\rho_A = \text{Tr}_B [\rho_{AB}]$ and trace is over system B 's degrees of freedom. For a pure state $\rho = |\Psi\rangle\langle\Psi|$ it follows that $\rho = \rho^2$; the purity equals 1, and for entangled states it is less than 1. Likewise, for pure states the entropy is zero, and an increase of the entropy corresponds to more correlation between the subsystems. If the composite system starts out in a pure state and evolve under (2.11), the composite entropy is identically zero throughout the evolution. This is, however, not true for the subsystems which may be entangled. It is possible to show that the purities are the same for the field and the atom $p_{atom}(t) = p_{field}(t)$, and when the initial state is pure we also have $S_{atom}(t) = S_{field}(t)$ [32].

2.2.2 Conditional atomic measurement

In general, after the passage of the atom, the cavity field and the atom will be in an entangle state as we have seen above. If the state of the atom is measured in either $|+\rangle$ or $|-\rangle$ after the interaction, it follows from (2.16) that the state of the field is modified by $a_+^\infty(n)$ or $a_-^\infty(n)$ depending on which state the atom is found in. This is called a *conditional measurement*. Depending on the outcome of the measurement, the field distribution will be (up to a normalization constant)

$$\begin{aligned} P_+(n) &= |a_+^\infty(n+1)|^2 |c_{n+1}|^2 \\ P_-(n) &= |a_-^\infty(n)|^2 |c_n|^2. \end{aligned} \quad (2.23)$$

The $|a_\pm^\infty(n)|^2$:s clearly reshape the photon distribution and are therefor called *filter functions*. If this process is repeated, the sequence of measured atoms determines the photon distribution, provided that the initial conditions are known.

If we measure a flip of the j :th atom according to $|\mp\rangle \rightarrow |\pm\rangle$, we let $k_j = \pm 1$ and for no flip $k_j = 0$. For a collected sequence \mathbf{k} , the photon distribution after m conditional atomic measurements is

$$P_{m,\mathbf{k}}(n) = \frac{1}{N} A_{m,\mathbf{k}}(n) P_0(n + \nu). \quad (2.24)$$

Here $A_{m,\mathbf{k}}(n)$ is the appropriate sequence of filter functions $|a_\pm^\infty(n)|^2$ as discussed in Paper III, $\nu = \sum_j k_j$ and N is the normalization constant. Note that the initial distribution is shifted by the same amount as the number of flips $|\nu|$. If the atom is excited, $P_0(n)$ is shifted towards lower photon numbers and vice versa for a de-excitation.

For a known normalized photon distribution $P = P(n)$, the probability to measure $|\pm\rangle$ becomes

$$\begin{aligned} P(+|P) &= \sum_n |a_+^\infty(n+1)|^2 P(n) \\ P(-|P) &= 1 - P(+|P), \end{aligned} \quad (2.25)$$

where the initial condition is $|a_-(n)|^2 = 1$. Iterating this, one gets the probability $P(\mathbf{k}|P_0)$ to have the sequence \mathbf{k} for an initial distribution $P_0(n)$. Note that the conditional probability $P(\mathbf{k}|P_0)$ is equal to the normalization constant N in equation (2.24).

In the situation of zero detuning and atoms initially in $|-\rangle$ the filter functions are

$$\begin{aligned} |a_+^\infty(n)|^2 &= \sin^2(\sqrt{n}A) \\ |a_-^\infty(n)|^2 &= 1 - |a_+^\infty(n)|^2 = \cos^2(\sqrt{n}A), \end{aligned} \quad (2.26)$$

where

$$A = \int_{-\infty}^{+\infty} g(t') dt'. \quad (2.27)$$

The dynamics will depend on the photon number n and the effective time $g_0 t$. Now suppose that the field is initially in a coherent state

$$P_0(n) = |c_n|^2 = \frac{\bar{n}^n e^{-\bar{n}}}{n!}, \quad (2.28)$$

and we do a conditional measurement on the atom and find it in its lower state, then the photon distribution becomes

$$P_-(n) = \frac{1}{N} \cos^2(\sqrt{n}A) \frac{\bar{n}^n e^{-\bar{n}}}{n!}, \quad (2.29)$$

with N being the normalization constant. An appropriate quantity to investigate in order to get some information about the properties of the field, is the Mandel Q value [28] defined as

$$Q = \frac{\langle n^2 \rangle - \langle n \rangle^2 - \langle n \rangle}{\langle n \rangle}. \quad (2.30)$$

For a Poissonian distribution, the Q -parameter is zero, for a super-Poissonian state it is greater than zero and for a non-classical sub-Poissonian state we have $-1 < Q < 0$.

In figure 1, the Mandel Q value is plotted as a function of the coupling area A for an initial coherent photon distribution with $\bar{n} = 20$. The figure clearly shows how the Q value at first collapses, but then it revive after some value A_r . This phenomena of collapse and revival can be understood from equation (2.29). When evaluating expectation values, we sum $P_-(n)$ over the photon numbers n . For zero coupling area $A = 0$ all terms in the sum are correlated. However, as A is increased the terms will oscillate with different frequencies, arising from \sqrt{n} in the cosine function. The correlation is then washed out leading to the collapse. When the terms come back in phase, we see a revival in Q . This collapse-revival phenomenon is repeated when A is further increased. Note that this is a pure quantum mechanical effect, which derives from the discreteness of the photon number in the cosine function. If n would have been continuous, as in a semi-classical treatment, we would have the collapse, but not the revivals. The collapse-revival phenomenon was first discovered by Eberly *et. al.* [5] and it has also been experimentally verified, see for example [14]. For the first revival we have (see [33])

$$A_r = \pi\sqrt{\bar{n}}. \quad (2.31)$$

So far we have only discussed how the atoms, measuring or not measuring their state, affect the properties of the cavity field. Likewise, the field affects the

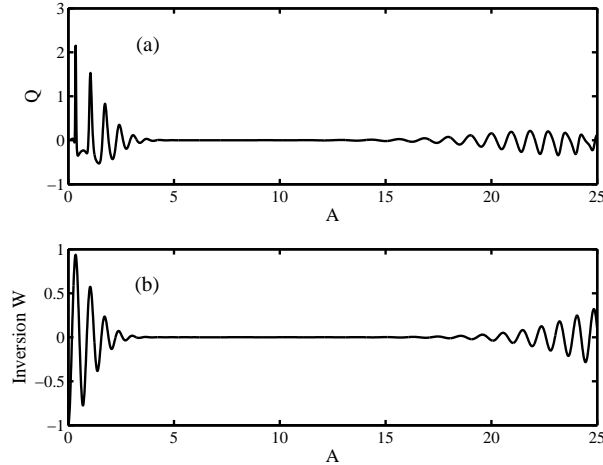


Figure 2.1: In (a) the Mandel Q value, as defined in equation (2.30), is plotted as a function of the coupling area A . The photon distribution, initially in a coherent state with $\bar{n} = 20$, is after the detection of a lower level atom given by (2.29). The quantum mechanical collapse-revival phenomenon is clearly seen. Figure (b) shows how the inversion (2.33) depends on the coupling area A with the same initial photon distribution. The same kind of collapse and revival is present as in (a) for the Mandel Q .

dynamics of the atoms. One quantity of interest, is the atomic inversion

$$\langle \sigma_z \rangle = \sum_{n=0}^{\infty} |c_n|^2 \left[|a_+^\infty(n)|^2 - |a_-^\infty(n)|^2 \right]. \quad (2.32)$$

With the filter functions (2.26) and assuming the initial field to be in a coherent state (2.28), the inversion becomes

$$\langle \sigma_z \rangle = 1 - 2 \sum_{n=0}^{\infty} \cos^2(\sqrt{n}A) \frac{\bar{n}^n e^{-n}}{n!}. \quad (2.33)$$

From the form of equation (2.33), we expect the same collapse-revival occurrence in the atomic inversion as for Q . This is confirmed in figure 2.1 where the inversion (2.33) is plotted for different values of A . The initial average photon number \bar{n} is again chosen to be 20.

If we instead had started out with an atom in its excited state $|+\rangle$, the filter functions (2.26) had been reversed and $\sqrt{n} \rightarrow \sqrt{n+1}$. For the mode initially in

vacuum, the inversion is given by

$$\langle \sigma_z \rangle = 1 - 2 \sin^2(A). \quad (2.34)$$

When A , which is proportional to the effective atom-field interaction time, increases, we note that, even though there are no photons in the cavity, the atom will Rabi flip between $|-\rangle$ and $|+\rangle$. This is the simplest example of an effect due to spontaneous emission.

2.2.3 Unconditional atomic measurement

If we do not select the atomic state after the interaction, we say that we perform a *nonselective* or *unconditional measurement*. The cavity field distribution must then be described as an ensemble average over all possible atomic outcomes

$$\tilde{P}_m(n) = \sum_{\text{All } \mathbf{k}} P(\mathbf{k}|P_0(n)) P_{m,\mathbf{k}}(n) = \sum_{\text{All } \mathbf{k}} A_{m,\mathbf{k}}(n) P_0(n + \nu) = \overline{P_{m,\mathbf{k}}(n)}. \quad (2.35)$$

In the second step, we have used the fact that the normalization constant N equals $P(\mathbf{k}|P_0(n))$ and in the last step $\overline{P_{m,\mathbf{k}}(n)}$ defines the ensemble average over all possible \mathbf{k} :s. Since, in general, there are 2^m different outcomes \mathbf{k} , the calculation of $\tilde{P}_m(n)$ may then be time consuming. Then it is more convenient to consider the density operator ρ^{field} of the field. This is, as discussed above, achieved by tracing the full density operator for the atom-field system over the atomic degrees of freedom

$$\rho^{field} = \text{Tr}_{atom}(\rho) = \sum_{n,n'} c_n c_{n'}^* \left[a_+^\infty(n) a_+^{\infty*}(n') |n-1\rangle \langle n'-1| + a_-^\infty(n) a_-^{\infty*}(n') |n\rangle \langle n' | \right]. \quad (2.36)$$

The diagonal elements $\langle n | \rho^{field} | n \rangle$ now give the ensemble average

$$\tilde{P}_m(n) = |a_+^\infty(n+1)|^2 \tilde{P}_{m-1}(n) + |a_-^\infty(n)|^2 \tilde{P}_{m-1}(n-1), \quad (2.37)$$

where we again have the initial condition $|a_-(n)|^2 = 1$. One special case of equation (2.37) has been investigated in [34].

When calculating expectation values, the order in which we take the averages does not matter

$$\langle \dots \rangle_m = \overline{\langle \dots \rangle_{m,\mathbf{k}}}. \quad (2.38)$$

Here $\langle \dots \rangle_m$ is the expectation value with respect to the distribution $\tilde{P}_m(n)$ and $\langle \dots \rangle_{m,\mathbf{k}}$ the same for the distribution $P_{m,\mathbf{k}}(n)$.

Chapter 3

Extended Jaynes-Cummings models

As the JC-model is the simplest non-trivial representation of two non-identical coupled systems, it has led to be experimentally verified due to its low number of degrees of freedom. With increasing progress in existing experimental techniques, extensions of the JC-model have become interesting. There is a huge number of different theoretical proposals, for example; [35, 36, 37, 38, 39]. Experimental works can be found in [40]. In this chapter we present some extended JC-models, while in the next we talk about their implementations. Writing down the extended Hamiltonian is often a straightforward task, but nevertheless the dynamics of the full system may be involved and complicated.

3.1 Multi-level Jaynes-Cummings models

A recent review of multi-level JC-models can be found in [41]. The model is either modified by coupling more electronic levels of the atom, more modes of the field or both of them. The bare energies of the field and atom is simply $\sum_i \hbar\omega_i a_i^\dagger a_i$ and $\sum_j \hbar\Omega_j |j\rangle\langle j|$ respectively, where subscripts i is for mode i and j for atomic internal state j . The specific form of the atom-field coupling terms are determined from atomic selection rules giving non-zero dipole elements. Since we throughout deal with dipole couplings, the coupling will only contain one-photon processes of the form $g(a^\dagger |j-1\rangle\langle j| + a|j\rangle\langle j-1|)$. However, below we will discuss effective models where levels that are hardly populated due to a large detuning can be eliminated, leading to multi-photon processes.

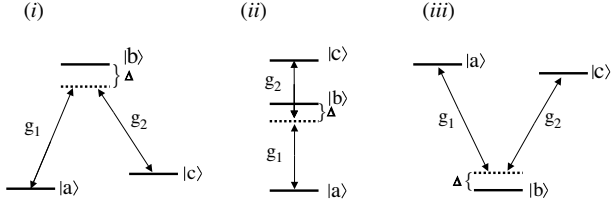
Λ -atom with two different modes


Figure 3.1: The three possible three-level atoms coupled to two modes 1 and 2. In all plots, the mode frequencies ω_1 and ω_2 are such that there is only one interesting detuning parameter Δ . The atomic configurations are called Λ (i), Ξ (ii) and V (iii).

One model that is of particular interest is a Λ -type of atom interacting with two cavity modes, as in figure 3.1 which shows the different 2-mode-3-level atoms. The Hamiltonian, in the rotating wave approximation, takes the form ($\hbar = 1$)

$$\begin{aligned} \tilde{H}_\Lambda &= \omega_1 a_1^\dagger a_1 + \omega_2 a_2^\dagger a_2 + \Omega_a |a\rangle\langle a| + \Omega_b |b\rangle\langle b| + \Omega_c |c\rangle\langle c| \\ &\quad + g_{ab} (a_1^\dagger |b\rangle\langle c| + a_1 |b\rangle\langle a|) + g_{bc} (a_2^\dagger |c\rangle\langle b| + a_2 |b\rangle\langle c|). \end{aligned} \quad (3.1)$$

The dynamics of this Hamiltonian has been studied in [42], using a unitary transformation. The solutions are rather complicated and one is interested in finding limiting approximations. The most common one is, as mentioned above, adiabatic elimination of far-off resonance levels that are weakly populated. The adiabatic methods are discussed in Appendix A, but the general idea of adiabatic elimination is to write down the Heisenberg equations of motion, and for those levels that are weakly populated, their derivatives are assumed zero before integrating the equations. This gives effective models and Hamiltonians. Due to the off resonance interaction, the effective models contain Stark shift terms proportional to the photon numbers $a_1^\dagger a_1$ and $a_2^\dagger a_2$, which are often neglected in the analyses. Defining the detunings as $\Omega_b - \Omega_a = \Delta_1 + \omega_1$ and $\Omega_b - \Omega_c = \Delta_2 + \omega_2$, we assume for the Λ -system the couplings of the upper level to be far-off resonance $|\Omega_a - \Omega_c| \ll |\Delta_1|, |\Delta_2|$ and that $\Delta = |\Delta_1 - \Delta_2| \ll |\Delta_1|, |\Delta_2|$. Then the upper level $|b\rangle$ can be eliminated and the atom acquires a two-level structure, coupled to the two modes [43, 44]:

$$H_\Lambda = \frac{\Delta}{2} \sigma_z + g_0 (a_1 a_2^\dagger \sigma^+ + a_1^\dagger a_2 \sigma^-), \quad (3.2)$$

where the Pauli matrixes act on the atomic states $|a\rangle$ and $|c\rangle$,

$$g_0 = \frac{g_{13}g_{23}}{\Delta}, \quad (3.3)$$

and we have transformed to an interaction picture; subtracting the proper term proportional to the constant of motion $N = a_1^\dagger a_1 + a_2^\dagger a_2 + \frac{1}{2}\sigma_z$. Here the Stark shift terms have been left out [43, 44]. The effective Hamiltonian governs a two-photon process, while keeping the total number of photons constant. In the bare basis that Hamiltonian is of Block form with 2×2 -blocks as the regular JC-model (2.12), with the Rabi frequency $g\sqrt{n(m+1)}$, where n and m are the photon numbers for mode 1 and 2 respectively. Thus, the solutions have the same form as for the standard JC-model replacing $g_0\sqrt{n}$ by $g_0\sqrt{n(m+1)}$. The combined system, two field modes plus the atom, shows examples of multistate entanglement. In the next chapter we will show how this model can be used for various applications like quantum information processing and state preparation. Note that if just one mode couples the two different transitions; $a_1 \rightarrow a_1$ and $a_2 \rightarrow a_1$, the Rabi frequency is proportional to n rather than \sqrt{n} , which has important consequences in for example the preparation of field Schrödinger cat states, see next chapter, and for the revivals, see equation (2.29).

Two-level atom with two identical modes

The second multi-level model we present is with one two-level atom interacting with two identical modes; having the same frequencies and polarization, [39]

$$\tilde{H}_{2m} = \omega a_1^\dagger a_1 + \omega a_2^\dagger a_2 + \frac{\Omega}{2}\sigma_z + g_1(a_1^\dagger \sigma^- + a_1 \sigma^+) + g_2(a_2^\dagger \sigma^- + a_2 \sigma^+). \quad (3.4)$$

By introducing the new Boson operators

$$A = K_{12}(g_2 a_1 - g_1 a_2), \quad B = K_{12}(g_1 a_1 + g_2 a_2), \quad (3.5)$$

where $K_{12} = (g_1^2 + g_2^2)^{-1/2}$, and going to the interaction picture with respect to number of excitations, the Hamiltonian can be written as

$$H_{2m} = \frac{\Delta}{2}\sigma_z + K_{12}^{-1}(B\sigma^+ + B^\dagger\sigma^-). \quad (3.6)$$

This transformation of the Hamiltonian is used in both Paper V and VIII. Thus, the solutions are again given by the solutions of the ordinary JC-model, where the number states are no longer the one mode states $|n\rangle$, but the two mode number states $|j\rangle = \frac{(B^\dagger)^j}{\sqrt{j!}}|0,0\rangle$.

Two identical two-level atoms and one mode

By adding an extra identical atom to the JC model one gets the Hamiltonian

$$H_{2a} = \Delta a^\dagger a + g [a^\dagger (\sigma_1^- + \sigma_2^-) + a (\sigma_1^+ + \sigma_2^+)], \quad (3.7)$$

where we have used that the number of excitations $N = a^\dagger a + \frac{1}{2}\sigma_{1z} + \frac{1}{2}\sigma_{2z}$ is conserved. The JC model with several atoms is sometimes referred to as *Travis-Cummings* or *Dicke model* [28]. With the four bare states $\{|n-1, +, -\rangle, |n, -, -\rangle, |n-1, -, +\rangle, |n-2, +, +\rangle\}$ the matrix representation of (3.7) is

$$H_{2a} = \begin{bmatrix} (n-1)\Delta & g\sqrt{n} & 0 & g\sqrt{n-2} \\ g\sqrt{n} & n\Delta & g\sqrt{n} & 0 \\ 0 & g\sqrt{n} & (n-1)\Delta & g\sqrt{n-1} \\ g\sqrt{n-2} & 0 & g\sqrt{n-1} & (n-2)\Delta \end{bmatrix}. \quad (3.8)$$

Let us give a last comment on similarities between the three models discussed in this section. If we consider the situation of lowest non-trivial excitations in the three models, we find that the three states $\{|1, 0\rangle|a\rangle, |0, 1\rangle|c\rangle, |0, 0\rangle|b\rangle\}$, where the last ket corresponds to the atomic state, are coupled by the Hamiltonian (3.1). In this basis the Hamiltonian is given by

$$\tilde{H}_\Lambda = \begin{bmatrix} \omega_1 + \Omega_1 & g_{13} & 0 \\ g_{13} & \Omega_3 & g_{23} \\ 0 & g_{23} & \omega_2 + \Omega_2 \end{bmatrix}. \quad (3.9)$$

For the second model the states $\{|1, 0, -\rangle, |0, 0, +\rangle, |0, 1, -\rangle\}$ are coupled by \tilde{H}_{2m} in equation (3.4), giving the matrix representation

$$\tilde{H}_{2m} = \begin{bmatrix} \omega - \frac{\Omega}{2} & g_1 & 0 \\ g_1 & \frac{\Omega}{2} & g_2 \\ 0 & g_2 & \omega - \frac{\Omega}{2} \end{bmatrix}. \quad (3.10)$$

And finally if $n = 1$ in the last model the fourth row and column of (3.8) goes away and if $\omega_1 + \Omega_1 = \omega_2 + \Omega_2$, the three matrices have identical form and show the same kind of dynamical features.

3.2 Time dependent Jaynes-Cummings models

The original JC-model and the extended examples in the previous section all assumed constant parameters, couplings and detunings, throughout the interaction, giving the time evolution

$$|\Psi(t)\rangle = e^{-iHt}|\Psi(t=0)\rangle. \quad (3.11)$$

However, this situation is only fulfilled when the atom is trapped at a specific location along the mode variations and therefor lacks center-of-mass motion. Most correct is to add the atomic motional term to the Hamiltonian together with the electric field variations of the particular mode, which is done in the next section. It is, however, in many experimental situations a good approximation to replace the momentum operator term by the classical momentum $p = mv$ and the position by $x = vt$, where $mv = p_0 = \langle p \rangle_{t=0}$. Since the kinetic energy term is substituted with a c -number, it means that p should approximately be a constant of motion, or the changes of p should be small compared to the variations of the internal interaction energy across the atomic wave-packet. Thus, if $\dot{p} \sim p/T$, for some characteristic time-scale T , is to be small, the time-scale is long, indicating some kind of adiabaticity. Going to a rotating frame $\exp(-ip_0^2/2m)H\exp(ip_0^2/2m)$, the Schrödinger equation for the JC-model becomes

$$i\frac{\partial}{\partial t}|\Psi(t)\rangle = H(t)|\Psi(t)\rangle, \quad (3.12)$$

and for a specific excitation number within one 2×2 block

$$i\frac{\partial}{\partial t} \begin{bmatrix} a_+(n, t) \\ a_-(n, t) \end{bmatrix} = \begin{bmatrix} \frac{\Delta}{2} & g\sqrt{n} \\ g\sqrt{n} & -\frac{\Delta}{2} \end{bmatrix} \begin{bmatrix} a_+(n, t) \\ a_-(n, t) \end{bmatrix}, \quad (3.13)$$

where Δ and g may be time-dependent. Any two-level system evolving by a hermitian 2×2 -Hamiltonian can always be transformed into the form of equation (3.13) [31]. Consequently, the differential equation of (3.13) has been of interest for physicists and mathematical physicists in a variety of different areas for a long time. In spite of its simple form, not many analytically solvable models exist. Usually the asymptotic solutions at $t = \infty$ are obtained, given some initial conditions at $t = -\infty$. We will most of the time pick $|a_-^0(n)| = 1$ as initial condition. The solution can be expressed in terms of a scattering matrix \mathcal{S} connecting initial and final amplitudes

$$\begin{bmatrix} a_+^\infty(n) \\ a_-^\infty(n) \end{bmatrix} = \begin{bmatrix} \sqrt{w_n} & e^{-i\phi_n}\sqrt{1-w_n} \\ -e^{i\phi_n}\sqrt{1-w_n} & \sqrt{w_n} \end{bmatrix} \begin{bmatrix} a_+^0(n) \\ a_-^0(n) \end{bmatrix}. \quad (3.14)$$

In table 2 some of the solvable models are presented and their specific dependence on time. These are the models that have been used in papers I-III, VI and VII, for other models see for example [45, 46, 47, 48]. Some of their solutions will be given later on, but as we will see in the next subsection, when being in the adiabatic regime the solutions become particularly simple.

| Model | $\Delta(t)/2$ | $g(t)\sqrt{n}$ |
|----------------------------|----------------------------|--|
| Zero detuning Paper II | $\Delta(t) \equiv 0$ | any $g(t)$ |
| Landau-Zener (LZ) [49, 50] | $\Delta_0 t$ | $g_0\sqrt{n}$ |
| Rosen-Zener (RZ) [51] | Δ_0 | $g_0\sqrt{n} \operatorname{sech}(t/T)$ |
| Demkov-Kunike 1 (DK1) [52] | $\bar{E} + E_0 \tanh(t/T)$ | $g_0\sqrt{n}$ |
| Demkov-Kunike 2 (DK2) [52] | $\bar{E} + E_0 \tanh(t/T)$ | $g_0\sqrt{n} \operatorname{sech}(t/T)$ |

Table 2. Parameter time-dependence for various analytically solvable 2×2 models. Note that for $E_0 = 0$ in the DK2 model one retains the RZ model.

3.2.1 Adiabatic evolution with level crossings

The adiabatic theorem states that if the rate of change in time of some time-dependent Hamiltonian becomes infinitely slow, an eigenstate of the initial Hamiltonian will remain in the corresponding eigenstate throughout the evolution. Thus, suppose $H(t)$ is given and $E_n(t)$ and $|\psi_n(t)\rangle$ are instantaneous eigenvalues and eigenstates of $H(t)$, then the theorem implies that $H(t)|\psi_n(t)\rangle = E_n(t)|\psi_n(t)\rangle$ is fulfilled for all t and any n . A more thorough discussion about the theorem and adiabaticity is given in Appendix A. The eigenstates of the JC-model were given in equations (2.13) and (2.14), and the eigenvalues in (2.15). The diagonal elements, the *bare eigenvalues* for $g_0 = 0$ become degenerate when $\Delta = 0$, and we say that the two energy levels cross. For non-zero coupling, $g_0 \neq 0$, the degeneracy is split and the energy levels $E_{1,2}(t)$ no longer cross, the crossing is *avoided*. The eigenstates (2.13) are called *dressed states*, while the states $|+, n-1\rangle$ and $|-, n\rangle$ are referred to as *bare states*. The bare and dressed states are only the same in the absence of coupling, or more precisely if $g/\Delta \rightarrow 0$, from which we conclude that the asymptotic initial and final bare and dressed states of the LZ, RZ and DK 2 models coincide.

According to the adiabatic theorem, we have $\langle\psi_1|\psi_2\rangle = 0$ for an infinitely slow change of the Hamiltonian. Assuming that the levels cross and that $g/\Delta \rightarrow 0$ in the asymptotic limits, a state initially in $|\psi_i\rangle = |+, n-1\rangle$ will adiabatically be transferred into the final state $|\psi_f\rangle = |-, n\rangle$. This is schematically shown in figure 3.2 which displays the eigenvalues $E_{1,2}(t)$ of the LZ and the DK 2 models for three different coupling strengths.

For models with no level crossings and $g/\Delta \rightarrow 0$, for example the RZ model and the DK 2 model with $\bar{E} > E_0$, the adiabatic evolution will result in no transitions between bare states.

3.2.2 STIRAP evolution in cavities

Stimulated Raman adiabatic passage, or shortly *STIRAP*, is a method for adiabatically transferring population from an initial state into a target state by virtually

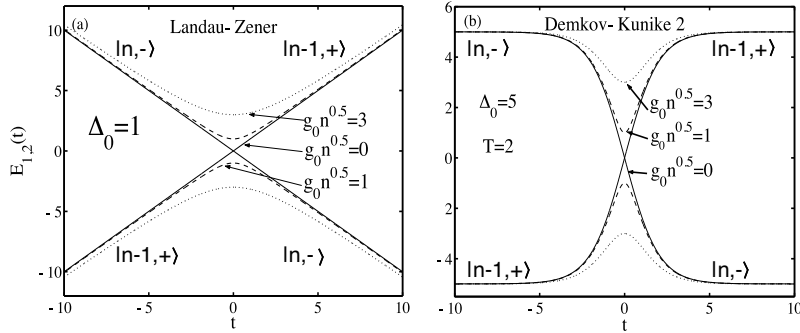


Figure 3.2: This figure shows the instantaneous time-dependent eigenvalues $E_{\pm}(t)$ of equation (2.15) for the LZ- (a) and the DK2 models (b). Three different examples are shown $g_0\sqrt{n} = 0, 1, 3$. In the figures are also inserted the corresponding bare states.

populating an intermediate state [24, 25]. It was first suggested for coherent population transfer between molecular levels. The scheme relies on letting the initial and target states couple through two laser-pulses to the intermediate level. The interesting point is that the two pulses occur in a counterintuitive order; first the empty target state is coupled to the intermediate state and then the initial, populated state is coupled to the middle state. However, in order to have any transfer the two pulses must overlap in time. Usually the shape of the pulses are taken to be Gaussian. The problem with Gaussian separated pulses is that they are not analytically solvable, but assuming a smooth change we may use the adiabatic theorem.

In the original model, a Λ -type of three level system is used and the lower states $|a\rangle$ and $|c\rangle$ are coupled by two laser pulses to the upper intermediate level $|b\rangle$. The Hamiltonian is given, in matrix representation, by

$$H_R = \begin{bmatrix} 0 & G_1(t) & 0 \\ G_1(t) & \Delta & G_2(t) \\ 0 & G_2(t) & 0 \end{bmatrix}, \quad (3.15)$$

where Δ is the detuning of the $|a\rangle \leftrightarrow |b\rangle$ and $|c\rangle \leftrightarrow |b\rangle$ -transitions. The form of (3.15) is identical to those of (3.9) and (3.10) apart from an overall constant term, suggesting that a STIRAP process may be realized also for those two cavity models. The pulses are then governed by the mode shape that the atom 'sees' as

it traverses two cavities. This is not an unrealistic situation, since for open Fabry-Perot cavities the transverse mode shape is very close to Gaussian, and for atoms with classical momentum we can transform the problem into a time-dependent one. The condition of overlapping pulses implies that the two cavities must also overlap in space.

The unitary matrix

$$U(t) = \begin{bmatrix} \sin \phi \sin \theta & \cos \theta & \cos \phi \sin \theta \\ \cos \phi & 0 & -\sin \phi \\ \sin \phi \cos \theta & -\sin \theta & \cos \phi \cos \theta \end{bmatrix} \quad (3.16)$$

with the angels $\tan \theta = G_1(t)/G_2(t)$ and $\tan 2\phi = 2G_0(t)/\Delta$, where $G_0^2 = G_1^2(t) + G_2^2(t)$ digonalizes H_R . The corresponding eigenvalues are

$$\begin{aligned} E_+(t) &= \frac{1}{2} \left(\Delta + \sqrt{\Delta^2 + 4G_0^2} \right) \\ E_0(t) &= 0 \\ E_-(t) &= \frac{1}{2} \left(\Delta - \sqrt{\Delta^2 + 4G_0^2} \right). \end{aligned} \quad (3.17)$$

The eigenvector $|\psi_0\rangle = \cos \theta |a\rangle - \sin \theta |c\rangle$ corresponding to the zero eigenvalue is called *dark state*, since it does not contain the upper $|b\rangle$ -state and therefore losses of the excited level are minimized. Choosing

$$\begin{aligned} \lim_{t \rightarrow -\infty} \frac{G_1(t)}{G_2(t)} &= 0, \quad \theta \rightarrow 0, \\ \lim_{t \rightarrow +\infty} \frac{G_2(t)}{G_1(t)} &= 0, \quad \theta \rightarrow \frac{\pi}{2} \end{aligned} \quad (3.18)$$

the dark state $|\psi_0\rangle$ evolves from $|a\rangle$ into $|c\rangle$, which is the idea behind STIRAP. With the given pulse sequence (3.18), the asymptotic unitary matrix (3.16) becomes

$$\begin{aligned} U(-\infty)_{\Delta=0} &= \begin{bmatrix} 0 & 1 & 0 \\ \frac{1}{\sqrt{2}} & 0 & -\frac{1}{\sqrt{2}} \\ \frac{1}{\sqrt{2}} & 0 & \frac{1}{\sqrt{2}} \end{bmatrix}, & U(+\infty)_{\Delta=0} &= \begin{bmatrix} \frac{1}{\sqrt{2}} & 0 & \frac{1}{\sqrt{2}} \\ \frac{1}{\sqrt{2}} & 0 & -\frac{1}{\sqrt{2}} \\ 0 & -1 & 0 \end{bmatrix}, \\ U(-\infty)_{\Delta \neq 0} &= \begin{bmatrix} 0 & 1 & 0 \\ 1 & 0 & 0 \\ 0 & 0 & 1 \end{bmatrix}, & U(+\infty)_{\Delta \neq 0} &= \begin{bmatrix} 0 & 0 & 1 \\ 1 & 0 & 0 \\ 0 & -1 & 0 \end{bmatrix}. \end{aligned} \quad (3.19)$$

Since the Hamiltonians (3.15) and (3.10) have the same form, the above arguments apply for both models, identifying the various terms. However, for the two-level atom two mode model of the previous section the adiabatic transition works for any photon numbers, not only the one photon case of the Hamiltonian (3.10) [53]. This is easily seen using the new boson operators (3.5). Since A and B commute, it follows that $[A, H] = 0$, and the states $|\psi_n\rangle = \frac{(A^\dagger)^n}{\sqrt{n!}}|0, 0, -\rangle$ are eigenstates to H_{2m} with eigenvalue zero; $H_{2m}|\psi_n\rangle = 0|\psi_n\rangle$. With the pulse sequence (3.18) it follows

$$A^\dagger = \begin{cases} a_2^\dagger, & t = -\infty \\ -a_1^\dagger, & t = +\infty \end{cases} \Rightarrow |\psi_n\rangle = \begin{cases} |0, n, -\rangle, & t = -\infty \\ (-1)^n |n, 0, -\rangle, & t = +\infty \end{cases}. \quad (3.20)$$

Thus, any Fock state $|n\rangle$ is adiabatically transferred from cavity 2 to cavity 1, from which it follows that any state can be transported between the cavities. For example, for a coherent state it means $|\alpha, 0, -\rangle \rightarrow |0, -\alpha, -\rangle$. The method is actually equivalent with multi-level STIRAP processes [54]. Note that the state $|\psi_n\rangle$ is a dark state, never populating the upper atomic state $|+\rangle$

3.3 The Jaynes-Cummings model with quantized motion

In most experimental realizations, the kinetic energy of the atoms greatly exceeds the interaction energy, implying a semi-classical treatment of the evolution; the kinetic energy term is not considered and the position is treated as time-dependent. However, by the use of laser cooling of the atomic motion, ultracold atoms can be prepared corresponding to temperatures of the order of $1 \mu\text{K}$. These energies are comparable with the interaction energies of cavity QED experiments and it is no longer legitimate to exclude the kinetic energy term from the Hamiltonian. In this section we discuss the theory of the JC model when the atomic motion is treated quantum mechanically and the shape of the mode appears in an x -dependent coupling.

The Schrödinger equation for a given excitation number n reads

$$\left\{ p^2 + \begin{bmatrix} \frac{\Delta}{2} & g(x)\sqrt{n} \\ g(x)\sqrt{n} & -\frac{\Delta}{2} \end{bmatrix} \right\} |\phi_\Sigma\rangle = E_\Sigma |\phi_\Sigma\rangle, \quad (3.21)$$

where Σ is the set of quantum numbers describing the eigenstate and we here use scaled parameters; $m = 1/2$ and $\hbar = 1$, see subsection 3.3.2.

3.3.1 Pulse-shaped atom-field coupling

As the atom traverses the cavity perpendicular to a longitudinal mode of a Fabry-Perot cavity the coupling will have a Gaussian shape. This problem is, however, not analytically solvable and we will therefore focus on a few other solvable situations with pulse shaped couplings.

The first, non-physical, case is to have a Mesa function shaped coupling

$$g(x) = \begin{cases} g_0, & 0 < x < L \\ 0, & \text{elsewhere} \end{cases}, \quad (3.22)$$

which has been studied in numerous papers [55, 56, 57, 58]. The first two refs. only consider the zero detuning case, while the last two treat the general situation. For the models of those papers, we will only analyze the zero detuning case here. In the literature this model has been called *mazer*, for "microwave amplification via z -motion-induced emission of radiation" (note here that we have x as the axis of propagation, not z). By working in the internal dressed state basis $\{|\psi_{\pm}\rangle = \frac{1}{\sqrt{2}}(|n-1,+\rangle \pm |n,-\rangle)\}$, the problems become those of a particle scattered against a potential barrier or well. The $|\psi_+\rangle$ -state sees the barrier, while $|\psi_-\rangle$ sees the well. There are four different scattering amplitudes, when expressed in bare states; transmission of the atom in excited or ground states, $T_{n-1,+}$ and $T_{n,-}$, and correspondingly for the reflections, $R_{n-1,+}$ and $R_{n,-}$. These are related to the scattering amplitudes ρ_n^{\pm} and τ_n^{\pm} for the internal dressed states according to

$$\begin{aligned} R_{n-1,+} &= \frac{1}{2}(\rho_n^+ + \rho_n^-), & T_{n-1,+} &= \frac{1}{2}(\tau_n^+ + \tau_n^-), \\ R_{n,-} &= \frac{1}{2}(\rho_n^+ - \rho_n^-), & T_{n,-} &= \frac{1}{2}(\tau_n^+ - \tau_n^-). \end{aligned} \quad (3.23)$$

Using dressed states decouples the equations in (3.21) into two 1-dimensional Schrödinger equations, which are solved to give the amplitudes ρ_n^{\pm} and τ_n^{\pm} . Starting with an excited atom, the solutions are [55]

$$\begin{aligned} \rho_n^{\pm} &= i\Delta_n^{\pm} \sin(k_n^{\pm}L), \\ \tau_n^{\pm} &= [\cos(k_n^{\pm}L) - i\Sigma_n^{\pm} \sin(k_n^{\pm}L)]^{-1}, \end{aligned} \quad (3.24)$$

with

$$\begin{aligned} k_n^\pm &= (k \mp \kappa_n^2)^{1/2}, \\ \Delta_n^\pm &= \frac{1}{2} \left(\frac{k_n^\pm}{k} - \frac{k}{k_n^\pm} \right), \\ \Sigma_n^\pm &= \frac{1}{2} \left(\frac{k_n^\pm}{k} + \frac{k}{k_n^\pm} \right), \\ \kappa_n &= \sqrt[4]{g_0^2(n+1)}. \end{aligned} \tag{3.25}$$

One quantity of interest is the atomic inversion defined as the expectation value $\langle \sigma_z \rangle$ (2.32), which is

$$\langle \sigma_z \rangle = 1 - 2P_{\text{emission}}(n), \quad P_{\text{emission}}(n) = |T_{n,-}|^2 + |R_{n,-}|^2. \tag{3.26}$$

For slow atoms, $k \ll \kappa_n$, the inversion has resonances at $\kappa_n L = m\pi$ ($m = 1, 2, 3, \dots$) when the cavity contains exactly n photons. These tunneling resonances occur when the atomic momentum corresponds to a deBroglie wavelength $\lambda_{dB} = 2L/m$.

A more physical solvable example of smooth pulse-shaped atom-field coupling is the zero detuning case with

$$g(x) = \operatorname{sech}^2 \left(\frac{x}{L} \right). \tag{3.27}$$

The solutions are [55]

$$\begin{aligned} \rho_n^\pm &= \frac{\Gamma(iKL)\Gamma(1-iKL)}{\Gamma(1/2+i\xi_n^\pm)\Gamma(1/2-i\xi_n^\pm)}, \\ \tau_n^\pm &= \frac{\Gamma[1/2-i(kL+\xi_n^\pm)]\Gamma[1/2-i(kL-\xi_n^\pm)]}{\Gamma(-ikL)\Gamma(1-ikL)}, \end{aligned} \tag{3.28}$$

where

$$\xi_n^\pm = \sqrt{\pm(\kappa_n L)^2 - 1/4}. \tag{3.29}$$

The atomic inversion again shows resonances, now for $\kappa_n L = \sqrt{m(m+1)}$ ($m = 1, 2, 3, \dots$). The resonances die out for large values $\kappa_n L$, and the faster the atoms the slower is the decay of the resonances. This indicates that the more adiabatic the process is, the less pronounced resonances. The asymptotic value of the inversion is zero, meaning that half the population is in the upper and half in the lower atomic state. In [58] a numerical simulation of a Gaussian mode shape is done, and as was also found in Paper II, the Gaussian mode profile shows less adiabatic features than the sech-pulse, due to the wide tails of the hyperbolic secant.

We end this subsection by presenting the solution of a third solvable model for general detunings. We let

$$\begin{aligned} g_0(x) &= \delta(x) \\ \Delta(x) &= \Delta_0 \end{aligned} \tag{3.30}$$

and by imposing the standard boundary conditions we get the solution for the transmission and reflection coefficients

$$\begin{aligned} R_{n-1,+} &= \tilde{k} \left| \frac{g_0^2 n}{g_0^2 n - 4\tilde{k}\tilde{k}'} \right|^2, & T_{n-1,+} &= \tilde{k} \left| \frac{4/\tilde{k}\tilde{k}'}{g_0^2 n + 4\tilde{k}\tilde{k}'} \right|^2, \\ R_{n,-} &= \tilde{k}' \left| \frac{g_0 \sqrt{n}/\tilde{k}}{g_0^2 n - 4\tilde{k}\tilde{k}'} \right|^2, & T_{n,-} &= \tilde{k}' \left| \frac{g_0 \sqrt{n}/\tilde{k}}{g_0^2 n + 4\tilde{k}\tilde{k}'} \right|^2, \end{aligned} \tag{3.31}$$

where $\tilde{k} = \sqrt{k^2 - \Delta/2}$ and $\tilde{k}' = \sqrt{k^2 + \Delta/2}$.

3.3.2 Periodic atom-field coupling

A Gaussian mode shape is obtained by a transverse passage of the atom through the cavity. If the atom, instead, propagates along the longitudinal mode shape, the coupling becomes $g(x) = g_0 \cos(qx)$, where $q = 2\pi/\lambda$ and λ is the photon wavelength. The JC model with such a coupling has been studied in several papers [37, 38]. Having a cavity length $L \gg \lambda$ the Hamiltonian is nearly periodic, the boundary effects should be small for an atom far from the edges of the cavity. Thus, the Hamiltonian is to a good approximation periodic, and from Bloch theory it is well known that an eigenstate/eigenvalue is described by two quantum numbers; $\nu = 1, 2, 3, \dots$ is called the *band index* and $-q < k < q$ is the *quasi momentum*. The range $[-q, q]$ defines the *Brillouin zone*. Some authors defines the Brillouin zone half the size, which implies that the set of eigenstates is disconnected into two parts [38]. From $2\cos(qx)|k\rangle = |k+q\rangle + |k-q\rangle$ it follows that the coupling of this form results not only a flip of internal atomic state, but also a momentum 'kick' in either direction. As already mentioned in the previous chapter, for zero detuning we may decouple the two equations leading to two one-dimensional Schrödinger equations with potentials $V(x) \propto \pm \cos(qx)$. These are the Mathieu equations [59], whose properties are well known. In the opposite limit, $g(x)/\Delta \rightarrow 0$, one may also decouple the equations by adiabatically eliminating the level that is initially unpopulated, giving one effective Schrödinger equation with potential $V(x) \propto \frac{g^2(x)}{\Delta} = \frac{1}{2}[1 + \cos(2qx)]$ also in Mathieu form. Note that the constant term represents a two photon process where the kicks have opposite directions, while $\cos(2qx)$ describes the situations when the kicks are in the same directions.

With scaled units, where the photon recoil energy $E_R = \hbar^2 q^2 / 2m$ sets an energy scale, the Hamiltonian is written as

$$H = -\frac{\partial^2}{\partial x^2} + \begin{bmatrix} \frac{\delta}{2} & V_0 \cos(x) \\ V_0 \cos(x) & -\frac{\delta}{2} \end{bmatrix}, \quad (3.32)$$

with

$$\begin{aligned} x &= q\tilde{x} & p &= \frac{\tilde{p}}{q} & t &= \tilde{t} \frac{E_R}{\hbar} \\ E &= \frac{\tilde{E}}{E_R} & V_0 &= \frac{2\tilde{g}_0\sqrt{n}}{E_R} & \delta &= \frac{\tilde{\Delta}}{E_R}, \end{aligned} \quad (3.33)$$

where the tilde \sim indicates unscaled quantities. The bare states coupled for a given initial momentum $p = k$ and internal state $|-\rangle_n \equiv |n, -\rangle$, are

$$|\psi_\mu(k)\rangle = \begin{cases} |k + \mu\rangle|-\rangle_n & \mu \text{ even} \\ |k + \mu\rangle|+\rangle_n & \mu \text{ odd,} \end{cases} \quad (3.34)$$

The momentum of a bare state $|\psi_\mu\rangle$ is $k + \mu$ and the set with even/odd flipped gives the orthogonal states with initial internal state $|+\rangle_n = |n - 1, +\rangle$. One may introduce the matrix $c_\nu^\mu(k)$ connecting dressed states, $H|\phi_\nu(k)\rangle = E_\nu|\phi_\nu(k)\rangle$, and bare states

$$\begin{aligned} |\phi_\nu(k)\rangle &= \sum_\mu c_\nu^\mu(k)|\psi_\mu(k)\rangle \\ |\psi_\mu(k)\rangle &= \sum_\nu c_\mu^\nu(k)|\phi_\nu(k)\rangle. \end{aligned} \quad (3.35)$$

The coefficients are solved from the Schrödinger equation written in matrix form with the bare states as basis. The Hamiltonian (3.32) is given by

$$\left[\begin{array}{cccccc} \ddots & \vdots & \vdots & \vdots & \vdots & \vdots \\ \dots & (k-2)^2 - \frac{\delta}{2} & \frac{V_0}{2} & 0 & 0 & 0 & \dots \\ \dots & \frac{V_0}{2} & (k-1)^2 + \frac{\delta}{2} & \frac{V_0}{2} & 0 & 0 & \dots \\ \dots & 0 & \frac{V_0}{2} & k^2 - \frac{\delta}{2} & \frac{V_0}{2} & 0 & \dots \\ \dots & 0 & 0 & \frac{V_0}{2} & (k+1)^2 + \frac{\delta}{2} & \frac{V_0}{2} & \dots \\ \dots & 0 & 0 & 0 & \frac{V_0}{2} & (k+2)^2 - \frac{\delta}{2} & \dots \\ \vdots & \vdots & \vdots & \vdots & \vdots & \vdots & \ddots \end{array} \right]. \quad (3.36)$$

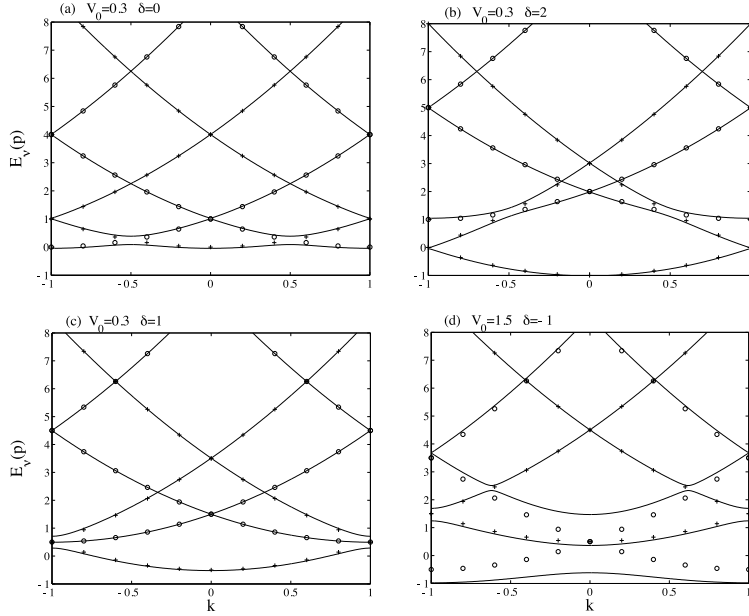


Figure 3.3: The lowest energy bands for different sets of parameters. Circles show the bare energy curves for excited atomic states $|+\rangle_n$ while plusses give the same for the $|-\rangle_n$ states. Note that when the coupling becomes large (d), the bare and dressed energy curves differ considerable for the lowest bands.

In order to numerically solve for the coefficients and the eigenvalues the matrix has to be truncated at some dimension, which has been discussed in Paper VI. An expression for the eigenvalues may be obtained in the form of a continued fraction as in equation (14) of paper VI. The eigenvalues $E_\nu(k)$ connecting energy and quasi momentum is often referred to as *dispersion curves* and their shapes influence the behaviour of Gaussian states evolving by the Hamiltonian (3.32). In order to see this we define Gaussian dressed and bare states. Let $\varphi_\nu(k)$ be a normalized Gaussian centered around some quasi momentum k_0 within the first Brillouin zone, then the *Gaussian dressed state* is

$$|\Phi_\nu\rangle = \int_{-1}^1 dk \varphi_\nu(k) |\phi_\nu(k)\rangle. \quad (3.37)$$

A *Gaussian bare state* is simply a bare state modulated by a normalized gaussian

distribution $\chi(p)$;

$$|\Psi\rangle = \int dp \chi(p) |p\rangle |-\rangle = \sum_{\mu} \int_{-1}^1 dk \chi(k + \mu) |\psi_{\mu}(k)\rangle. \quad (3.38)$$

The two distributions are related through $\chi(k) = \varphi_{\nu}(k - \mu) c_{\nu}^{\mu}(k - \mu)$. If one of the coefficients $c_{\nu}^{\mu}(k)$ clearly dominates for all k , it means that the Gaussian bare and dressed states are very similar, has a large overlap. The time evolution of a Gaussian dressed state is

$$|\Phi_{\nu}(t)\rangle = \int_{-1}^1 dk \varphi_{\nu}(k) e^{-iE_{\nu}(k)t} |\phi_{\nu}(k)\rangle. \quad (3.39)$$

Assuming the width Δ_k^2 of $\varphi_{\nu}(k)$ to be narrow compared to the Brillouin zone and consequently the variation of $E_{\nu}(k)$ we may expand the dispersion curve around k_0

$$\begin{aligned} E_{\nu}(k) &\approx E(k_0) + v_g(k_0)(k - k_0) + \frac{1}{2} \frac{1}{m^*(k_0)} (k - k_0)^2 \\ &= E_0 + \frac{1}{2m_0(k_0)} k_0^2 + \frac{1}{m_1(k_0)} k_0 (k - k_0) + \frac{1}{2m_2(k_0)} (k - k_0)^2, \end{aligned} \quad (3.40)$$

Using this approximation one may derive the evolution of a Gaussian dressed state in the x -representation (see paper VI)

$$|\Phi_{\nu}(t)\rangle = \frac{1}{\sqrt[4]{2\pi \left(\frac{1}{2\Delta_k} + \frac{i\Delta_k t}{m_2} \right)^2}} \exp \left[-\frac{(x - v_g t)^2}{4 \left(\frac{1}{4\Delta_k^2} + \frac{it}{2m_2} \right)} \right] |\phi_{\nu}(k_0)\rangle \quad (3.41)$$

with the time-dependent width $\Delta_x(t) = |\frac{1}{2\Delta_k} + \frac{i\Delta_k t}{m_2}|$ and

$$v_g = \left. \frac{\partial E_{\nu}(k)}{\partial k} \right|_{k=k_0} \quad \text{and} \quad \frac{1}{m_2} = \left. \frac{\partial^2 E_{\nu}(k)}{\partial k^2} \right|_{k=k_0}. \quad (3.42)$$

Thus, the first derivative of the dispersion curve around the center of the wave-packet gives the group velocity, while the second derivative determines the amount of spreading of the wave-packet. The wave-packet consequently evolve as a free particle with effective parameters v_g and m_2 . The mass m_2 is usually named the *effective mass* dating back from the theory of electrons exposed to an external force within metallic crystals. In figure 3.3 the lowest bands are shown for four different sets of parameters, circles mark bare energies for excited atoms $|+\rangle_n$ and

crosses for ground state atoms $|-\rangle_n$. Note how the gaps in general decrease for higher values of ν indicating that the bands are less strongly coupled, which is expected since the corresponding bare energy curves couple through multi photon processes.

In figure 3.4 the variation of the effective mass m_2 and the group velocity v_g of the lowest band in figure 3.3 (a) is plotted. Note that m_2 becomes singular before and after the crossings at $k = \pm 1/2$, and at those points the group velocities are maximum, indicating that the Gaussian wave-packet propagates without spreading.

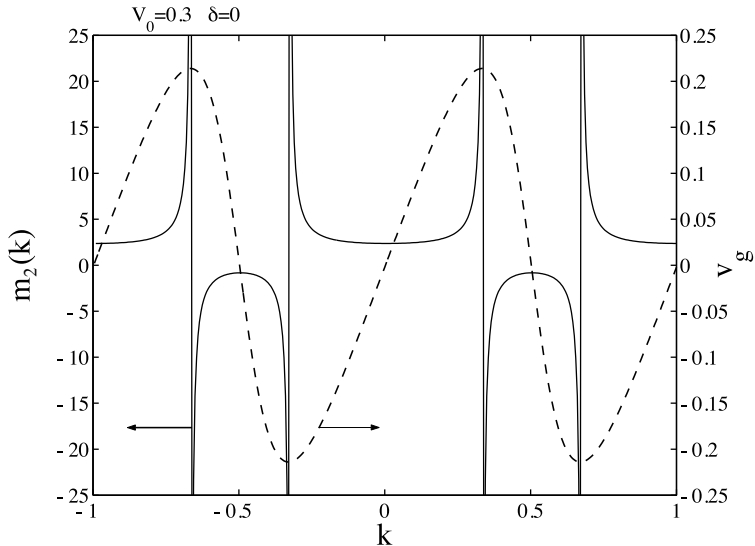


Figure 3.4: The effective mass m_2 and group velocity v_g as function of quasi momentum for the lowest band in figure 3.3 (a).

3.3.3 Washboard potential

An interesting phenomenon occurs when a linear force, giving the potential Fx , is affecting the atom within the standing wave in the cavity [38]. Instead of a constant acceleration of the atom, it is possible to have an oscillatory motion called *Bloch oscillation* dating back to the papers [60]. In the large detuning case the two-level structure can be effectively approximated by a one-level system, and for such systems the Bloch oscillations have been seen experimentally in a variety of fields

[61]. The amplitude of F compared to the size of the band gap determines whether the atom will accelerate constantly or oscillate. The force could be, for example, gravity felt by the atom.

The eigenstates of the tipped light potential $V_0 \cos(x) + Fx$ are clearly not bound and eventually any wave-packet will approach $x \rightarrow -\infty$. If V_0 is large compared to F , one may describe the eigenstates as quasi bound and localized around some local minimum of the washboard potential, with corresponding eigenvalues complex. The imaginary part of the eigenvalues gives the decay or tunneling rate of the particle out from the local minimum. The spectrum of discrete complex eigenvalues

$$\mathcal{E}_{\nu,n} = \bar{E}_\nu + dFn - i\Gamma_\nu, \quad n = 0, \pm 1, \pm 2, \dots \quad (3.43)$$

is called a *Wannier-Stark ladder* [62] and here \bar{E}_ν is the average energy of the ν th energy band and d is the period of the potential. These are equally spaced similar to the eigenvalues of the harmonic oscillator, indicating that an oscillatory behaviour should be seen as long as the decay terms Γ_ν are small. As mentioned, higher bands are less coupled to the surrounding bands giving smaller band gaps and the decay terms are therefore increasing for larger values of ν .

As the Wannier-Stark ladder explains the oscillations of the atomic motion and its decay, one may also understand it using the band spectrum of figure 3.3. Assuming that the force is small compared to the potential depths, the quasi momentum behaves 'classically' and grows linearly in time

$$k = k_0 - Ft \Rightarrow |\varphi(k, t)|^2 = |\varphi(k_0 - Ft)|^2 \quad (3.44)$$

This is called *the acceleration theorem* and is derived in Appendix A. This is the same as saying that the atom moves adiabatically due to the force F and coupling to nearby energy curves can be neglected. Since the dispersion curves $E_\nu(k)$ are periodic in k , and consequently the effective parameters (3.42), the motion of the wave-packet will also be periodic. The adiabaticity constraints are most likely to break down when the energy curves are close, which occur at the avoided crossings in figure 3.3. If transition between different states takes place only as the quasi momentum is swept across a crossing one may estimate the amount of transferred population by truncating the Hamiltonian (3.36) to contain just the states involved and linearize the time dependent diagonal terms around the crossing. For a crossing with two states in the lowest band with $\delta = 0$ one gets

$$H = \begin{bmatrix} Ft & \frac{V_0}{2} \\ \frac{V_0}{2} & -Ft \end{bmatrix} \quad (3.45)$$

and for a three level crossing

$$H = \begin{bmatrix} 2Ft & \frac{V_0}{2} & 0 \\ \frac{V_0}{2} & 0 & \frac{V_0}{2} \\ 0 & \frac{V_0}{2} & -2Ft \end{bmatrix}. \quad (3.46)$$

The first one is the standard Landau-Zener model [49, 50] with asymptotic probability $P = \exp(-\Lambda/2)$ for transition out of the band, where $\Lambda = \pi V_0^2/4F$. The second Hamiltonian is the three level version of the Landau-Zener model and it is also analytically solvable [63], with transition probabilities similar to standard Landau-Zener model, see [63] or Paper VII.

3.3.4 External atomic trap-potential

Here we consider the system described by the Hamiltonian

$$H_{trap} = p^2 + V(x) + \begin{bmatrix} \frac{\Delta}{2} & g_0\sqrt{n} \\ g_0\sqrt{n} & -\frac{\Delta}{2} \end{bmatrix}, \quad (3.47)$$

where $V(x)$ may be any potential acting equally on both atomic internal states. This may be decoupled by using the dressed states of (2.13), giving two regular Schrödinger equations

$$\left[p^2 + V(x) \pm \sqrt{\left(\frac{\Delta}{2}\right)^2 + g_0^2 n} \right] \Psi_j(x) |\psi_{1,2}\rangle = E_j \Psi_j(x) |\psi_{1,2}\rangle. \quad (3.48)$$

Especially interesting are the situations when $V(x)$ has bound states forming a trap of the atom inside the cavity. During the last years, experiments with atoms trapped in external traps inside cavities have been performed [67]. This field combine ion trap experiments with cavity QED, and now both the motional state of the atom/ion and its internal states store the quantum information. If we assume a harmonic potential trap we get $\Psi_j(x) = H_j(x)$, where $H_j(x)$ is the j 'th Hermite polynomial. Note that if g_0 or Δ becomes position dependent, H_{trap} is no longer diagonalized in its two-level structure by an x -independent unitary operator which commutes with p .

Chapter 4

Dynamics of extended Jaynes-Cummings models

4.1 State preparation

Together with the progress of isolating simple quantum mechanical systems from the environment, greater demands on the preparation of desirable initial quantum states has been called for [64]. In chapter 2 it was discussed how excited Rydberg levels of the atom and how cold superconducting cavities are used to initialize a vacuum state of the field. It is not only pure states of the individual subsystems that are of interest, being able to prepare entanglement in a controlled fashion is highly desirable. These states are at the heart of quantum mechanics, representing a sort of correlation not seen in classical physics. They serve as a main building block in all kinds of quantum information processing. Any state showing non-classical behaviours, for example Fock states and Schrödinger cat states, are, of course, very interesting, giving an insight into quantum nature. Much of the methods presented in this section rely on having an adiabatic evolution. This has several advantages, where the most important one is the robustness of the scheme, not sensitive to parameter amplitudes. Being in the adiabatic regime often means that simple analytic expressions are obtainable.

4.1.1 Adiabatic preparation of Fock states

Fock states or number states, $a^\dagger a|n\rangle = n|n\rangle$, have a well defined number of photons n . These states are highly non-classical, showing singularities or negative values of the quasi probability distributions, such as the Wigner distribution. Fock states also have several applications in quantum computations, and one is interested in

being able to prepare any number state $|n\rangle$ on demand. In general, the higher photon number n , the harder it is to create. As was mentioned in chapter 2, the decoherence usually grows with the number of degrees of freedom, and in many situations, it is also true for the ‘amplitude’ of the state, see subsection 4.1.3. The idea behind these scheme for preparing the Fock states is to let the detuning slowly change as the atom is inside the cavity. By having a slow variation, the state follows adiabatically the instantaneous eigenstates. If the detuning changes sign during the interaction, it means that the bare energy curves cross, while for the eigenenergy curves the crossing is avoided. The adiabatic evolution was explained in subsection 3.2.1, and see figure 3.2.

In order to get a measure of non-adiabatic contributions we use the DK 2 model of table 3.2, where the coupling is of a hyperbolic secant form and the detuning a hyperbolic tangent, as given in table 3.2. The asymptotic solutions for the filter functions, if we choose $\bar{E} = 0$, are [52]

$$\begin{aligned} |a_+^\infty(n)|^2 &= \cos^2\left(\pi T \sqrt{g_0^2 n - E_0^2}\right) \operatorname{sech}^2(\pi T E_0), \\ |a_-^\infty(n)|^2 &= 1 - |a_+^\infty(n)|^2, \end{aligned} \quad (4.1)$$

where we have assumed that the atom enters the cavity in its upper state. The adiabaticity parameter that determines the degree of adiabaticity, for this model is $\Lambda = TE_0$. The larger Λ the more adiabatic the process, and letting $\Lambda \rightarrow \infty$ we note that $|a_-^\infty(n)|^2 \rightarrow 1$, meaning that all atoms leave the cavity in their ground state. Every atom shifts the photon distribution by unity; $P_m(n) = P_{m-1}(n-1)$. Thus, the field is heated up, and if we choose the initial field to be the vacuum, $P_{m=0}(n) = \delta_{n0}$, it follows that after the passage of m atoms, the field contains exactly m photons, $P_m(n) = \delta_{mn}$. A similar scheme is presented in [65]. The method also works for cooling down the field by letting the atom enter the cavity in their lower states, and every atom adiabatically absorbs one photon. The atom acts as *field erasers* [66]. If $E_0 < g_0$, the square root in (4.1) stays real for all $n > 1$, and the cos-term oscillates within ± 1 and does not blow up. If we pick a typical atom-field coupling from a microwave experiment of $g_0 = 10$ kHz, then it follows that if $E_0 \approx g_0$ an interaction time of $T \sim 100$ μ s gives an adiabatic process. This timescale is much shorter than the decay times of microwave experiments.

If the filter functions $|a_\pm^\infty(n)|^2$ can be made constant for $n > 1$ there is an analytical closed form expression for the ensemble average photon distribution (2.37), given that the field is initially in vacuum, see Paper III. The solution becomes

$$\tilde{P}_m(n) = \binom{m}{n} \kappa^{m-n} (1-\kappa)^n, \quad (4.2)$$

where $|a_+^\infty(n)| = \kappa$ for $n \neq 0$ and zero if $n = 0$. The distribution is a binomial with mean $\langle \tilde{n} \rangle = m\kappa$ and variance $\tilde{\Delta}n_m^2 = m\kappa(1-\kappa)$. Note that if $\kappa = 0$ $\tilde{P}_m(n) = \delta_{nm}$

corresponding to the Fock state preparation scheme above. We saw an example of having constant filter functions with $\kappa = 1/2$ in subsection 3.3.1 and another example will be shown in subsection 4.3.4. These kind of filter functions may also be obtained by using time-asymmetric atom-field couplings [47].

4.1.2 Adiabatic preparation of entangled states, chirped case

In the previous subsection it was shown how non-classical number states could be achieved by slowly changing the detuning while the atom interacted with the field mode. The excitation, initially sitting on the atom, was adiabatically transferred to the field. This could be understood by the level-crossing of bare energy curves in an energy-time plot. By extending the system to contain more degrees of freedom by adding new subsystems, the parameter dimension of the Hamiltonian grows and consequently the number of energy curves. For example, if our two-level atom interacts with two identical modes and the detuning is varied so that it changes sign (having a level-crossing), the excitation in the atom must be transferred equally to the two modes due to symmetry.

In section 3.1 we saw that for the lowest non-trivial excitation situations, containing the states $\{|0, +, -\rangle, |1, -, -\rangle, |0, -, +\rangle\}$ or $\{|1, 0, -\rangle, |0, 0, +\rangle, |0, 1, -\rangle\}$, the Hamiltonian in matrix form could be written as

$$H_2 = \begin{bmatrix} 0 & g_1 & 0 \\ g_1 & \Delta & g_2 \\ 0 & g_2 & 0 \end{bmatrix} \quad (4.3)$$

for the models with '2-atom-1-mode' and '2-mode-1-atom'. If we let $\Delta = \lambda t$ for some real constant λ , the Hamiltonian becomes a special case of the analytically solvable three-level Landau-Zener model [63] presented in subsection 3.3.3. For the initial condition $|\mathbf{a}^{-\infty}| = (0, 1, 0)^T$ and assuming symmetry $g_1 = g_2 = g_0$ the final bare probabilities become

$$|\mathbf{a}^{+\infty}|^2 = \begin{bmatrix} \frac{1}{2} \left(1 - \exp \left(-\pi \frac{4g_0^2}{\lambda} \right) \right) \\ \exp \left(-\pi \frac{4g_0^2}{\lambda} \right) \\ \frac{1}{2} \left(1 - \exp \left(-\pi \frac{4g_0^2}{\lambda} \right) \right) \end{bmatrix}. \quad (4.4)$$

These are the probabilities and do not contain the phases, which, however, from symmetry implies that levels 1 and 3 must have identical phases. The adiabaticity parameter is here $\Lambda = \pi g_0^2 / \lambda$ and we note that when it becomes large $|\mathbf{a}^{+\infty}|^2 \rightarrow (1/2, 0, 1/2)^T$. For the two models with 'two atoms - one mode' and 'two modes -

one atom', this adiabatic evolution prepares the following EPR-states

$$\begin{aligned} |\text{EPR}\rangle_{2m} &= \frac{1}{\sqrt{2}} (|1,0\rangle + |0,1\rangle) |-\rangle \\ |\text{EPR}\rangle_{2a} &= \frac{1}{\sqrt{2}} (|+, -\rangle + |-, +\rangle) |0\rangle, \end{aligned} \quad (4.5)$$

for the two modes and two atoms respectively. The excitation has been transferred from the atom into the two modes in the first case and from the mode to the two atoms in the second. This scheme could be used for preparing the two atoms in an EPR-state if they interact with the cavity simultaneously and if they have different directions of propagation in space, they could be sent to two spatially separated locations for the implementation of, for example, quantum cryptography with atoms. However, one must take into account the decoherence of the atoms while traveling in free space, which could be decreased with the use of Λ -atoms instead.

Finally a remark on the form of the time-dependent three-level system (4.3). With the notation $\mathbf{a} = (a_1, a_2, a_3)$, one notes that by introducing the parameter $b = a_1 + a_3$, the system reduces to a two-level one for the amplitudes (a_2, b)

$$i \frac{\partial}{\partial t} \begin{bmatrix} a_2 \\ b \end{bmatrix} = \begin{bmatrix} \frac{\Delta}{2} & g_0 \\ g_0 & -\frac{\Delta}{2} \end{bmatrix} \begin{bmatrix} a_2 \\ b \end{bmatrix}. \quad (4.6)$$

Thus, one may use the solutions to the known two-level time-dependent problems, for example those given in table 3.2. As argued, for atoms traversing Fabry-Perot cavities perpendicular to the standing wave modes, a more physically realistic model is the DK 2 model with smooth pulse-shaped couplings. However, the adiabatic solutions are similar for any crossing model.

4.1.3 Adiabatic preparation of entangled states, STIRAP case

The idea of adiabatic population transfer between various states using time-dependent delayed pulses was presented in subsection 3.2.2, and was called STIRAP. The shapes of the pulses are important in the final results of the states; smoothness is needed for fulfilling the adiabaticity constraints and the relative asymptotic amplitudes at $t = \pm\infty$ of the pulses directly determine the adiabatic states. By choosing various pulse sequences, the final population may not need to end in a single quantum state, but it may populate several states, and it is then possible to prepare various entangled states. The STIRAP Hamiltonian (3.15) describes a three-level system, but it has been shown that multi-level STIRAP generalizations are possible [54].

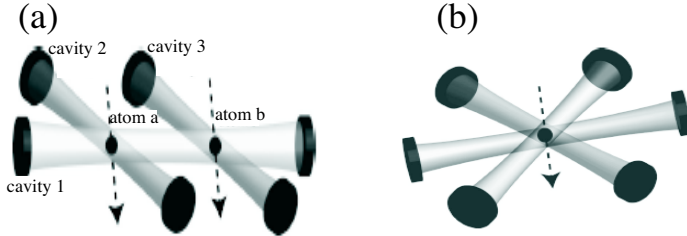


Figure 4.1: The two setups, H-configuration (a) and Star-configuration (b).

The original idea used in this subsection for applying the STIRAP formalism to cavity QED systems was published in [53] and then extended to more complicated systems in Paper V. Here we discuss two such extensions shown in figure 4.1, where in (a) there are three cavities 1,2 and 3 overlapping and two atoms a and b involved, while in (b) only one atom interacts with M cavities. The two setups will be referred to as H-configuration and Star-configuration.

H-configuration

The Hamiltonian describing the H-configuration, in the interaction picture with respect to the excitation number, reads

$$H = \Delta_a(\sigma_{az} + 1) + \Delta_b(\sigma_{bz} + 1) + [(g_{1a}\hat{a}_1 + g_{2a}\hat{a}_2)\sigma_a^+ + (g_{1b}\hat{a}_1 + g_{3b}\hat{a}_3)\sigma_b^+ + h.c.], \quad (4.7)$$

where we have set all mode frequencies the same $\omega_1 = \omega_2 = \omega_3 = \omega$ and $\Delta_j = (\Omega_j - \omega)/2$ with $j = a, b$. For the various couplings we have

$$g_{i\nu}(t) = G_{i\nu} \exp\left(-\frac{(t - t_{i\nu})^2}{\sigma_{i\nu}^2}\right), \quad (4.8)$$

so that $G_{i\nu}$ gives the amplitude, $t_{i\nu}$ the pulse center and $\sigma_{i\nu}$ the width. Throughout this thesis we use dimensionless parameters by introducing some characteristic scales. The bare basis states are given with the standard notation $|n_1, n_2, n_3, \pm_a, \pm_b\rangle$, where the first three entries gives the photon numbers of the modes and the last two refer to the atomic states. The operator

$$A^\dagger(t) = K(t) \left(\frac{g_{1a}(t)}{g_{2a}^*(t)} a_2^\dagger - a_1^\dagger + \frac{g_{1b}^*(t)}{g_{3b}(t)} a_3^\dagger \right), \quad (4.9)$$

where $K(t)$ is a normalisation constant, commutes with H implying that the adiabatic states $|\psi_n\rangle = \frac{(A^\dagger)^n}{\sqrt{n!}} |0, 0, 0, -, -\rangle$ are eigenstates of H with eigenvalue zero.

Thus for an adiabatic evolution, an initial state $f[A^\dagger(t = -\infty)] |0\rangle$ will transform into $f[A^\dagger(t = +\infty)] |0\rangle$, for any analytic function f and where $|0\rangle$ is the ground state of the combined system. For the particular choice of couplings obeying

$$\begin{aligned} |g_{1a}g_{3b}| &\gg |g_{1b}g_{2a}|, & \text{for } t \rightarrow -\infty \\ |g_{1a}g_{3b}| &\ll |g_{1b}g_{2a}|, & \text{for } t \rightarrow +\infty \\ |g_{1a}g_{3b}|^2 + |g_{1b}g_{2a}|^2 &\gg |g_{2a}g_{3b}|^2, & \text{all } t \end{aligned} \quad (4.10)$$

any field state initially in cavity 2 will be transferred to cavity 3 without ever populating cavity 1. Figure 4.2 shows the result of a numerical simulation of a one photon transfer between cavity 2 and 3, for one example of pulse sequence satisfying (4.10). The size of the Hilbert space spanned by the coupled states for a given excitation number rapidly blows up for larger number of excitations, resulting in harder numerical simulations.

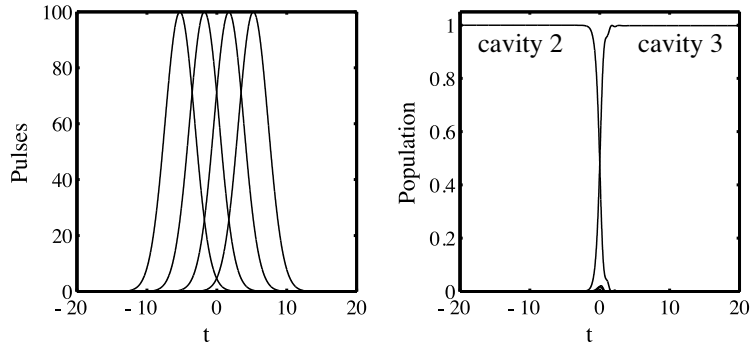


Figure 4.2: The figure to the left shows the first example of a pulse sequence for realizing complete population transfer from cavity 2 to cavity 3 with minimal population in the intermediate cavity 1 for the H-configuration. The pulses are ordered in a completely counterintuitive way, from left to right g_{3b} , g_{1b} , g_{1a} and g_{2a} . The widths of the pulses are all $\sigma = 3$ and the maximum amplitudes are $G = 100$. The other plot shows the populations of the five states involved as functions of the scaled interaction time t . It is clear that population is transferred adiabatically from the second cavity to the third cavity (both marked in the figure), without significant population in cavity 1. The final population in the third cavity is 99.8 %, and maximum population of cavity 1 during the process is 0.2 %.

If we chose another pulse sequence according to

$$\begin{aligned} |g_{1a}g_{3b}|, |g_{1b}g_{2a}| &\ll |g_{2a}g_{3b}|, \quad \text{for } t \rightarrow -\infty \\ |g_{1a}g_{3b}|, |g_{1b}g_{2a}| &\gg |g_{2a}g_{3b}|, \quad \text{for } t \rightarrow +\infty \\ g_{1a} = g_{1b}, & \quad \text{all } t \\ g_{2a} = g_{3b}, & \quad \text{all } t \end{aligned} \tag{4.11}$$

it results in that any initial field state in cavity 1 can be transferred into cavities 2 and 3; $f(a_1^\dagger)|0\rangle \rightarrow f(a_2^\dagger + a_3^\dagger)|0\rangle$. For the one photon case, the final state is of EPR type between cavity mode 2 and 3

$$|\text{EPR}\rangle_{23} = \frac{1}{\sqrt{2}}(|1,0\rangle + |0,1\rangle). \tag{4.12}$$

The experimental procedure to achieve the pulse sequence of equation (4.11) would be to let atom a and b pass simultaneously through the setup with no delays. They first enter the empty cavities 2 and 3 and then the populated cavity 1. A numerical simulation is given in figure 4.3. Note that the necessary amplitude of the pulses is much smaller in this example due to the fact that not so many intermediate levels are virtually populated as in figure 4.2.

Star-configuration

In the Star-configuration it is assumed that $M-1$ identical cavities are initially empty and lie in a plane, while one non-empty cavity is slightly off the plane, but still overlapping with the other cavities. The atom passes through the M cavities at the center point, first entering the $M-1$ cavities and then the M th cavity. The effective Hamiltonian is

$$H = \Delta(\sigma_a + 1) + \left[g_{Ma}\hat{a}_M\sigma_a^+ + g_a \sum_{i=1}^{M-1} \hat{a}_i\sigma_a^+ + h.c. \right], \tag{4.13}$$

where $g_{ia} = g_a$ for $i = 1, 2, \dots, M-1$. The adiabatic operator that gives the adiabatic dark states $|\psi_n\rangle = \frac{(A^\dagger)^n}{\sqrt{n!}}|0, \dots, 0, -\rangle$ is

$$A^\dagger = K(t) \left(-g_{Ma}a_1^\dagger - g_{Ma}a_2^\dagger - \dots - g_{Ma}a_{M-1}^\dagger + g_a a_M^\dagger \right). \tag{4.14}$$

For the case of a single photon and

$$\lim_{t \rightarrow -\infty} \left(\frac{g_{Ma}}{g_a} \right) = 0, \quad \text{and} \quad \lim_{t \rightarrow +\infty} \left(\frac{g_a}{g_{Ma}} \right) = 0, \tag{4.15}$$

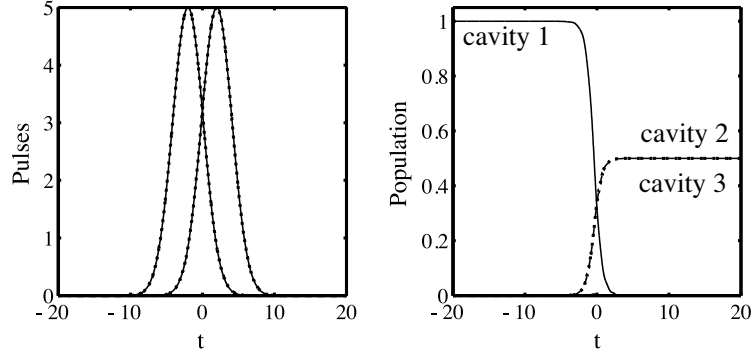


Figure 4.3: This shows the numerical simulation of preparation of EPR states between cavity 2 and 3. To the left we show the pulses, with the parameters $G = 5$, $t_{1a} = 2$, $t_{2a} = -2$, $t_{3b} = -2$ and $t_{1b} = 2$ and $\sigma_{1a} = \sigma_{2a} = \sigma_{1b} = \sigma_{3b} = 3$. The right plot gives the populations, and how the photon initially in cavity 1 (solid line) is transferred equally to cavity 2 and 3 (dotted and dashed lines). For the fidelity (overlap between the numerically obtained state with the target state) we have $F = |\langle EPR|\psi(t = +\infty)\rangle| = 0.9999$.

the final states will be, for $M = 3$, an EPR-state in cavities 1 and 2, for $M = 4$ a W-state,

$$|W\rangle = \frac{1}{\sqrt{3}} (|1, 0, 0\rangle + |0, 1, 0\rangle + |0, 0, 1\rangle), \quad (4.16)$$

and for higher M s the natural generalization of these states. For a general number state $|n\rangle$ in cavity M we get

$$|0, \dots, 0, n, -\rangle \longrightarrow \sum_{k_1 + \dots + k_{M-1} = n} \frac{1}{N} \frac{n!}{k_1! \dots k_{M-1}!} \left(\hat{a}_1^\dagger\right)^{k_1} \dots \left(\hat{a}_{M-1}^\dagger\right)^{k_{M-1}} |0, \dots, 0-\rangle. \quad (4.17)$$

Note the similarities of this scheme with that of beam-splitters, S. Haroche in [1].

Generation of Schrödinger cat states by selectiv atomic measurements

An Ancilla state is an auxiliary state for achieving desirable operations. It is a subsystem in a particular state $|\psi_A\rangle$ that is initially not entangled with the main system and after the operation it still is disentangled from the system and in the same original state; $|\Psi\rangle_{sys} \otimes |\psi_A\rangle \rightarrow |\tilde{\Psi}\rangle_{sys} \otimes |\psi_A\rangle$. In the STIRAP scheme above, the atomic state $|\psi_A\rangle = |-, -, \dots\rangle$ (depending on the number of atoms) and $|\Psi\rangle_{sys}$

is the states of the various modes. In order to create entanglement it is often useful to introduce another level $|q\rangle$ that does not interact with the system, due to a large detuning, selection rules or any other reason for a zero coupling. Then it follows $|\Psi\rangle_{sys}(c_q|q\rangle + c_A|\psi\rangle_A) \rightarrow c_q|\Psi\rangle_{sys}|q\rangle + c_A|\tilde{\Psi}\rangle_{sys}|\psi\rangle_A$ for any constants c_q and c_A . Note that in general an Anchilla state is not needed, $|\psi\rangle_A$ could be any state interacting with the system.

Let us go back to the situation of just two overlapping cavities and a single atom discussed in sections 3.1 and 3.2.2. With the third atomic level $|q\rangle$ introduced and from equation (3.20) it follows that

$$\begin{aligned} |0, \alpha, -\rangle &\longrightarrow |-\alpha, 0, -\rangle \\ |0, \alpha, q\rangle &\longrightarrow |0, \alpha, q\rangle. \end{aligned} \quad (4.18)$$

Thus,

$$|0, \alpha\rangle|\chi\rangle_{\pm}^a \longrightarrow \frac{1}{\sqrt{2}}(|-\alpha, 0\rangle|-\rangle^a \pm |0, \alpha\rangle|q\rangle^a), \quad (4.19)$$

which defines the atomic states $|\chi\rangle_{\pm}$. If an atomic measurement is done after the interaction in the $|\chi\rangle_{\pm}$ -basis, the two modes will be

$$|\psi_{field}\rangle = \frac{1}{\sqrt{2}}(|-\alpha, 0\rangle \pm |0, \alpha\rangle), \quad (4.20)$$

where we have assumed $\langle\alpha|0\rangle \approx 0$, and we have a plus sign if the measured and initial states are the same, otherwise a minus sign. By using the property of the displacement operator, $D(\beta)|\alpha\rangle = e^{i\text{Im}(\alpha\beta^*)}|\alpha + \beta\rangle$, and letting both β and α be real and $\alpha = 2\beta$ we get

$$D_{mode1}(-\beta)D_{mode2}(-\beta)|\psi_{field}\rangle = \frac{1}{\sqrt{2}}(|-\beta, \beta\rangle \pm |\beta, -\beta\rangle). \quad (4.21)$$

This state describes a maximally entangled two-mode state, see Paper IV and V and [68]. For another type of cat-states, see [69]. It is highly non-classical since it is entangled and also a mesoscopic superposition assuming that β is large. It is known that the larger the amplitude $|\beta|$ of the cat, the faster the decoherence. Following [13] assuming decay according to

$$\frac{\partial\rho}{\partial t} = \frac{\Gamma}{2} \left(2a_1\rho a_1^\dagger - a_1^\dagger a_1\rho - \rho a_1^\dagger a_1 \right) + \frac{\Gamma}{2} \left(2a_2\rho a_2^\dagger - a_2^\dagger a_2\rho - \rho a_2^\dagger a_2 \right) \quad (4.22)$$

we find that the diagonal and off-diagonal terms of ρ dissipate as

$$\rho(t) = N \sum_{\gamma_1, \gamma_2=\pm\beta} \langle\gamma_1|\gamma_2\rangle^{2-2e^{-\Gamma t}} |\gamma_1 e^{-\Gamma t/2}, -\gamma_1 e^{-\Gamma t/2}\rangle \langle\gamma_2 e^{-\Gamma t/2}, -\gamma_2 e^{-\Gamma t/2}|. \quad (4.23)$$

Note that the off-diagonal terms, the coherence terms, decay much faster due to the small overlap $\langle \beta| -\beta \rangle$.

Manipulation of atomic states

From the similarities between the 2-mode-1-atom and the 2-atom-1-mode Hamiltonians (3.10) and (3.8), one understands that the methods above could be applied for preparing certain states of the atoms. We conclude this subsection by looking at a simple model of two atoms and one mode, and show how the dynamics of two systems looking alike can differ considerably. Let us first consider a single two-level atom, initially in the upper state $|+\rangle$, passing resonantly through an empty cavity with a Gaussian mode shape. The time-evolution of the system is

$$|\psi(t)\rangle = \cos(A)|0,+\rangle - i \sin(A)|1,-\rangle \quad (4.24)$$

with

$$A = \int_{-\infty}^t dt' g_1(t') \quad (4.25)$$

being the pulse-area. Thus, inside the cavity, the atom Rabi-oscillates, and the final state is determined by the pulse-area. Now, assume that during the passage of the atom through the cavity, another atom is constantly interacting with the cavity with a coupling g_2 . The second atom is initially in its ground state, and since the cavity mode is initially in the vacuum state, no exchange of energy is taking place between the mode and the second atom, as long as the first atom is not interacting with the mode. When the process is adiabatic, the system will follow the dark state

$$|\psi_{ad}\rangle = N(g_2|0,+,-\rangle - g_1(t)|0,-,+\rangle). \quad (4.26)$$

The system starts and ends in the state $|0,+,-\rangle$, while during the passage the population is distributed between the states $|0,+,-\rangle/|0,-,+\rangle$ as $g_2/g_1(t)$. Note that the cavity mode is only virtually populated, regardless the spatial distance between the atoms. The second atom, sitting inside the cavity, could be used as a measuring device; 'klick' when an atom passes through the cavity.

4.1.4 Non-adiabatic preparation of entangled states, Λ -atom case

In the previous subsection the couplings changed in time, and adiabaticity was used to explain the dynamics of various state preparation schemes. The Λ -atom systems presented in 3.1 have similarities with the models of the previous subsection, but now we will, however, assume no time-dependence of the Hamiltonian, and describe

some non-adiabatic state preparation methods. We will, however, use the effective Hamiltonian obtained after adiabatic elimination of the upper atomic level. See Appendix A, where the elimination is carried out. After the elimination and neglecting Stark-shift terms, the Hamiltonian is in the zero detuning case

$$H_\Lambda = g \left(a_2^\dagger a_1 \sigma^- + a_2 a_1^\dagger \sigma^+ \right), \quad (4.27)$$

in our standard notation. An initial state $|\Psi(0)\rangle = \sum_{n,m} C_n^{(1)} C_m^{(2)} |n, m\rangle [\gamma|a\rangle + \delta|c\rangle]$ evolves as

$$\begin{aligned} |\Psi(t)\rangle = & \sum_{n,m} C_n^{(1)} C_m^{(2)} \left\{ \gamma \left[\cos(gt\sqrt{(n+1)m}) |n, m, a\rangle \right. \right. \\ & - i \sin(gt\sqrt{(n+1)m}) |n+1, m-1, c\rangle \Big] \\ & \left. \left. + \delta \left[\cos(gt\sqrt{(m+1)n}) |n, m, c\rangle \right. \right. \right. \\ & \left. \left. - i \sin(gt\sqrt{(m+1)n}) |n-1, m+1, a\rangle \right] \right\}. \end{aligned} \quad (4.28)$$

Large initial fields

In the papers [6] it was shown that for large initial coherent states in the standard JC model, the atom disentangles from the field at certain times regardless of its initial state. This has recently been demonstrated experimentally [15]. Let us assume that the photon distributions have means \bar{n} and \bar{m} and that we can replace $C_{n\pm 1}^{(1)} C_{m\mp 1}^{(2)}$ by $C_n^{(1)} C_m^{(2)} e^{i\varphi_{nm}^{(\pm)}}$. We also put the phase to a constant value, $\varphi_{nm}^{(\pm)} = \pm\varphi$, under the assumption that the phases $\varphi_{nm}^{(\pm)}$ of the two fields are slowly varying around the average photon numbers \bar{n} and \bar{m} . In order to understand the evolution better we introduce the atomic states $|\phi_\pm\rangle = \frac{1}{\sqrt{2}}(e^{i\varphi}|a\rangle \pm |c\rangle)$, and if the distributions are sharply peaked around their means we use the approximation

$$\sqrt{(m+1)n} - \sqrt{(n+1)m} \approx \frac{1}{2} \left(\sqrt{\frac{\bar{n}}{\bar{m}}} - \sqrt{\frac{\bar{m}}{\bar{n}}} \right), \quad (4.29)$$

to obtain the following approximate evolution, see Paper IV,

$$\begin{aligned}
|\Psi(t)\rangle_{\pm} &\approx \frac{1}{\sqrt{2}} \sum_{n,m} C_n^{(1)} C_m^{(2)} e^{\mp i g t \sqrt{(m+1)n}} \times \\
&\quad \times \left[e^{i\varphi} e^{\pm i g t [\sqrt{(m+1)n} - \sqrt{(n+1)m}]} |a\rangle \pm |c\rangle \right] |n, m\rangle \\
&\approx \frac{1}{\sqrt{2}} \left(\exp \left[i\varphi \pm i \frac{gt}{2} \left(\sqrt{\frac{\bar{n}}{\bar{m}}} - \sqrt{\frac{\bar{m}}{\bar{n}}} \right) \right] |a\rangle \pm |c\rangle \right) \times \quad (4.30) \\
&\quad \times \sum_{n,m} C_n^{(1)} C_m^{(2)} e^{\mp i g t \sqrt{(m+1)n}} |n, m\rangle \\
&= \frac{1}{\sqrt{2}} \left(\exp \left[i\varphi \pm i \frac{gt}{2} \left(\frac{\kappa - 1}{\sqrt{\kappa}} \right) \right] |a\rangle \pm |c\rangle \right) |\psi_{\mp}\rangle.
\end{aligned}$$

The last line defines the field states $|\psi_{\pm}\rangle$ and the parameter κ is \bar{n}/\bar{m} . The interesting observation is that for effective interaction times

$$gt_0^{(j)} = (2j + 1) \frac{\pi \sqrt{\kappa}}{|\kappa - 1|}, \quad j = 0, 1, 2, \dots \quad (4.31)$$

the atomic states of (4.30) become equal, meaning that any atomic state disentangle from the fields at these times. In Paper IV we investigated the approximations leading to equation (4.30) and how well the atom did disentangle from the field. In Paper VIII the same approximations are considered in a similar model. We noted that the approximations did not hold so well when we used coherent initial states with moderate means \bar{n} and \bar{m} . By using more localized states in form of squeezed states, the method improved.

For large enough means we can expand the term $\sqrt{(m+1)n}$ around \bar{n} and \bar{m} to first order to obtain the field states

$$|\psi_{\pm}(t)\rangle \approx e^{\pm i \frac{\sqrt{\kappa} gt}{2}} |\nu e^{\pm i \frac{gt}{2\sqrt{\kappa}}} \rangle |\mu e^{\pm i \frac{\sqrt{\kappa} gt}{2}} \rangle. \quad (4.32)$$

When the atom disentangles from the fields for the first time $gt_0^{(0)}$, the states become

$$|\psi_{\pm}(gt_0^{(0)})\rangle \approx e^{\pm i \frac{\pi \kappa}{2|\kappa - 1|}} |\nu e^{\pm i \frac{\pi}{2} \frac{1}{|\kappa - 1|}} \rangle |\mu e^{\pm i \frac{\pi}{2} \frac{\kappa}{|\kappa - 1|}} \rangle. \quad (4.33)$$

For an example take $\kappa = 3$, giving the phase modulations of the coherent states $\exp(\pm i\pi/4)$ and $\exp(\pm i3\pi/4)$. If the atom is initially in say $|1\rangle$, the field at the disentanglement times is

$$|\psi_{field}(gt_0^{(j)})\rangle = \frac{1}{N} (|\psi_+(gt_0^{(j)})\rangle + |\psi_-(gt_0^{(j)})\rangle), \quad (4.34)$$

where N is a normalization constant. With $\kappa = 3$ and $j = 0$ this state is an entangled two-mode Schrödinger cat

$$|\Psi(gt_0^{(0)})\rangle = \frac{1}{\sqrt{2}} (i|a\rangle + |b\rangle) \otimes \frac{i}{N} \left(|\nu e^{-i\pi/4}\rangle |\mu e^{-i3\pi/4}\rangle - |\nu e^{i\pi/4}\rangle |\mu e^{i3\pi/4}\rangle \right). \quad (4.35)$$

This is confirmed in figure 4.4 which shows the Q -functions of the reduced density operators for the two fields. In the figure we have used initially squeezed states with

$$C_n^{(l)} = \frac{\tanh(r)^{n/2}}{\sqrt{n! 2^n \cosh(r)}} e^{-|\nu|^2(1-\tanh(r))/2} H_n \left(\frac{\nu}{\sqrt{\sinh(2r)}} \right), \quad l = 1, 2 \quad (4.36)$$

if ν is chosen real and H_n is the n 'th Hermite polynomial. From the figure one cannot easily tell whether the two modes are in a statistical mixture or really are entangled. This has been checked by calculating the mode purity of any of the states $|\psi_{\pm}\rangle$ defined in equation (4.30), which is the same for the two states, to be $P_{\text{mode}} \approx 0.96$, indicating entanglement.

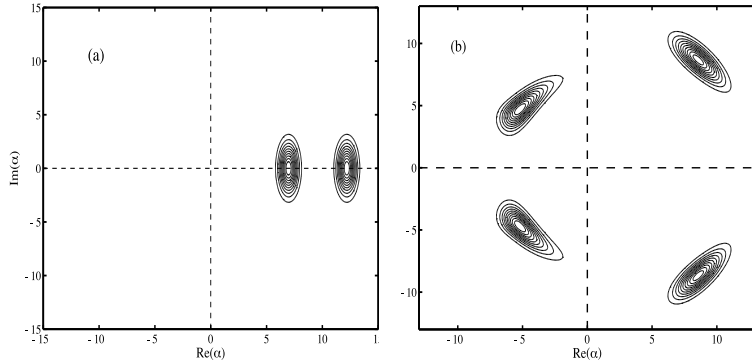


Figure 4.4: These two contour plots show the various reduced Q -functions $Q_{1,2}^{\pm}(\alpha, t) = \langle \alpha | \rho_{1,2}^{\pm}(t) | \alpha \rangle$, at (a) the time zero, and (b) first disentanglement time $gt_0^{(1)}$. The two modes are initially in squeezed states with $\bar{n} = 150$, $\bar{m} = 50$ and $r_1 = r_2 = 1$, which are seen in (a). In figure 5 (b) it is clear how the two separate modes' initial states split up into two parts, characterizing a Schrödinger cat. Note that the phases of the fields agree well with the predicted phases from the approximations, see, for example, equation (4.35). The shapes of the Q -functions for mode two, with lower average number of photons, have changed more during the evolution than for mode one.

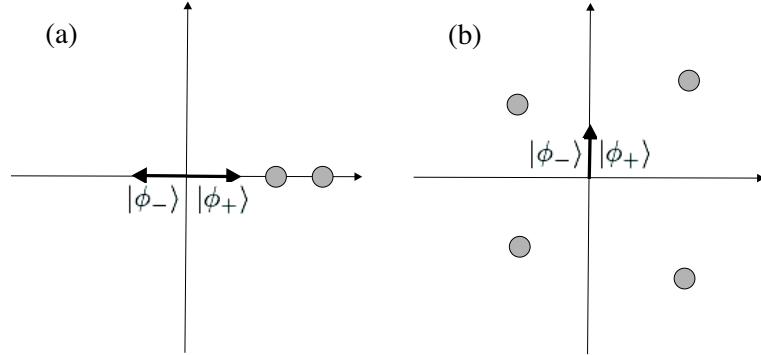


Figure 4.5: Schematic representation of how the Bloch dipole states $|\phi_{\pm}(t)\rangle$ rotate. At the first disentanglement time (b), the two states have rotated $\pm\pi/2$ and they become equal, and consequently disentangle from the field.

One way to get a physical idea of the atomic disentanglement is to consider the atomic dipole states $|\phi_{\pm}\rangle$. On the Bloch sphere they represent two states opposite to each other, as time evolves the states start to rotate in opposite directions, while the field states split up into two counter rotating parts. In the phase plane we represent the dipole states as arrows, and at the first disentanglement time they have rotated $\pm\pi/2$ respectively, see figure 4.5.

EPR-states

By choosing $gt = \pi/4$ we get, according to equation (4.28), the following evolution

$$|0, 1\rangle|a\rangle \rightarrow \frac{1}{\sqrt{2}}(|0, 1\rangle|a\rangle - i|1, 0\rangle|c\rangle). \quad (4.37)$$

By measuring the atom in the $\left\{\frac{1}{\sqrt{2}}(|a\rangle \pm |c\rangle)\right\}$ -basis after the interaction the field of the two modes is left in one of the states

$$\begin{aligned} |\text{EPR}\rangle_{-} &= \frac{1}{\sqrt{2}}(|0, 1\rangle - i|1, 0\rangle) \\ |\text{EPR}\rangle_{+} &= \frac{1}{\sqrt{2}}(|0, 1\rangle + i|1, 0\rangle). \end{aligned} \quad (4.38)$$

GHZ-states

We now assume that two atoms pass the cavity one after the other and that the two modes have been prepared in the superposition states $|\pm\rangle = \frac{1}{\sqrt{2}}(|0\rangle \pm |3\rangle)$.

The interaction times are for both atoms $gt\sqrt{3} = \pi$. From (4.28), it follows that the states of the two modes will be flipped if the atoms pass the cavity in different initial states $|a\rangle_1|c\rangle_2$ or $|c\rangle_1|a\rangle_2$, while if they have the same initial states the cavity fields are not changed, for example

$$|+,+\rangle \frac{1}{\sqrt{2}}(|a\rangle_1 \pm |c\rangle_1)|a\rangle_2 \rightarrow \frac{1}{\sqrt{2}}(|+,+,a\rangle_1 \pm |-, -, c\rangle_1)|a\rangle_2. \quad (4.39)$$

The two cavities plus atom 1 is in a so called GHZ-state, an entangled three-partite state. Note that the order of the atoms does not matter. The above idea will be used in the next section for implementing a phase-gate.

4.1.5 Dispersive preparation of entangled states, V -atom case

In the previous subsection we have shown how an effective model after elimination of one level may be used to prepare various states. In that case, one out of three levels was removed and did not couple to the other levels, while the remaining two levels coupled by some effective coupling. Thus, if population is initially in the uncoupled level, the interaction does not give any population transfer, but some phase shifts. The reason why it was legitimate to remove one level was due to a large detuning, resulting in small population transfer. As already mentioned, the effective model will contain Stark-shift terms of the various energy levels. These terms were neglected in the previous subsection, and they are proportional to the field amplitudes $a_i^\dagger a_i$. In this subsection we use an equivalent model as the Λ one, except that we assume the eliminated level is the lowest level instead of the upper level. This has only been done in order to have low losses, by using a ground state instead of an excited one. The atom is initially in the eliminated level, which does not couple to the other levels, so that no energy exchange is taking place between the atom and the fields. However, the interaction will result in phase-modulations as will be shown.

We denote the atomic level that interacts dispersely with the field as $|a\rangle$ and we again use a level $|q\rangle$ not interacting with the field. From equation (A.19) of the Appendix A we find the Hamiltonian

$$\tilde{H} = \Omega_q|q\rangle\langle q| + \Omega'_{22}|b\rangle\langle b| + \left(\lambda_1 a_1^\dagger a_1 + \lambda_2 a_2^\dagger a_2\right)|b\rangle\langle b| \quad (4.40)$$

and with $g_{12} = g_{23} = g$ and $\Delta_1 = \Delta_3 = \Delta$ we have

$$\Omega'_2 = \Omega_2 + \frac{2g^2}{\Delta}, \quad \lambda_1 = \lambda_2 = \frac{g^2}{\Delta}. \quad (4.41)$$

By removing the first two purely atomic terms we find

$$H = \lambda \left(a_1^\dagger a_1 + a_2^\dagger a_2\right)|b\rangle\langle b| \quad (4.42)$$

which is our dispersive Hamiltonian. The evolution of initial coherent states of the modes is especially simple

$$\begin{aligned}
|\Psi(t)\rangle &= e^{-iHt} |\alpha, \beta\rangle \frac{1}{\sqrt{2}} (|q\rangle \pm |b\rangle) \\
&= \frac{1}{\sqrt{2}} \left(|\alpha, \beta, q\rangle \pm e^{-|\alpha|^2/2 - |\beta|^2/2} \sum_{n,m} \frac{(\alpha e^{-i\lambda t})^n}{\sqrt{n!}} \frac{(\beta e^{-i\lambda t})^m}{\sqrt{m!}} |n, m, b\rangle \right) \\
&= \frac{1}{\sqrt{2}} (|\alpha, \beta, q\rangle \pm |\alpha e^{-i\lambda t}, \beta e^{-i\lambda t}, b\rangle).
\end{aligned} \tag{4.43}$$

Projecting onto the basis states $\left\{ \frac{1}{\sqrt{2}} (|q\rangle \pm |b\rangle) \right\}$ leaves the two modes in an entangled Schrödinger cat state. Note that by using different effective couplings λ_1 and λ_2 the phase-modulations of the two fields would be different. A similar method is presented in Paper VIII for generation of entangled Schrödinger cat states. There it is shown that one only needs a two-level atom for the preparation, in the case of identical frequencies of the two modes.

In a recent paper [70] the corresponding dispersive interaction in the Standard JC model was proposed for the realization of a quantum walk. The quantum walk is similar to the classical random walk, but the 'coin' used in the classical theory for going left or right is changed to a qubit in the quantum version. The qubit may be in any linear combination of 'head' and 'tail' and there is no randomness in the quantum walk. In [70] the two-level atom serves as the coin, and depending whether it is in the $|+\rangle$ or in the $|-\rangle$ state, a coherent state of the mode is rotated clockwise or anti-clockwise. From (4.43) it is clear that the interaction time directly determines the angle of rotation. In the quantum walk scheme, the atom interacts dispersively with the field for a time τ and then a Hadamard operation is imposed on the atom and the atom interacts another time τ with the field and so on. The Hadamard acts on the atomic states $|\pm\rangle$ (or in our case $\{|q\rangle, |b\rangle\}$) as

$$U_{Had} = \frac{1}{\sqrt{2}} \begin{bmatrix} 1 & -1 \\ 1 & 1 \end{bmatrix}, \tag{4.44}$$

and one may say that it represent the tossing of the coin. The interaction described above, rotating two modes is not a generalization to a two-dimensional quantum walk, since both mode always take the same steps in the 'walk'. However, one could use one of the modes as a reference for a field measurement. In that way the field is not 'destroyed' by the measurement.

4.2 Quantum computing

In this section we show how the extended JC models may be used to carry out various quantum gate operations needed for quantum computing. In realizing a quantum computer, a whole set of constraints must be fulfilled. These are: 1) The system must be isolated from external disturbances in the form of decoherence. It will always couple irreversible to the surrounding environment, and the larger system the more irreversible losses. Thus one needs to isolate the system extremely well. 2) One must be able to prepare the whole system in a desired initial state. 3) One needs a universal set of unitary operations that can be implemented in a controllable way on the qubits of the system. 4) One needs a scheme for read-out of the state vector after the computation has been performed. 5) Finally, the system must be scalable, so that all the above constraints hold for a large number of qubits. In the previous section we discussed various state preparation schemes and now we will analyze constraint 3), to find unitary operations that realize the gates. Note, however, that the preparation and the operation schemes are often related; the unitary evolution in the previous section could be seen as performing gates on the qubits.

As for the state preparation, it is often convenient to be in the adiabatic limit, since in this regime we often do not need to worry about various 'pulse areas'. Thus the evolution is insensitive to parameter values and interaction times. However, adiabaticity is by its definition a 'slow' process, giving long operation times and realizing many gates before decoherence becomes significant may be hard. Adiabatic quantum computing has been considered in several papers, see for example [71].

4.2.1 Adiabatic quantum computing, with field qubits

We will always use the adiabatic theory of level-crossings for transferring population between bare states. With a crossing and in this limit, $w_n = 0$ in the scattering matrix (3.14). It then follows

$$a_{\pm}^0(n) \rightarrow \mp e^{\pm i\phi_n} a_{\mp}^{\infty}(n) \quad (4.45)$$

where the phase ϕ_n due to the passage of a crossing depends on the various parameters, not only n . Even if the population transfer between the bare states $a_{\pm}(n)$ is not sensitive to parameter changes, the phase is, which is a problem for some of our quantum gates. For the LZ model the phase is

$$\phi_n = -\frac{\pi}{4} - \Lambda + \Lambda \ln(\Lambda) - \arg[\Gamma(\Lambda)], \quad (4.46)$$

where

$$\Lambda = \frac{g_0^2 n}{2\Delta_0} \quad (4.47)$$

and $\Gamma()$ is the gamma function. Note that in the adiabatic limit for a crossing model we have for repeated applications of the scattering matrix \mathcal{S} (3.14)

$$\begin{aligned}\mathcal{S}^1 &= \mathcal{S}, & \mathcal{S}^2 &= -1, \\ \mathcal{S}^3 &= -\mathcal{S}, & \mathcal{S}^4 &= 1.\end{aligned}\quad (4.48)$$

Thus, passing a crossing twice results in an overall minus sign, which is exactly the same as rotating a spin 1/2-particle 2π . This fact may be used in order to achieve a phase gate.

Controlled-phase gate

A single two-level atom enters a cavity in its lower state far out of resonance with two different modes 1 and 2. The atomic transition frequency is then tuned adiabatically across mode 1's frequency ω_1 and then it is tuned across mode 2's frequency ω_2 . After the two crossings, the atomic frequency is reversed, first cross mode 2 and then mode 1. Thus finally it has crossed both modes frequencies twice. The field qubits are either the vacuum or the one photon Fock state. By indicating the adiabatic crossing of mode i by A.C. i , we get the following scheme

$$\begin{aligned}|0, 0, -\rangle &\xrightarrow{\text{A.C.1,2}} |0, 0, -\rangle \xrightarrow{\text{A.C.1,2}} |0, 0, -\rangle \\ |0, 1, -\rangle &\xrightarrow{\text{A.C.1,2}} e^{-i\phi_1} |0, 0, +\rangle \xrightarrow{\text{A.C.1,2}} -|1, 0, -\rangle \\ |1, 0, -\rangle &\xrightarrow{\text{A.C.1,2}} -|0, 1, -\rangle \xrightarrow{\text{A.C.1,2}} |1, 0, -\rangle \\ |1, 1, -\rangle &\xrightarrow{\text{A.C.1,2}} -e^{-i(\phi_1-\phi_2)} |0, 1, -\rangle \xrightarrow{\text{A.C.1,2}} |1, 1, -\rangle,\end{aligned}\quad (4.49)$$

which simplified without the Anchilla state $|-\rangle$ and the intermediate states becomes

$$\begin{aligned}|0, 0\rangle &\rightarrow |0, 0\rangle \\ |0, 1\rangle &\rightarrow -|0, 1\rangle \\ |1, 0\rangle &\rightarrow |1, 0\rangle \\ |1, 1\rangle &\rightarrow |1, 1\rangle.\end{aligned}\quad (4.50)$$

This is a controlled phase gate; the state flips sign if mode 1 is in vacuum and mode 2 is in a one photon state, otherwise the state remains the same.

One qubit gates

Having the phase gate (4.50) plus one qubit gates one has a universal set of gates and out from them it is possible to build any desirable gate. The one qubit

gates are the set of rotations or reflections of two-level state vectors. Experimentally it is much easier to rotate the atomic states $|\pm\rangle$, than the field basis states $|0\rangle, |1\rangle$. Thus, it would be desirable if the field state could be transferred onto the atom and then the gate

$$U_{atom}(a, b) = \begin{bmatrix} a & b \\ -b^* & a^* \end{bmatrix}, \quad |a|^2 + |b|^2 = 1 \quad (4.51)$$

is performed on the atom and finally the state is transferred back to the field. By using the adiabatic crossing idea we get

$$\begin{aligned} & [\alpha|0\rangle + \beta|1\rangle] |-\rangle \xrightarrow{\text{A.C.}} |0\rangle [\alpha|-\rangle + \beta e^{-i\phi_1}|+\rangle] \xrightarrow{U_{atom}} \\ & |0\rangle [(\alpha a^* - \beta b^* e^{-i\phi_1}) |-\rangle + (\alpha b + \beta a e^{-i\phi_1}) |+\rangle] \xrightarrow{\text{A.C.}} \\ & [(\alpha a^* - \beta b^* e^{-i\phi_1}) |0\rangle - (\alpha b e^{i\phi_1} + \beta a) |1\rangle] |-\rangle. \end{aligned} \quad (4.52)$$

This operation may be written as the unitary operation acting on the field qubit

$$U = \begin{bmatrix} -1 & 0 \\ 0 & 1 \end{bmatrix} U_{field}(a, b e^{i\phi_1}). \quad (4.53)$$

For example, we get

$$\begin{aligned} a = -\frac{1}{\sqrt{2}}, \quad b = -\frac{e^{-i\phi_1}}{\sqrt{2}} \quad \Rightarrow \quad U_1 &= \frac{1}{\sqrt{2}} \begin{bmatrix} 1 & 1 \\ 1 & -1 \end{bmatrix} \\ a = 0, \quad b = -e^{-i\phi_1} \quad \Rightarrow \quad U_2 &= \begin{bmatrix} 0 & 1 \\ 1 & 0 \end{bmatrix} \\ a = -1, \quad b = 0 \quad \Rightarrow \quad U_3 &= \begin{bmatrix} 1 & 0 \\ 0 & -1 \end{bmatrix}. \end{aligned} \quad (4.54)$$

The first gate is a Hadamard gate, $U_1 = U_{Had}$, the second a Not-gate $U_2 = \sigma_x = U_{Not}$, the third one a 'inversion' gate $U_3 = \sigma_z$ and $U_3 U_2 = i\sigma_y$. Note that the atomic one qubit gate defined in equation (4.51) has a determinant equal to 1, while the field gate (4.53) has determinant -1.

4.2.2 Adiabatic quantum computing, with atom qubits

Performing single atomic gates is usually done by applying external laser fields. For resonant fields the effect on the atom is to transfer population between the

bare states $|\pm\rangle$ and by using off-resonant fields, the phases of the atomic state may be controlled. Thus having the tool of single qubit gates we only need to find, for example, a controlled phase-gate in order to have a universal set of gates. As argued above the 2-mode-1-atom and the 1-mode-2-atom systems behave very similarly in the lowest order of excitations. We may therefore translate the phase-gate of the previous subsection to the situation with two atoms a and b and one mode. We assume the atoms to interact far off resonance with the mode, then atom a 's transition frequency is tuned adiabatically across the mode frequency once, then atom b is tuned twice, back and forth, across the mode frequency, and finally atom a is again tuned adiabatically through a crossing. In the adiabatic limit and using the scattering matrix (3.14) we get

$$\begin{aligned} |0, -, -\rangle &\xrightarrow{\text{A.C.}a} |0, -, -\rangle \xrightarrow{\text{A.C.}b,b} |0, -, -\rangle \xrightarrow{\text{A.C.}a} |0, -, -\rangle \\ |0, -, +\rangle &\xrightarrow{\text{A.C.}a} |0, -, +\rangle \xrightarrow{\text{A.C.}b,b} -|0, -, +\rangle \xrightarrow{\text{A.C.}a} -|0, -, +\rangle \\ |0, +, -\rangle &\xrightarrow{\text{A.C.}a} -e^{i\phi_1}|1, -, -\rangle \xrightarrow{\text{A.C.}b,b} -e^{i\phi_1}|1, -, -\rangle \xrightarrow{\text{A.C.}a} |0, +, -\rangle \\ |0, +, +\rangle &\xrightarrow{\text{A.C.}a} -e^{i\phi_1}|1, -, +\rangle \xrightarrow{\text{A.C.}b,b} -e^{i\phi_1}|1, -, +\rangle \xrightarrow{\text{A.C.}a} |0, +, +\rangle, \end{aligned} \tag{4.55}$$

which simplified can be written as

$$\begin{aligned} |-, -\rangle &\rightarrow |-, -\rangle \\ |-, +\rangle &\rightarrow -|-, +\rangle \\ |+, -\rangle &\rightarrow |+, -\rangle \\ |+, +\rangle &\rightarrow |+, +\rangle. \end{aligned} \tag{4.56}$$

The gate may be realized by trapping both atom inside a cavity and by external lasers driving the separated atoms' transition frequencies. This, however, assumes that individual addressing of the two atoms is possible.

4.2.3 Non-adiabatic quantum computing, with field qubits

We conclude this section by giving an example of a two mode controlled phase-gate using the Λ -atom of subsection 4.1.4. Thus the dynamics is governed by the Hamiltonian (4.27) giving the general solution (4.28). Let us assume the field computational basis to be $\{|0\rangle, |3\rangle\}$ and pick the interaction time $g_0 t \sqrt{3} = \pi$; then

we find that the initial atomic states $|a\rangle$ or $|b\rangle$ will evolve according to

$$\begin{aligned} |0, 0, a\rangle &\rightarrow |0, 0, a\rangle & |0, 0, b\rangle &\rightarrow |0, 0, b\rangle \\ |0, 3, a\rangle &\rightarrow -|0, 3, a\rangle & |0, 3, b\rangle &\rightarrow |0, 3, b\rangle \\ |3, 0, a\rangle &\rightarrow |3, 0, a\rangle & |3, 0, b\rangle &\rightarrow -|3, 0, b\rangle \\ |3, 3, a\rangle &\rightarrow |3, 3, a\rangle & |3, 3, b\rangle &\rightarrow |3, 3, b\rangle. \end{aligned} \tag{4.57}$$

4.3 Effects due to a quantized atomic motion

In this section we treat the full quantum system with both the spatial variations of the cavity mode and the quantized center-of-mass motion of the atom included in the analysis. For physical cavity QED models one is mainly interested in a pulse shaped or a periodic coupling and as mentioned, there are only a few models that are analytically solvable; the sech^2 -mode model with zero detuning [55] and the mesa-mode model with arbitrary detuning [57, 58]. The situation of zero detuning and periodic mesa-barriers separates into standard Kronig-Penny models [72], where the spectrum is obtainable. The case when the coupling is a simple trigonometric function $\cos(kx)$ is identical to the Mathieu equations [59] in the limit of zero detuning. In the pulse models one may have tunneling resonances which affects the dynamics compared to a semi-classical treatment with a constant velocity. For periodic models, the band-spectrum determines the evolution of the atom-field system.

4.3.1 Effective parameters

In Paper VI we studied the evolution of either Gaussian dressed (3.37) or bare (3.38) states, exposed to the periodic coupling. The numerical methods used for the wave-packet propagation is the so called *split operator method* and it is briefly discussed in Appendix B. In order to talk about effective parameters describing the motion, the Gaussian states should have a relatively localized quasi-momentum. A Gaussian bare state is approximately a linear combination of Gaussian dressed states all with the same widths but shifted by an integer number of q 's, or equivalently they have the same mean k_0 but belong to different bands. Then, within the approximation limits, each component in the linear combination will evolve according to equation (3.41), where the effective parameters are calculated using (3.42) for the corresponding bands. Figure 4.6 shows the time evolution of a Gaussian dressed (left) and bare (right) state. The bare state splits up in three smaller ones while the dressed state remains fairly Gaussian. The inset displays the momentum distribution at the final time, indicating the three dressed components.

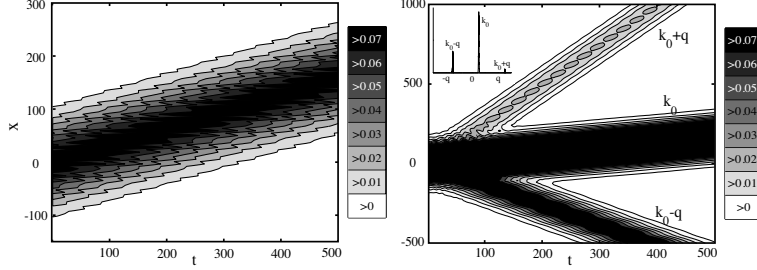


Figure 4.6: The evolution of Gaussian states, left dressed and right bare. From the figure it is clear that the bare wave-packet splits up into its three main dressed components, while the dressed state stays localized. The inset shows the final momentum distribution $|\langle k | \Psi \rangle|^2$. The parameters are $g_0 = 0.002$, $\Delta = 0$, $x_0 = 0$, $k_0 = 1/4$ and $\Delta_k^2 = 1/10000$.

We now want to verify numerically the effective parameters (3.42) using the wave-packet propagation methods and in order to do that we use the following

$$\begin{aligned} v_g &= \frac{\langle x \rangle_f - \langle x \rangle_0}{t_f}, \\ \Delta_x^2 &= \langle x^2 \rangle_t = \frac{1}{4\Delta_k^2} + \left(\frac{\Delta_k}{m_2} \right)^2 t^2. \end{aligned} \tag{4.58}$$

Here subscript f stands for final and 0 for initial. When calculating the expectation values $\langle x \rangle_{f,0}$ for the bare states only one component of the atomic wave-packet is used $\langle x \rangle = \frac{\langle -|x|-\rangle}{\langle -|-\rangle}$. When the coupling is not too large, the overlap between bare and dressed states is dominated for one atomic state, for example, for zero detuning and a small coupling, the lowest band with $-1/2 < k < 1/2$ is dominated by the bare state $|-\rangle$. This is the reason for only using one of the states in the calculations. Experimentally this means that a projective measurement must be performed onto the atomic bare states. As the bare wave-packets evolve, it is seen in figure 4.6 that it splits up into its dressed components, these might be very small, but since they are located on the tails they contribute significantly to the variance. In the calculation, we therefor 'cut' the wave-packet for $|x| > 150$. The results from the three different cases; Gaussian dressed, Gaussian bare, and Floquet approach (3.42), are displayed in figure 4.7. It shows great agreement between all three curves.

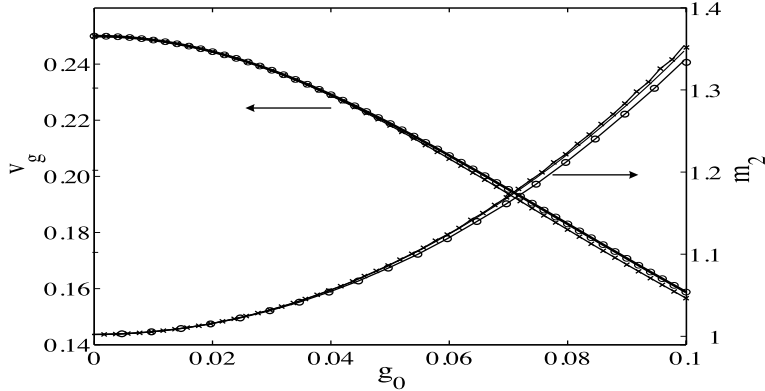


Figure 4.7: This figure shows the numerical results of the group velocity v_g and effective mass m_2 as function of the coupling strength. Circles show the results from bare state propagation, crosses for dressed states and solid line for the parameter values from direct calculation of the derivatives (3.42). In the calculation of v_g the initial momentum was $k_0 = 1/4$ while for m_2 it was picked at $k_0 = 0$. The other parameters are final time $t_f = 500$, $\Delta = 0$, $\Delta_x^2 = 2500$ (group velocity) and $\Delta_x^2 = 1500$ (effective mass).

4.3.2 Atom optics

Recently the area of atom optics has grown considerably, including, for example, Bose-Einstein condensates, atom cooling, atom lasers and mechanical light-forces on atoms. An overview can be found in the book [73]. We have already talked about forces from the light field felt by the atom in terms of effective parameters. In this subsection we take one further step to investigate the analogy with propagation of classical light pulses. In atom optics, the light-matter situation is often reversed; the matter waves, or the wave-packets act as the classical light pulse, while the field serves as the medium in which the 'pulse' propagates. We define the effective matter wave index of refraction as

$$n^a = \frac{v_0}{v} \quad (4.59)$$

or in three dimensions

$$\mathbf{n}^a = (v_{0x}/v_x, v_{0y}/v_y, v_{0z}/v_z), \quad (4.60)$$

where v_0 is the atomic center-of-mass velocity in the absence of fields. The velocity v is given by the group velocity, giving that the index of refraction is the same

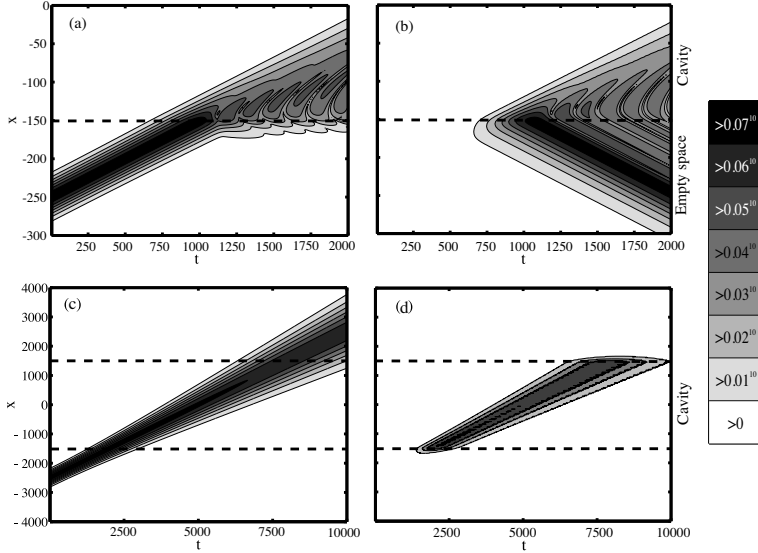


Figure 4.8: The scattering of a wave-packet against a cavity mode. In (a) and (b), the energy of the free space wave-packet coincide with the first energy gap ($k_0 = 1/2$) of the energy band spectrum corresponding to the standing wave mode in the cavity, and in (c) and (d) the kinetic energy of the atom is 'allowed' to enter the cavity field ($k_0 = 1/4$). The left plots show the upper atomic state while the right plots display the lower atomic states, and the cavity is schematically marked by the dashed lines. We note that in the first two plots approximately all of the wave-packet is reflected, while in the last two the atom is transmitted through the cavity. Note also that in the second example, the lower atomic state is only populated while being inside the cavity, which, however, from the contour scale indicates that it is only weakly populated. Here the parameters are $g_0 = 0.02$, $\Delta = 0$, $\Delta_x^2 = 2500$ and $x_1 = 1500$.

as the effective mass ratio m_1/m , where m is the 'free' mass. We first assume that an atom moves in free space in the x direction and enters upon a cavity with a standing wave mode in the same direction. In order to represent the cavity numerically we multiply the standing wave mode with the function

$$\bar{g} = \frac{1}{2} \left[\tanh\left(\frac{x + x_1}{x_e}\right) - \tanh\left(\frac{x - x_1}{x_e}\right) \right]. \quad (4.61)$$

This function goes to zero for large $|x|$ and is centered around $x = 0$, the cavity length is given by $2x_1$, and the 'slope' how fast it turns on/off is determined by

x_e . The length of the cavity is assumed to be much longer than the wavelength, which in scaled units reads $x_1 \gg \pi$. If the energy of the incoming atomic wave-packet is such that it coincides with an energy gap in the cavity spectrum, the effective parameters go to infinity and the atom cannot enter. Due to energy and momentum conservation the atom must be reflected with its initial velocity. If the atom is initially in its upper state and has a momentum corresponding to the first energy gap $k = 1/2$ ($\Delta = 0$), the reflecting state will have momentum $k = -1/2$ and the atom will be in its lower state leaving one photon to the cavity field. On the other hand, if the atom enters the cavity with an energy falling within the allowed energy bands it will enter. As it traverses the cavity, the two bare states will couple, so if the atom is initially excited, the lower atomic state will be populated while inside the cavity. For weak couplings this population will be small. In figure 4.8 we show the results of numerical wave-packet simulations, which clearly confirm our predictions. The contour scale has been chosen such that the tails of the wave-packets are seen, which might give a false impression of the actual non-logarithmic shapes.

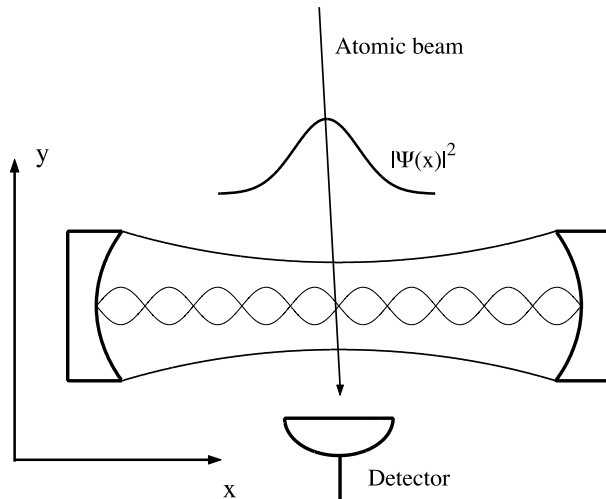


Figure 4.9: A possible experimental setup. The angle of the atomic beam sets the initial velocity k_0 in the x direction.

In order to have kinetic energies of the incoming atoms that fall into the first energy band the atom must be cooled down to temperatures order of magnitudes colder than μK scale, which is presently out of reach with current techniques. So in order to experimentally realize the scenario above, the scattering must take

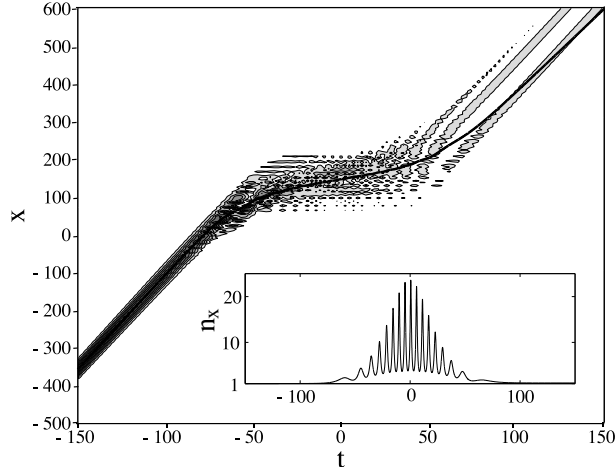


Figure 4.10: The passage of an excited atom through a cavity setup as in the previous figure. The atom is clearly slowed down while traversing the cavity, which means that the effective index of refraction (shown in the insert), or equivalently the inverse of the group velocity, increases. The Gaussian shape of n_x has a narrower width than the coupling amplitude $g_0(t)$. The plot shows the full atomic wave packet; $|\Psi(x, t)|^2 = |\langle + | \langle x | \Psi \rangle|^2 + |\langle - | \langle x | \Psi \rangle|^2$. The solid line gives $\langle x \rangle_t$.

place within higher energy bands. The band gaps decrease with the band index, but in cavity QED experiments, the coupling strength g_0 is very large giving clear band gaps also higher up in the spectrum. However, there is another possibility where arbitrary low velocities are achievable shown in figure 4.9. The velocity in the y direction is assumed classical so that the y -dependence of the coupling can be substituted by $v_{0y}t$, while the small angle of the atomic beam gives very small velocities v_{0x} . Thus, we may have the effective coupling $g(x, t) = g_0(t) \cos(x)$, where $g_0(t)$ has a Gaussian shape. Assuming a classical velocity gives the effective index of refraction $n_y = 1$ throughout the propagation, while n_x will change inside the cavity. Since the coupling amplitude changes in time, so will n_x . In figure 4.10 we have simulated the scattering of figure 4.9 by plotting the full, both upper and lower atomic state wave-packets. The atom is initially excited and the cavity empty, and we use a Gaussian time-dependence of the mode amplitude with a width $\Delta_t^2 = 2025$. The thick line gives $\langle x \rangle_t$ and the index of refraction, $n_x = v_{0x} / (d\langle x \rangle_t / dt)$, is shown in the inset. Note the oscillations of the index of refraction caused by the population exchange between internal states $|\pm\rangle$.

4.3.3 Generalized Bloch oscillations and tunneling

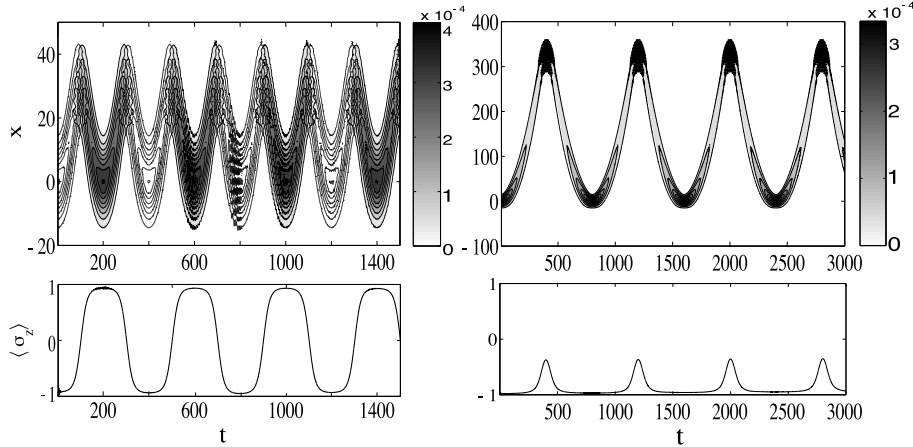


Figure 4.11: The wave-packet evolution and the atomic inversion $\langle \sigma_z \rangle$. In the left plots the detuning is zero while in the right one it is $\delta = 1$ corresponding to figure 3.3 (a) and (c) respectively. The coupling is $V_0 = 0.2$ in both plots and $F = 0.005$ for the zero detuning case and $F = 0.0025$ in the other case. Filled contour lines shows the upper atomic state wave-packet in the left plot and lower atomic states in the right plot and reversely for unfilled curves. Note how the internal state is flipped between every oscillation in the zero detuning case, but not in the detuned one. This is easily understood from the band spectrum of figure 3.3

In subsection 3.3.3 we discussed the behaviour of a wave-packet in the periodic potential exposed to a linear force. The effective light potential thus has the form $V_0 \cos(x) + Fx$ and we argued that if F is small compared to V_0 , a Gaussian dressed state wave-packet will oscillate in x -space. When the force F was weak we could apply the acceleration theorem saying that the quasi-momentum grows linearly in time; $k = k_0 - Ft$. Population within one band remains in the same band also after traversing the level-crossings, and from figure 3.4 it was seen that the group velocity will oscillate around zero. The evolution of initial bare state Gaussian wave-packets are shown in figure 4.11 for two different detunings; $\delta = 0$ left plots and $\delta = 1$ right plots. From figure 3.3 (a) and (c) we note that these two examples have two different kinds of level-crossings, in the first (a) only two levels cross, while in the second (c) three different levels cross. In (a) and in the limit of weak coupling V_0 , the lowest band consist of alternating upper and lower atomic internal states, resulting in that when k is swept, the internal state is flipped between $|+\rangle$

and $|-\rangle$. In (c), on the other hand, the lower state solely consist of upper state atomic states. This is verified in figure 4.11 where the atomic inversions are also plotted. In the right plot of the inversion, it is seen that a small part of the upper atomic state is populated during the passage through a crossing, which indicates that when the energy curves become close the dressed states are mixtures of both internal states $|\pm\rangle$.

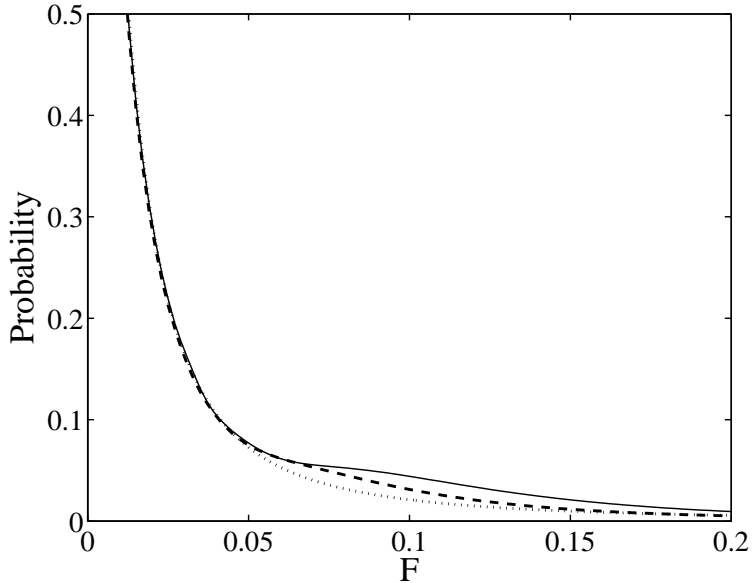


Figure 4.12: The probability of remaining in the same band after a passage of a level-crossing, similar to that one of figure 3.3 (d). The initial state is a Gaussian bare state wave-packet $|+\rangle$ with $k_0 = -1/2$ and it has been propagated to $k = 1/2$. Solid line is the probability of finding the atom in the upper state with momentum $-1 < p < 0$, dotted line is the probability of finding the atom in the lowest band $\nu = 1$ and dashed line displays the analytic result from linearization of the energy curves around the crossing. For large forces F the probabilities approach zero saying that the adiabaticity is all gone and the atom accelerates freely according to the linear force. The parameters are $V_0 = 0.2$, $k_0 = 1/2$ and $\Delta_x^2 = 50$.

As mentioned in subsection 3.3.3 one may estimate the non-adiabatic transitions between nearby energy bands by linearizing the models around a crossing. This has been done in [74] for the case of two-level crossings, while in Paper VII we do it for the three-level crossings. Using the three-level Landau-Zener model in-

troduced in subsection 3.3.3 one finds the probability to remain in the lowest band after one passage of a crossing $(1 - P)^2$ where $P = \exp(-\Lambda/2)$ with $\Lambda = \pi V_0^2/4F$. This analytic result is compared with results obtained from wave-packet simulations in figure 4.12. The analytic result is shown with the dashed line while the dotted line gives the probability of ending up in the lowest band $\nu = 1$ and solid line the probability of staying in the bare state $|+\rangle$. The initial state is here a Gaussian bare state in $|+\rangle$ with $k_0 = -1/2$ and it has been propagated to $k = 1/2$ across one crossing, see figure 3.3 (d). The coupling is fairly small, $V_0 = 0.2$, indicating that the lowest dressed state has a large overlap with $|+\rangle$ at $k = \pm 1/2$. The three curves clearly show the same trend, but differ slightly around $F = 0.1$.

4.3.4 STIRAP with quantized motion

The STIRAP Hamiltonian was introduced in equation (3.15), and the idea behind it is to have an adiabatic evolution and control the pulses $G_1(t)$ and $G_2(t)$ so that population can be transferred between different bare states. We saw that if the pulses were switched on and off in a counterintuitive way population is transferred coherently from $|c\rangle$ to $|a\rangle$. In the standard experimental setup [24], an atom/molecule traverses two overlapping laser beams with Gaussian mode shapes. Usually the approximation of replacing the kinetic energy and the position operators by its classical counterparts, giving a semi-classical model, is in general only justified for the dark state evolution, as will be shown. To my knowledge, the wave-packet treatment with spatially dependent pulses has not been studied. In [75], the STIRAP situation is considered with wave-packets, but for time-dependent pulses.

The fully quantized STIRAP Hamiltonian is then given by

$$H_S = -\frac{\partial^2}{\partial x^2} + \begin{bmatrix} 0 & G_1(x) & 0 \\ G_1(x) & \Delta & G_2(x) \\ 0 & G_2(x) & 0 \end{bmatrix} \quad (4.62)$$

and the bare state vectors are on the form

$$\langle x|\Psi(t)\rangle = \begin{bmatrix} \psi_a(x, t) \\ \psi_b(x, t) \\ \psi_c(x, t) \end{bmatrix}. \quad (4.63)$$

The initial state is given by only one $\psi_i(x, 0) = \chi(x)$ with $\chi(x)$ a Gaussian, so that we start with a Gaussian bare state wave-packet. The x -dependent pulses are assumed Gaussian with an amplitude g_0 , and to be applied in a counterintuitive order. The dressed states of the second part of the above Hamiltonian were given in

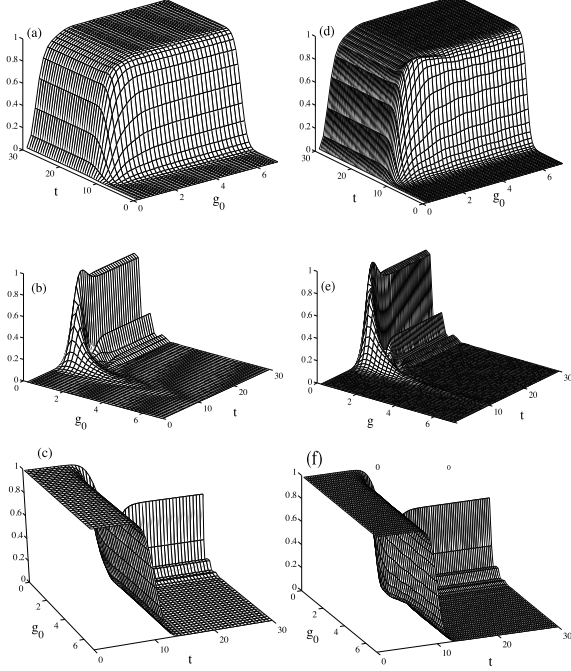


Figure 4.13: The norms $\int |\psi_i(x,t)|^2 dx$, $i = a, b, c$ respectively as function of t and g_0 for quantized motion (a)-(c) and semi-classical motion (d)-(f). This figure shows the dark state evolution, and it is clear that the two treatments agree considerably. The non complete transfer for small couplings is due to non-adiabatic evolution. The pulses $G_{1,2}(x)$ have widths $\sigma_G = 15$ and are located at $x = \pm 20$.

equation (3.16). For the counterintuitive pulse sequence, population is assumed to be transferred between the states $|c\rangle$ and $|a\rangle$, and for the dark state the upper atomic level $|b\rangle$ is only virtually populated. However, in subsection 3.3.1 it was shown that the dressed states effectively see a potential well or barrier, which for momentum smaller than the height gave tunneling resonances. Classically such states should be reflected, but quantum mechanically states fulfilling these resonance conditions may be transmitted. The STIRAP eigenvalues are given in equation (3.17) and we note that the first gives a barrier, the second a free propagation and the last a potential well. Thus, since the eigenvalue is identically zero for the dark state, there should be no scattering resonances, and all population should be transmitted. This is indeed the case and has been verified numerically. In figure 4.13 (a)-(c), the norms $\int |\psi_i(x,t)|^2 dx$, $i = a, b, c$ obtained from wave-packet propagation, are

shown as functions of the coupling amplitudes g_0 for an initial atomic momentum $p_0 = 5$ and zero detuning $\Delta = 0$. The STIRAP works perfectly for couplings $g_0 \sim 2$ or larger, which can be understood from the adiabatic theorem saying that the adiabaticity is directly related to the distance between energy eigenstates. In (d)-(f) the same is shown but now when the problem has been turned into a time-dependent one by substituting $x \rightarrow vt$ in the pulses $G_{1,2}(x)$ and neglecting the kinetic energy term. The coupled first order three-level differential equations have been solved numerically using the Runge-Kutta method. The agreement is nearly perfect, which is, however, a consequence of the 'free' evolution of the dressed dark state due to the zero eigenvalue. We expect less agreement for a state with non-zero eigenvalue components. In figure 4.14 we again show the norms from wave-packet simulations with an initial Gaussian bare state $|a\rangle$, but only for the final time when the system has reached its asymptotic limit. The rest of the parameters are as in figure 4.13. The oscillations between the two states $|b\rangle$ and $|c\rangle$ die out for increasing coupling amplitudes, and at $g_0 \sim 25$ ($p_0 = 5 \Rightarrow p_0^2 = 25$) parts of the wave-packet start to be reflected. At even larger couplings we note that tunneling resonances become important. The adiabatic solutions from the time-dependent model are given by equation (3.19), which clearly differ from the full quantum solutions in figure 4.14.

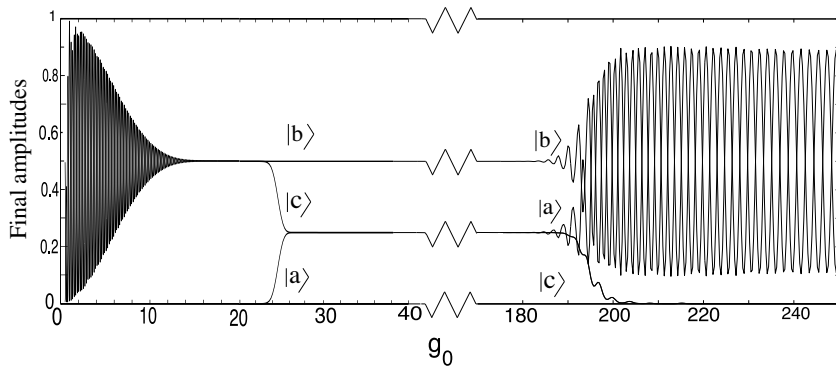


Figure 4.14: The asymptotic norms $\int |\psi_i(x)|^2 dx$, $i = a, b, c$ as function of g_0 for quantized motion. The atom is initially in the state $|a\rangle$, otherwise the parameters are as in figure 4.13. Note how the oscillations between the two states collapse, which is not the case in the semi-classical time-dependent model (not shown here) see (3.19), then at around $g_0 \approx 25$ ($= p_0^2$) the barrier becomes larger than the kinetic energy and the wave-packet starts to be reflected and finally for couplings larger than 200 we see the tunneling resonances.

Finally we plot in figure 4.15 the evolution of the wave-packets in x -space to show how the transfer takes place. The parameters are $p_0 = 5$ and $g_0 = 5$, and the transfer is nearly perfect.

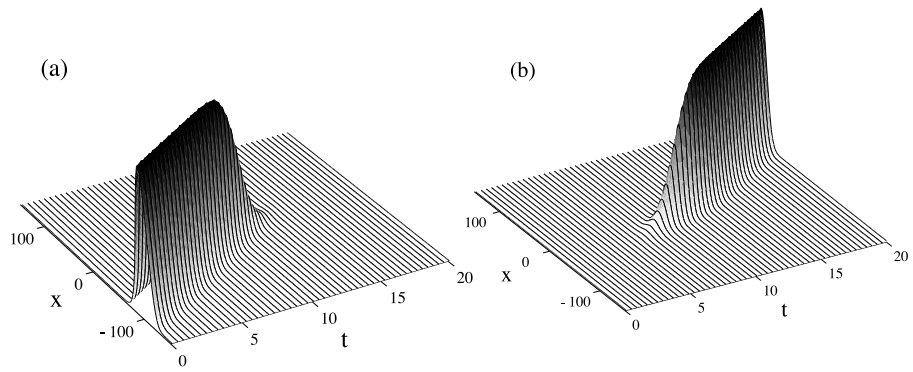


Figure 4.15: The Evolution of the wave-packets $|\psi_i(x,t)|^2$, $i = c$ (plot a) and $i = a$ (plot b). The final population in the state $|a\rangle$ is 100 %. Here $g_0 = 5$ and the other parameters are as in the previous figure 4.13.

Chapter 5

Conclusion

The dynamics of the most simple quantum systems has often proved to be more complex than first expected. Even for the especially simple JC model, a wide range of interesting phenomena has been discovered since its introduction in the 60's [3]. When experiments showed that the model correctly described the observed results, it gained even more interest. As the experiments developed, some modifications or extensions of the original JC model was in order. Several generalizations and more complex versions of the JC model have been published since. Here, in this thesis, I have summarized our results and studies done on some of these extensions when applied to cavity QED.

It has been divided into three groups: multi-level JC models, time-dependent JC models and position-momentum dependent JC models. Various models known from other areas in physics have been applied in order to find correct or approximated results. For all three groups, adiabaticity and the adiabatic theorem has served as a motivation and explanation of the dynamics. Simple expressions for different quantities are often obtained in the adiabatic limit, and the validity of these results has been tested both using analytical and numerical investigations. The central part is the understanding of the evolution of the systems, but several applications, such as state preparation and quantum computing, are given. For the last group, x - p -dependent JC models, numerical studies of wave-packet propagations for different kind of atom-field couplings have been carried out. These results have been compared to results from either direct numerical integration of the Schrödinger equations, analytical approximations or effective treatments of the models. Good agreement between the different approaches was found, and deviations were discussed. Dissipation and decoherence have not been included in the analysis, assuming that the coherent time-scales are much shorter than the decoherent ones. This is usually the case for single Rydberg atoms passing through

a high Q cavity, but often it is desirable to let several atoms pass the cavity one after the other, and the separate interaction times add. As mentioned, many of the results rely on being in the adiabatic regime, and adiabaticity directly means slow changes in time giving long interaction times. Thus, there is a conflict of achieving high fidelities in short times. However, the adiabatic regime may still be much shorter than typical decay times, but nonetheless it sets a bound on the number of operations achievable.

The models discussed in this thesis are not, by any means, exhaustive, and there are many possible continuations, where the limit is set by ones imagination. For the multi-level JC models, new atom-field configurations are constantly popping up, and interesting effective Hamiltonians with nice properties are derived. JC models with a non-linear medium, or *Kerr* models [76], have not been discussed here, and one may apply ideas from this thesis to such systems. Driven models [77] have just been mentioned briefly here and one may explore such cases. The time-dependent treatment of the original two-level JC model mostly uses analytically solvable models, and one could go beyond these models and try to numerically find other time-dependences of the parameters that gives interesting filter functions. For example, what time-dependence would give a filter function that selects one particular Fock state, such that by a successful conditional atomic measurement the field is reduced to one single Fock state? The examples of atom-cavity configurations giving the multi-STIRAP models could be examined further to find other set-ups with desirable properties. The section on quantum computing with time-dependent JC models may be analyzed further, to find new gates or even simple algorithms. The wave-packet simulation for atoms with quantized center-of-mass motion, is not a very well studied area in the literature and there one could, for example, look into more physically realizable models, with realistic parameters. The STIRAP with quantized motion is not a completed chapter, and the concept of a quantized motion could be tested on any of the multi-level JC models. The fresh areas of combining ion traps together with cavities [26, 78] or solid state qubit devices together with cavities [79] have not been considered. Our analysis of the extended JC models have been focusing on cavity QED systems, and it is likely that much of the studies are applicable to other fields where the JC or similar models are used. Finally, the research is purely theoretical and the relevance of the results concerning the existing current experiments has not been investigated in great detail.

Appendix A

Adiabaticity

In this appendix we briefly discuss the adiabatic theorem [80] and we perform two calculations; one of adiabatic elimination of a largely detuned atomic level using canonical transformations and we also derive the acceleration theorem. Throughout this thesis, we have seen examples of adiabatic evolution and argued that within the adiabatic limit, simple analytic expressions are obtained for the final populations. We have also mentioned some solvable time-dependent models, where the most known one is the Landau-Zener model, and these have been used for finding a measure of non-adiabatic contributions.

Given a time-dependent Hamiltonian $H(t)$ and where $E_n(t)$ and $|\psi_n(t)\rangle$ are the instantaneous n 'th eigenvalues and eigenstates, then the theorem states that for an infinitely slow process we have

$$H(t)|\psi_n(t)\rangle = E_n(t)|\psi_n(t)\rangle, \quad \forall t. \quad (\text{A.1})$$

Let $U(t)$ be the unitary operator that diagonalizes $H(t)$ and $|\tilde{\psi}_n(t)\rangle = U^{-1}(t)|\psi_n(t)\rangle$, then the time-dependent Schrödinger equation can be written as

$$H_d(t)|\tilde{\psi}_n(t)\rangle = i\partial_t|\tilde{\psi}_n(t)\rangle - i[\partial_t U^{-1}(t)]U(t)|\tilde{\psi}_n(t)\rangle. \quad (\text{A.2})$$

The solution of the Schrödinger equation can be expressed in the instantaneous eigenstates as

$$|\Psi(t)\rangle = \sum_n a_n(t) e^{-i \int_0^t E_n(\tau) d\tau} |\psi_n(t)\rangle, \quad (\text{A.3})$$

which after substitution into the Schrödinger equation and multiplication with $\langle\psi_k(t)|$ gives

$$\partial_t a_k(t) = - \sum_n a_n(t) \langle\psi_n(t)|\partial_t|\psi_n(t)\rangle e^{-i \int_0^t \delta E_{nk}(\tau) d\tau}, \quad (\text{A.4})$$

where $\delta E_{nk}(t) = E_n(t) - E_k(t)$. Taking the time derivative of equation (A.1) and multiplying with $\langle \psi_k(t) |$ one finds

$$\langle \psi_k(t) | \partial_t | \psi_n(t) \rangle = \frac{\langle \psi_k(t) | [\partial_t H(t)] | \psi_n(t) \rangle}{\delta E_{nk}(t)}. \quad (\text{A.5})$$

Thus, equation (A.4) becomes

$$\partial_t a_k(t) = -a_k(t) \langle \psi_k(t) | \partial_t | \psi_k(t) \rangle - \sum_{n \neq k} a_n(t) \frac{\langle \psi_k(t) | [\partial_t H(t)] | \psi_n(t) \rangle}{\delta E_{nk}(t)} e^{-i \int_0^t \delta E_{nk}(\tau) d\tau}, \quad (\text{A.6})$$

meaning that if

$$\left| \frac{\langle \psi_k(t) | [\partial_t H(t)] | \psi_n(t) \rangle}{\delta E_{nk}(t)} \right| \ll |\delta E_{nk}(t)|, \quad \forall t \quad (\text{A.7})$$

the individual eigenstates evolve independently. Equation (A.7) is to be given as a general condition for having adiabatic evolution.

In subsection 3.2 it was shown that within certain conditions the time-independent Hamiltonian could be approximated by a time-dependent one lacking the operators x and p . For the resulting time-dependent system one may apply the adiabatic theorem. Below, when deriving the acceleration theorem, we show how to obtain a time-dependent problem from a stationary one. Thus, adiabaticity is not just a matter for systems depending explicitly on time and one would like to have some kind of constraints also for the evolution of some time-independent systems. We are especially interested in Jaynes-Cummings type of models

$$H = -\partial_x^2 + \begin{bmatrix} \frac{\Delta}{2} & g_0(x)\sqrt{n} \\ g_0(x)\sqrt{n} & -\frac{\Delta}{2} \end{bmatrix}. \quad (\text{A.8})$$

By using the unitary operator of equations (2.13) and (2.14)

$$U = \begin{bmatrix} \cos(\theta/2) & -\sin(\theta/2) \\ \sin(\theta/2) & \cos(\theta/2) \end{bmatrix}, \quad \tan[\theta(x)] = -\frac{g_0(x)\sqrt{n}}{\Delta(x)} \quad (\text{A.9})$$

one finds the transformed Hamiltonian

$$\begin{aligned} \tilde{H} = U H U^{-1} &= -\partial_x^2 - \begin{bmatrix} 0 & -\partial_x \theta \\ \partial_x \theta & 0 \end{bmatrix} \partial_x + \frac{1}{2} \begin{bmatrix} 0 & -\partial_x^2 \theta \\ \partial_x^2 \theta & 0 \end{bmatrix} \\ &+ \begin{bmatrix} E_+(x) + (\partial_x \theta/2)^2 & 0 \\ 0 & E_-(x) + (\partial_x \theta/2)^2 \end{bmatrix}, \end{aligned} \quad (\text{A.10})$$

where $E_{\pm}(x)$ are the eigenvalues (2.15). Using the definition of the angle θ we have

$$\partial_x \theta = \frac{\Delta \sqrt{n} \partial_x g_0(x)}{\Delta^2 + 4ng_0^2(x)}. \quad (\text{A.11})$$

The adiabatic couplings, the off-diagonal terms of equation (A.10), measure the variation of the effective potential and hence the force on the atom. In order to have an adiabatic evolution we request the kinetic energy to be greater than the off-diagonal adiabatic corrections

$$\frac{2\pi}{\lambda_{dB}} \gg \left| \frac{\Delta \sqrt{n} \partial_x g_0(x)}{\Delta^2 + 4ng_0^2(x)} \right|, \quad (\text{A.12})$$

where λ_{dB} is the deBroglie wave-length related to the atomic momentum. For further discussions of the adiabatic theorem see, for example, [80] and [81].

Adiabatic elimination of the upper level in a Λ -atom

We will follow the method used in [44], applying a unitary transformation to the Hamiltonian. This is, however, not the standard way of how adiabatic elimination usually is performed. Using the notation of [44] the Hamiltonian is

$$H_{\Lambda} = \sum_{i=1}^3 \Omega_i \sigma_{ii} + \omega_1 a_1^\dagger a_1 + \omega_2 a_2^\dagger a_2 + g_{12} (a_1 \sigma_{21} + a_1^\dagger \sigma_{12}) + g_{32} (a_2 \sigma_{32} + a_2^\dagger \sigma_{23}), \quad (\text{A.13})$$

where $\sigma_{ij} = |i\rangle\langle j|$ and state $|2\rangle$ is the upper atomic state. We further introduce the detunings $\Delta_1 = \Omega_2 - \Omega_1 - \omega_1$ and $\Delta_3 = \Omega_2 - \Omega_3 - \omega_2$ and the unitary operator

$$U = e^S, \quad (\text{A.14})$$

where

$$S = \alpha (a_1 \sigma_{21} - a_1^\dagger \sigma_{12}) + \beta (a_2 \sigma_{32} - a_2^\dagger \sigma_{23}). \quad (\text{A.15})$$

Here α and β are constants that will be determined later. Let us also note that

$$\begin{aligned} \sum_{i=1}^3 \Omega_i \sigma_{ii} &= \frac{1}{3} (\Omega_1 + \Omega_2 + \Omega_3) + \frac{1}{3} (3\Omega_3 - \Omega_1 - \Omega_2) (\sigma_{33} - \sigma_{11}) \\ &\quad - \frac{1}{3} (\Omega_3 + \Omega_1 - 2\Omega_2) (\sigma_{22} - \sigma_{11}). \end{aligned} \quad (\text{A.16})$$

We now make a perturbative analysis keeping terms to second order in the coupling constants. We denote transformed operators by prime and use the following relation

$$X' = e^S X e^{-S} = X + [S, X] + \frac{1}{2!} [S, [S, X]] + \dots. \quad (\text{A.17})$$

The various transformed operators become

$$\begin{aligned}
a'_1 &= a_1 + \alpha\sigma_{12} + \frac{\alpha^2}{2}a_1(\sigma_{22} - \sigma_{11}) - \frac{\alpha\beta}{2}a_2\sigma_{13}, \\
a'_2 &= a_2 + \beta\sigma_{32} + \frac{\beta^2}{2}a_2(\sigma_{33} - \sigma_{22}) - \frac{\alpha\beta}{2}a_1\sigma_{31}, \\
\sigma'_{12} &= \sigma_{12} + \alpha a_1(\sigma_{22} - \sigma_{11}) - \beta a_2\sigma_{13}, \\
\sigma'_{23} &= \sigma_{23} - \beta a_2^\dagger(\sigma_{33} - \sigma_{22}) - \alpha a_1^\dagger\sigma_{13}, \\
\sigma'_{22} - \sigma'_{11} &= (\sigma_{22} - \sigma_{11}) - 2\alpha a_1\sigma_{21} - 2\alpha a_1^\dagger\sigma_{12} - \beta a_2\sigma_{23} - \beta a_2^\dagger\sigma_{32} - (2\alpha^2 + \beta^2)\sigma_{22} \\
&\quad - 2\alpha^2 a_1^\dagger a_1(\sigma_{22} - \sigma_{11}) + \beta^2 a_2^\dagger a_2(\sigma_{33} - \sigma_{22}) + \frac{3}{2}\alpha\beta(a_2^\dagger a_1\sigma_{31} + a_1^\dagger a_2\sigma_{13}), \\
\sigma'_{33} - \sigma'_{11} &= (\sigma_{33} - \sigma_{11}) - \alpha a_1\sigma_{21} - \alpha a_1^\dagger\sigma_{12} + \beta a_2\sigma_{23} + \beta a_2^\dagger\sigma_{32} \\
&\quad + (\beta^2 - \alpha^2)\sigma_{22} - \alpha^2 a_1^\dagger a_1(\sigma_{22} - \sigma_{11}) - \beta^2 a_2^\dagger a_2(\sigma_{33} - \sigma_{22}). \tag{A.18}
\end{aligned}$$

By choosing $\alpha = g_{12}\Delta_1$ and $\beta = g_{23}/\Delta_3$ the terms linear in the field operators vanish and the transformed Hamiltonian is given by

$$\begin{aligned}
H'_\Lambda &= \Omega_1\sigma_{11} + \Omega_3\sigma_{33} + \left(\Omega_2 + \frac{g_{12}^2}{\Delta_1} + \frac{g_{23}^2}{\Delta_3}\right)\sigma_{22} + \frac{g_{12}^2}{\Delta_1}a_1^\dagger a_1(\sigma_{22} - \sigma_{11}) + \frac{g_{23}^2}{\Delta_1}a_2^\dagger a_2(\sigma_{22} - \sigma_{33}) \\
&\quad + \omega_1 a_1^\dagger a_1 + \omega_2 a_2^\dagger a_2 - \frac{g_{12}g_{23}}{2}\left(\frac{1}{\Delta_1} + \frac{1}{\Delta_2}\right)(a_1^\dagger a_2\sigma_{23} + a_2^\dagger a_1\sigma_{31}). \tag{A.19}
\end{aligned}$$

From the structure of H'_Λ we note that the upper level $|2\rangle$ is not coupled to the other two levels, while those two levels couple through a two photon process. The Stark-shift terms of levels $|1\rangle$ and $|3\rangle$ are proportional to $a_1^\dagger a_1$ and $a_2^\dagger a_2$ respectively, while level $|2\rangle$ is affected by both field amplitudes.

Acceleration theorem

We here derive the acceleration theorem used in subsections 3.3.3 and 4.3.3.

We start with the Schrödinger equation

$$\begin{aligned} i\partial_t \Psi(x, t) &= (-\partial_x^2 + \frac{\delta}{2}\sigma_z + g_0 \cos(x)\sigma_x - Fx) \Psi(x, t) \Leftrightarrow \\ i\partial_t \Phi(k, t) &= k^2 \Phi(k, t) + \frac{\delta}{2}\sigma_z \Phi(k, t) + g_0 \sigma_x (\Phi(k-1, t) + \Phi(k+1, t)) - iF \partial_k \Phi(k, t). \end{aligned} \quad (\text{A.20})$$

In the absent of a force the dressed states are given by

$$k^2 |\phi_\nu(k)\rangle + \frac{\delta}{2} \sigma_z |\phi_\nu(k)\rangle + g_0 \sigma_x (|\phi_\nu(k-1)\rangle + |\phi_\nu(k+1)\rangle) = E_\nu(k) |\phi_\nu(k)\rangle, \quad (\text{A.21})$$

which we use for expanding the states $\Phi(k, t)$ according to

$$\Phi(k, t) = \sum_\nu d_\nu(k, t) e^{-iE_\nu(k)t} |\phi_\nu(k)\rangle. \quad (\text{A.22})$$

Substitution of this state in the time-dependent Schrödinger equation gives

$$\begin{aligned} i\partial_t \Phi(k, t) &= i \sum_\nu [\partial_t d_\nu(k, t)] e^{-iE_\nu(k)t} |\phi_\nu(k)\rangle + \sum_\nu E_\nu(k) d_\nu(k, t) e^{-iE_\nu(k)t} |\phi_\nu(k)\rangle \\ &= \sum_\nu d_\nu(k, t) e^{-iE_\nu(k)t} \underbrace{\left[k^2 |\phi_\nu(k)\rangle + \frac{\delta}{2} \sigma_z |\phi_\nu(k)\rangle + g_0 \sigma_x (|\phi_\nu(k-1)\rangle + |\phi_\nu(k+1)\rangle) \right]}_{= E_\nu(k) |\phi(k)\rangle} \\ &\quad - iF \partial_k \sum_\nu d_\nu(k, t) e^{-iE_\nu(k)t} |\phi_\nu(k)\rangle, \end{aligned} \quad (\text{A.23})$$

which after simplification and projection onto $e^{+iE_\mu(k)t} \langle \phi_\nu(k) |$ becomes

$$\begin{aligned} i\partial_t d_\mu(k, t) &= -iF \partial_k d_\mu(k, t) - F t V_\mu(k) d_\mu(k, t) \\ &\quad - iF \sum_\nu d_\nu(k, t) e^{-i[E_\nu(k) - E_\mu(k)]t} \langle \phi_\mu(k) | \partial_k | \phi_\nu(k) \rangle, \end{aligned} \quad (\text{A.24})$$

where

$$V_\mu = \frac{dE_\mu(k)}{dx}. \quad (\text{A.25})$$

We write the coefficients as

$$d_\mu(k, t) = A_\mu(k - Ft, t) e^{+iF \int_0^t \tau V_\mu(k - Ft + F\tau) d\tau} \quad (\text{A.26})$$

and substitute in the above expression, where we use $\partial_{(1)}$ and $\partial_{(2)}$ for derivatives

with respect to the first and second argument respectively

$$\begin{aligned}
& i\partial_t \left[A_\mu(k - Ft, t) e^{+iF \int_0^t \tau V_\mu(k - Ft + F\tau) d\tau} \right] \\
&= -iF \left[\partial_{(1)} A_\mu(k - Ft, t) \right] e^{+iF \int_0^t \tau V_\mu(k - Ft + F\tau) d\tau} \\
&\quad + i \left[\partial_{(2)} A_\mu(k - Ft, t) \right] e^{+iF \int_0^t \tau V_\mu(k - Ft + F\tau) d\tau} \\
&\quad + iA_\mu(k - Ft, t) (iFtV_\mu(k)) e^{+iF \int_0^t \tau V_\mu(k - Ft + F\tau) d\tau} \\
&\quad + iA_\mu(k - Ft, t) \left(iF(-F) \int_0^t \tau V'_\mu(k - Ft + F\tau) d\tau \right) e^{+iF \int_0^t \tau V_\mu(k - Ft + F\tau) d\tau} \\
&= -iF\partial_k \left[A_\mu(k - Ft, t) e^{+iF \int_0^t \tau V_\mu(k - Ft + F\tau) d\tau} \right] \\
&\quad - FtV_\mu(k) \left[A_\mu(k - Ft, t) e^{+iF \int_0^t \tau V_\mu(k - Ft + F\tau) d\tau} \right] \\
&\quad - iF \sum_\nu d_\nu(k, t) e^{-i(E_\nu(k) - E_\mu(k))t} \langle \phi_\mu(k) | \partial_k | \phi_\nu(k) \rangle \\
&= -iF \left[\partial_{(1)} A_\mu(k - Ft, t) \right] e^{+iF \int_0^t \tau V_\mu(k - Ft + F\tau) d\tau} \\
&\quad - iFA_\mu(k - Ft, t) \left(iF \int_0^t \tau V'_\mu(k - Ft + F\tau) d\tau \right) e^{+iF \int_0^t \tau V_\mu(k - Ft + F\tau) d\tau} \\
&\quad - FtV_\mu(k) \left[A_\mu(k - Ft, t) e^{+iF \int_0^t \tau V_\mu(k - Ft + F\tau) d\tau} \right] \\
&\quad - iF \sum_\nu d_\nu(k, t) e^{-i(E_\nu(k) - E_\mu(k))t} \langle \phi_\mu(k) | \partial_k | \phi_\nu(k) \rangle. \tag{A.27}
\end{aligned}$$

This leads to

$$\begin{aligned}
\partial_{(2)} A_\mu(k - Ft, t) &= -F \sum_\nu A_\nu(k - Ft, t) e^{iF \int_0^t \tau V_\nu(k - Ft + F\tau) d\tau} e^{-iF \int_0^t \tau V_\mu(k - Ft + F\tau) d\tau} \\
&\quad \times e^{-i(E_\nu(k) - E_\mu(k))t} \langle \phi_\mu(k) | \partial_k | \phi_\nu(k) \rangle. \tag{A.28}
\end{aligned}$$

The exponent may be rewritten as

$$iF \int_0^t \tau V_\mu(k - Ft + F\tau) d\tau = \dots = itE_\nu(k) - i \int_0^t E_\nu(k - ft + F\tau) d\tau. \tag{A.29}$$

From this derivation we conclude that in the absence of coupling between the bands (also known as *single band approximation* [82]) the coefficients in the expansion (A.22) obey

$$d_\mu(k, t) = A_\mu(k - Ft) e^{+iF \int_0^t \tau V_\mu(k - Ft + F\tau) d\tau}, \quad (\text{A.30})$$

which proves the acceleration theorem. Note the additional phase-factor that modifies the amplitudes, see also [83]. The corrections due to band-couplings are given by

$$\begin{aligned} \partial_{(2)} A_\mu(k - Ft, t) &= -F \sum_\nu A_\nu(k - Ft, t) e^{+i \int_0^t E_\nu(k - Ft + F\tau) d\tau} e^{-i \int_0^t E_\mu(k - Ft + F\tau) d\tau} \\ &\times \langle \phi_\mu(k) | \partial_k | \phi_\nu(k) \rangle \Big|_{k \rightarrow k - Ft}. \end{aligned} \quad (\text{A.31})$$

Note that the coupling is weak when the bands are far apart or when $\langle \phi_\mu(k) | \partial_k | \phi_\nu(k) \rangle$ is small, in agreement with general adiabatic evolution.

Appendix B

Split operator method

There are several numerical methods for solving the Schrödinger equation [84]

$$-i\frac{\partial}{\partial t}\Psi(x, t) = -\frac{\partial^2}{\partial x^2}\Psi(x, t) + V(x)\Psi(x, t) \quad (\text{B.1})$$

and we have used the *split operator method* [85]. The procedure is to 'split' the time evolution operator into two parts; one containing the position operator x and one containing the momentum operator p . For any two operators A and B we may in first order of small δt write

$$e^{A\delta t+B\delta t} \approx e^{A\delta t}e^{B\delta t} \quad (\text{B.2})$$

and next order would be to write $\exp(A\delta t+B\delta t) \approx \exp(A\delta t/2)\exp(B\delta t)\exp(A\delta t/2)$. However, we have used the form of equation (B.2). Now, the higher terms neglected in (B.2) are of the orders δt^n , $n = 2, 3, \dots$ and may be assumed small. The split operator method applied to the Schrödinger equation (B.1) becomes

$$\Psi(x, \delta t + t_0) = e^{-i\frac{\partial^2}{\partial x^2}\delta t - iV(x)\delta t}\Psi(x, t_0) \approx e^{-i\frac{\partial^2}{\partial x^2}\delta t}e^{-iV(x)\delta t}\Psi(x, t_0). \quad (\text{B.3})$$

Having $\Psi(x, t_0)$ we first multiply by $\exp(-iV(x)\delta t)$, then Fourier transform the x -propagated wave-function to momentum space p and multiply by the kinetic term $\exp(-ip^2\delta t)$, and finally Fourier transform back to x -representation. This whole routine is repeated N times to give the wave-function at the time $t = t_0 + N\delta t$. During the propagation one obtains the wave-functions or wave-packets both in x - and p -representation

$$\Psi(x, t_0 + n\delta t), \quad \Phi(p, t_0 + n\delta t), \quad (\text{B.4})$$

for all $n = 0, 1, 2, \dots, N$. This is appropriate for calculating time variations of expectation values of the form $\langle x^j \rangle$ and $\langle p^j \rangle$ for integers j . However, calculating expectation values of the form $\langle x^j p^i \rangle$ is not straightforward with the split operator method and the Crank-Nicholson method [84] might be more suited. Note that the procedure is also applicable for time-dependent potential $V(x, t)$, where the potential with 'correct' time is used in each N steps. When we have a two-level system as, for example, the Jaynes-Cummings model, the potential is a 2×2 matrix and we may use the formula

$$e^{-i\alpha \cdot \sigma \delta t} = \cos(|\alpha| \delta t) - i \sin(|\alpha| \delta t) \frac{\alpha \cdot \sigma}{|\alpha|}, \quad (\text{B.5})$$

where $\alpha = (\alpha_1, \alpha_2, \alpha_3)$ and $\sigma = (\sigma_x, \sigma_y, \sigma_z)$. In subsection 4.3.4 where wave-packet propagations are performed for three-level systems the above formula does not work, and instead we use the MATLAB command `expm`, which numerically calculates the exponential of a matrix M using $e^M = V \cdot e^D \cdot V^{-1}$, where V is the matrix of M 's eigenvectors and D is the diagonal matrix of M 's eigenvalues.

Bibliography

- [1] *Quantum entanglement and information processing*, edited by D. Estve, J.-M. Raimond, and J. Dalibard, (Elsevier, 2004).
- [2] G. Raithel, Ch. Wagner, H. Walther, L. M. Narducci and M. O. Scully, 1994, *Cavity Quantum Electrodynamics, Advances in Atomic, molecular and Optical Physics, Supplement 2*, , editor P. R. Berman (Academic Press).
- [3] E. T. Jaynes and F. W. Cummings, Proc. IEEE **51**, 89 (1963).
- [4] B. W. Shore and P. L. Knight, J. Mod. Opt. **40**, 1195 (1993).
- [5] J. H. Eberly, N. B. Narozhny and J. J. Sanchez-Mondragon, Phys. Rev. Lett. **44**, 1323 (1989).
- [6] J. Gea-Banacloche, Phys. Rev. Lett. **65**, 3385 (1990). J. Gea-Banacloche, Phys. Rev. A **44**, 5913 (1991).
- [7] S. J. D. Phoenix and P. L. Knight, Phys. Rev. A **44**, 6023 (1991). S. J. D. Phoenix and P. L. Knight, Phys. Rev. Lett. **66**, 2833 (1991).
- [8] P. Meystre and M. S. Zybaury, Phys. Lett. A **89**, 390 (1982). A. Heidmann, J.M. Raimond and S. Reynaud, Phys. Rev. Lett. **54**, 326 (1985). J. R. Kukliński and J. L. Madajczyk, Phys. Rev. A **37**, 3175 (1988).
- [9] P. J. Bardsroff, E. Mayr, W. P. Schleich, Phys. Rev. A **51**, 4963 (1995). M. Brune, S. Haroche, V. Lefevre, J. M. Raimond and N. Zugary, Phys. Rev. Lett. **65**, 976 (1990).
- [10] C. T. Bodendorf, G. Antesberger, M. S. Kim and H. Walther, Phys. Rev. A **57**, 1371 (1997). M. S. Kim, G. Antesberger, C. T. Bodendorf and H. Walther, Phys. Rev. A **58**, R65 (1998).

- [11] M. Franca Santos, E. Solano and R. L. de Matos Filho, Phys. Rev. Lett. **87**, 093601 (2001).
- [12] J. M. Raimond and S. Haroche, Atoms and Cavities: The birth of a Schrödinger cat of the radiation field, in *International Trends in Optics and Photonics*, ed. T. Asakura (Springer Verlag, Heidelberg 1999), pp 40-53. V. Bužek, H. Moya-Cessa and P. L. Knight, Phys. Rev. A **45**, 8190 (1992).
- [13] D. F. Walls and G. J. Milburn, Phys. Rev. A **31**, 2403 (1985). G. S. Agarwal, M. O. Scully and H. Walther, Phys. Rev. Lett. **86**, 4271 (2001).
- [14] G. Rempe and H. Walther, Phys. Rev. Lett. **58**, 353 (1987).
- [15] A. Auffeves, P. Maioli, T. Meunier, S. Gleyzes, G. Nogues, M. Brune, J. M. Raimond and S. Haroche, Phys. Rev. Lett. **91**, 230405 (2003).
- [16] C.J. Hood, T.W. Lynn, A.C. Doherty, A.S. Parkins, and H.J. Kimble, Science **287**, 1447 (2000).
- [17] M. Brune, F. Schmidt-Kaler, A. Maali, J. Dreyer, E. Hagley, J. M. Raimond and S. Haroche, Phys. Rev. Lett. **76**, 1800 (1996). M. Brune, P. Nussenzveig, F. Schmidt-Kaler, F. Bernardot, A. Maali, J. M. Raimond and S. Haroche, Phys. Rev. Lett. **72**, 3339 (1994). S. Brattke, B. T. H. Varcoe and H. Walther, Phys. Rev. Lett. **86**, 3534 (2001). G. Nogues, A. Rauschenbeutel, S. Osnaghi, M. Brune, J.M. Raimond and S. Haroche, Nature **400**, 239 (1999). P. Bertet, S. Osnaghi, P. Milman, A. Auffeves, P. Maioli, M. Brune, J. M. Raimond and S. Haroche, Phys. Rev. Lett. **88**, 143601 (2002). B. T. H. Varcoe, S. Brattke, M. Weidinger and H. Walther, Nature **403**, 743 (2000).
- [18] M. Brune, E. Hagley, J. Dreyer, X. Maître, A. Maali, C. Wunderlich, J. M. Raimond and S. Haroche, Phys. Rev. Lett. **77**, 4887 (1996). J. M. Raimond, M. Brune and S. Haroche, Phys. Rev. Lett. **79**, 1964 (1997).
- [19] G. Nogues, A. Raushenbeutel, S. Osnaghi, M. Brune, J. M. Raimond and S. Haroche, Nature **400**, 239 (1999). P. Bertet, S. Osnaghi, P. Milman, A. Auffeves, P. Maioli, M. Brune, J. M. Raimond and S. Haroche, Phys. Rev. Lett. **88**, 143601 (2002).

- [20] S. Brattke, B. T. H. Varcoe and S. Walther, Opt. Express **8**, 131 (2001). P. Bertet, S. Osnaghi, P. Milman, A. Auffeves, P. Maioli, M. Brune, J. M. Raimond and S. Haroche, Phys. Rev. Lett. **88**, 143601 (2002). S. Brattke, B. T. H. Varcoe and H. Walther, Phys. Rev. Lett. **86**, 3534 (2001).
- [21] G. Rempe, F. Schmidt-Kaler and H. Walther, Phys. Rev. Lett. **64**, 2783 (1990).
- [22] M. A. Nielsen and I. L. Chuang, *Quantum Computation and Quantum Information*, (Cambridge, 2000).
- [23] J. M. Raimond, M. Brune and S. Haroche, Rev. Mod. Phys. **73**, 565 (2001). A. Rauschenbeutel, G. Nogues, S. Osnaghi, P. Bertet, M. Brune, J. M. Raimond and S. Haroche, Phys. Rev. Lett. **83**, 5166 (1999). X. Maître, E. Hagley, G. Nogues, C. Wunderlich, P. Goy, M. Brune, J. M. Raimond and S. Haroche, Phys. Rev. Lett. **79**, 769 (1997). C. Wagner, R. J. Brecha, A. Schenzle and H. Walther, Phys. Rev A **47**, 5068 (1993). A. Rauschenbeutel, G. Nogues, S. Osnaghi, P. Bertet, M. Brune, J.M. Raimond and S. Haroche, Science **288**, 2024 (2000). H. Walther, Phys. Rep.-Rev. Phys. Lett. **219**, 263 (1992). J. I. Cirac, P. Zoller, H. J. Kimble and H. Mabuchi, Phys. Rev. Lett. **78**, 3221 (1997). E. Hagley, X. Maitre, G. Nogues, C. Wunderlich, M. Brune, J. M. Raimond and S. Haroche, Phys. Rev. Lett. **79**, 1 (1997). A. Rauschenbeutel, P. Bertet, S. Osnaghi, G. Nogues, M. Brune, J. M. Raimond and S. Haroche, Phys. Rev. A **64** 050301 (2001). B. G. Englert and H. Walther, Opt. Comm. **179**, 283 (2000).
- [24] K. Bergman, H. Theuer and B. W. Shore, Rev. Mod. Phys. **70**, 1003 (1998).
- [25] F. T. Hioe, Phys. Lett. **99A**, 150 (1983). N. V. Vitanov and S. Stenholm, Phys. Rev A **55**, 648 (1997). N. V. Vitanov and S. Stenholm, Opt. Comm. **135**, 394 (1997). L. P. Yatsenko, S. Gue'rin and H. R. Jauslin, Phys. Rev. A **65**, 043407 (2002). T. A. Laine and S. Stenholm, Phys. Rev. A **53**, 2501 (1996).
- [26] P.W.H. Pinkse, T. Fisher, P. Maunz, and G. Rempe, Nature **404**, 365 (2000). J. A. Sauer, K. M. Fortier, M. S. Chang, C. D. Hamley and M. S. Chapman, Phys. Rev. A **69**, 051804 (2004).
- [27] D. Meschede, H. Walther, and G. Müller, Phys. Rev. Lett. **54**, 551 (1985).

- [28] L. Mandel and E. Wolf, *Optical Coherence and Quantum Optics*, (Cambridge, 1995).
- [29] M. O. Scully and M. S. Zubairy, *Quantum Optics*, (Cambridge, 1997).
- [30] J. E. Bayfield, *Quantum evolution*, (John-Weily and Sons, 1999).
- [31] M. V. Berry, Proc. R. Soc. London A, **429**, 61 (1990).
- [32] H. Araki E. Lieb, Comm. math. Phys. **18**, 160 (1970).
- [33] N. B. Narozhny, J. J. Sanchez-Mondragon and J. H. Eberly, Phys. Rev. A **23**, 236 (1981).
- [34] G. Harel and G. Kurizki, Phys. Rev. A **54**, 5410 (1996). J. Krause, M. O. Scully and H. Walther, Phys. Rev. A **36**, 4547 (1987).
- [35] C. C. Gerry, Phys. Rev. A **37**, 2683 (1988). I. Ashraf, J. Gea-Banacloche and M. S. Zubairy, Phys. Rev A **42**, 6704 (1990). P. L. Knight and T. Quang, Phys. Rev. A **41**, 6255 (1990). X.-S. Li, D. L. Lin and C.-D. Gong, Phys. Rev. A **36**, 5209 (1987).
- [36] A. Dasgupta, J. Opt. B **1**, 14 (1999). A. Joshi and S. V. Lawande, Phys. Rev. A **48**, 2276 (1992). Mao-Fa Fang, Physica A **259**, 193 (1998). R. R. Schlicher, Opt. Comm. **70**, 97 (1989). A. Joshi and S. V. Lawande, Phys. Rev. A **42**, 1752 (1990). A. Joshi, Phys. Rev. A **58**, 4662 (1998).
- [37] J.T. Zhang, X.L Feng, W.Q. Zhang and Z.Z. Xu, Chin. Phys. Lett. **19**, 670 (2002). Y.T. Chough, S.H. Youn, H. Nha, S.W. Kim and K. An, Phys. Rev. A **65**, 023810 (2002). M. Wilkens, E. Schumacher and P. Meystre, Phys. Rev. A **44**, 3130 (1991). I. Cusumano, A. Vaglica and G. Vetri, Phys. Rev. A **66**, 043408 (2002). C.J. Hood, M.S. Chapman, T.W. Lynn and H.J. Kimble, Phys. Rev. Lett. **80**, 4157 (1998). F. Saif, F.L. Kien and M.S. Zubairy, Phys. Rev. A **64**, 043812 (2001). G. Compagno, J.S. Peng and F. Persico, Phys. Rev. A **26**, 2065 (1982). A.Z. Muradyan and G.A. Muradyan, J. Phys. B **35**, 3995 (2002). A. Vaglica, Phys. Rev. A **52**, 2319 (1995).
- [38] A. R. Kolovsky, J. Opt. B **4**, 218 (2002). W. Ren and H.J. Carmichael, Phys. Rev. A **51**, 752 (1995).
- [39] C. Wildfeuer and D. H. Schiller, Phys. Rev. A **67**, 053801 (2003).

- [40] M. Brune, J. M. Raimond, P. Goy, L. Davidovich and S. Haroche, Phys. Rev. Lett. **59**, 1899 (1987). W. Lange, G. S. Agarwal and H. Walther, Phys. Rev. Lett. **76**, 3293 (1996). A. Rauschenbeutel, P. bertet, S. Osnaghi, G. Nogues, M. Brune, J. M. Raimond and S. Haroche, Phys. Rev. A **64**, 050302(R) (2001).
- [41] A. Messina, S. Maniscalco and A. Napoli J. Mod. Opt. **50**, 1 (2003).
- [42] Y. Wu, Phys. Rev. A **54**, 1586 (1996).
- [43] C.C. Gerry and J.H Eberly, Phys. Rev. A **42**, 6805 (1990).
- [44] M. Alexanian and S.K. Bose, Phys. Rev. A **52**, 2218 (1995).
- [45] E. E. Nikitin and S. Ya. Umenskii, *Theory of Slow Atomic Collisions*, (Springer Verlag, Heidelberg, 1999), sections 7-9. B. M. Garraway and K.-A. Suominen, Rep. Progr. Phys. **58**, 365 (1995). B. W. Shore, *The Theory of Coherent Atomic Excitation*, (John Wiley & Sons, New York 1990), sections 5.5 and 5.6.
- [46] S. Stenholm in *Quantum dynamics of simple systems*, Edited by G.-L. Oppo, S. M. Barnett, E. Riis and M. Wilkinson, (Bristol: Institute of Physics Publishing, 1997)
- [47] E. J Robinson, Phys. Rev. A **24**, 2239 (1981). N. V. Vitanov, J. Phys. B **27**, 1351 (1993). A. Bambini and P. R. Berman, Phys. Rev. A **23**, 2496 (1981).
- [48] E. J. Robinson, J. Phys. B **18**, 3687 (1985). E. J. Robinson , Phys. Rev. A **29**, 1665 (1984).
- [49] L. D. Landau, Phys. Z. Sowjet Union **2**, (1932); L. D. Landau and E. M. Lifshitz, *Quantum Mechanics, 3rd ed.* (Pergamon Press, Oxford, 1977).
- [50] C. Zener, Proc. Roy. Soc. Lond. A, **137**, 696 (1932).
- [51] N. Rosen and C. Zener, Phys. Rev. **40**, 502 (1932).
- [52] Yu. N. Demkov and M. Kunike, Vestn. Leningr. Univ. Ser. Fiz. Khim. **16**, 39 (1969). see also, F. T. Hioe, Phys. Rev. A **30**, 2100 (1984).
- [53] F. Mattinson, M. Kira and S. Stenholm, J. Mod. Opt. **48**, 889 (2001). F. Mattinson, M. Kira and S. Stenholm, J. Mod. Opt. **49**, 1649 (2002).

- [54] N. V. Vitanov, Phys. Rev. A **58**, 2295 (1998). Y. B. Band and P. S. Julienne, J. Chem. Phys. **95**, 5681 (1991). N. V. Vitanov and S. Stenholm, Phys. Rev. A **60**, 3820 (1999). B. W. Shore, K. Bergman, J. Oreg and S. Rosenwaks, Phys. Rev. A **44**, 7442 (1991). V. S. Malinovsky and D. J. Tannor, Phys. Rev. A **56**, 4929 (1997).
- [55] G. M. Meyer, M. O. Scully and H. Walther, Phys. Rev. A **56**, 4142 (1997). M. Löffler, G. M. Meyer, M. Schröder, M. O. Scully and H. Walther, Phys. Rev. A **56**, 4153 (1997). M. Schröder, K. Vogel, W. P. Schleich, M. O. Scully and H. Walther, Phys. Rev. A **56**, 4164 (1997). R. Arun and G. S. Agarwal, arXiv:quant-ph/0103015.
- [56] B. G. Englert, J. Schwinger, A. O. Barut and M. O. Scully, Europhys Lett. **14**, 25 (1991).
- [57] T. Bastin and J. Martin, Phys. Rev. A **67**, 053804 (2003), J. Martin and T. Bastin, Euro. Phys. Jour. D **29**, 133 (2004), T. Bastin and E. Solano, Opt. Commun. **217**, 239 (2003).
- [58] T. Bastin and E. Solano, Comp. Phys. Commun. **124**, 197 (2000).
- [59] *Handbook of Mathematical Functions*, Natl. Bur. Stand. Appl. Math. Ser. No. 55, edited by M. Abramowitz and I.A. Stegun (U.S. GPO, Washington, DC, 1972).
- [60] H. Jones, and C. Zener, Proc. Roy. Soc. A **144**, 101 (1934). F. Bloch, Z. Phys. **52**, 555 (1928).
- [61] M.B. Dahan, E. Peik, J. Reichel, Y. Castin, and C. Salomon, Phys. Rev. Lett. **76**, 4508 (1996). E. Peik, M.B. Dahan, I. Bouhoule, Y. Castin, and C. Salomon, Phys. Rev. A **55**, 2989 (1997). S.R. Wilkinson, C.F. Bharucha, K.W. Madison, Q. Niu, and M.G. Raizen, Phys. Rev. Lett. **76**, 4512 (1996). O. Morsch, J.H. Müller, M. Cristiani, D. Ciampini, and E. Arimondo, Phys. Rev. Lett. **87**, 140402 (2001). M. Cristiani, O. Morsch, J.H. Müller, D. Ciampini, and E. Arimondo, Phys. Rev. A **65**, 063612 (2002). G.C. Chu, T. Dekorsy, H.J. Bakker, H. Kurz, A. Kohl, and B. Opitz, Phys. Rev. B **54**, 4420 (1996).
- [62] M. Glück, A. R. Kolovsky and H. J. Korsch, Phys. Rep. **366**, 103 (2002).
- [63] C. E. Carrol and F. T. Hioe, J. Phys. A: Math. Gen. **19**, 2061 (1986).

- [64] W. P. Schleich and M. G. Raymer, editors, J. Mod. Opt. **44**, 2021 (1997).
- [65] P. Domokos, M. Brune, J. M. Raimond and S. Haroche, Eur. Phys. J. D **1**, 1 (1998).
- [66] J. M. Raimond, M. Brune and S. Haroche, Rev. Mod. Phys. **73**, 565 (2001).
- [67] A. B. Mundt, A. Kreuter, C. Becher, D. Leibfried, J. Eschner, F. Schmidt-Kaler and R. Blatt, Phys. Rev. Lett. **89**, 103001 (2002). A. Kreuter, C. Becher, G. P. T. Lancaster, A. B. Mundt, C. Russo, H. Haffner, C. Roos, J. Eschner, F. Schmidt-Kaler and R. Blatt, Phys. Rev. Lett. **92**, 203002 (2004). S. Nussmann, M. Hijkema, B. Weber, F. Rohde, G. Rempe and A. Kuhn, arXiv:quant-ph/0506088.
- [68] E. Solano, G. S. Agarwall and H. Walther, Phys. Rev. Lett. **90**, 027903 (2003), G. S. Agarwal and R. R. Puri, Phys. Rev. A **40**, 5179 (1989).
- [69] P.L. Knight and B. W. Shore, Phys. Rev. A **48**, 642 (1993).
- [70] B. C. Sanders, S. D. Bartlett, B. Tregenna and Peter L. Knight, Phys. Rev. A **67**, 042305 (2003).
- [71] E. Farhi, J. Goldstone, S. Gutmann, J. Lapan, A. Lundgren and D. Preda, Science **292**, 472 (2001). M. S. Shahriar, J. A. Bowers, B. Demsky, P. S. Bhatia, S. Lloyd, P. R. Hemmer and A. E. Craig, Opt. Comm. **195**, 411 (2001). J. Roland and N. J. Cerf, Phys. Rev. A **65**, 042308 (2002). E. Farhi, J. Goldstone, S. Gutmann and M. Sipser, arXiv:quant-ph/0001106. A. M. Childs, E. Farhi and J. Preskill, Phys. Rev. A **65**, 012322 (2002).
- [72] D. J. Goldstein, *States of matter*, (Dover Publications, 1985).
- [73] P. Meystre, *Atom Optics*, (Springer Verlag, Heidelberg, 2001).
- [74] M. Holthaus, J. Opt. B: Quantum Semiclass. Opt. **2**, 589 (1999).
- [75] B. M. Garraway and K.-A. Suominen, Phys. Rev. Lett **80**, 932 (1998).
- [76] J. Liu and Y. Wang, Phys. Rev. A **54**, 2326-2333 (1996). G. S. Agarwal and R. R. Puri, Phys. Rev. A **39**, 2969-2977 (1989). A. Joshi and R. R. Puri, Phys. Rev. A **45**, 5056-5060 (1992).

- [77] P. Lougovski, F. Casagrande, A. Lulli, B.-G. Englert, E. Solano and H. Walther, Phys. Rev. A **69**, 023812 (2004). E. Solano, G. S. Agarwal and H. Walther Phys. Rev. Lett. **90**, 027903 (2003). C. C. Gerry, Phys. Rev. A **65**, 063801 (2002). J. Gea-Banacloche, T. C. Burt, P. R. Rice, and L. A. Orozco, Phys. Rev. Lett. **94**, 053603 (2005). P. Alsing, D.S. Guo, and H. J. Carmichael, Phys. Rev. A **45**, 5135-5143 (1992)
- [78] J. Pachos and H. Walther, Phys. Rev. Lett. **89**, 187903 (2002). D. E. Browne, M. B. Plenio and S. F. Huelga, Phys. Rev. Lett. **91**, 067901 (2003).
- [79] E. Paspalakis and N. J. Kylstra, Jour. Mod. Opt. **51**, 1679 (2004). Z. Kis and E. Paspalakis, Phys. Rev. B **69**, 024510 (2004).
- [80] A. Messiah, *Quantum Mechanics*, Vol. II, (North-Holland, Amsterdam, 1961). D. Bohm, *Quantum Theory*, (Prentice-Hall, Englewood Cliffs, 1951). S. Gasiorowicz, *Quantum Physics*, (Weily, 1992).
- [81] M. S. Sarandy, L. -A. Wu and D. A. Lidar, Quant. Inf. Proc. **3**, 331 (2004).
- [82] T. Hartmann, F. Keck, H.J. Korsch, and S. Mossmann, New J. Phys. **6**, 2 (2004).
- [83] V. Grecchi and A. Sacchetti, quant-ph/0506057.
- [84] B. M. Garraway and K. -A., Suominen, Rep. Prog. Phys. **58**, 365 (1995).
- [85] M. D. Feit, J. A. Fleck and A. Steiger, J. Comp. Phys. **47**, 412 (1982).